



National Library
of Canada

Canadian Theses Service

Ottawa, Canada
K1A 0N4

Bibliothèque nationale
du Canada

Services des thèses canadiennes

CANADIAN THESES

THÈSES CANADIENNES

NOTICE

The quality of this microfiche is heavily dependent upon the quality of the original thesis submitted for microfilming. Every effort has been made to ensure the highest quality of reproduction possible.

If pages are missing, contact the university which granted the degree.

Some pages may have indistinct print especially if the original pages were typed with a poor typewriter ribbon or if the university sent us an inferior photocopy.

Previously copyrighted materials (journal articles, published tests, etc.) are not filmed.

Reproduction in full or in part of this film is governed by the Canadian Copyright Act, R.S.C. 1970, c. C-30. Please read the authorization forms which accompany this thesis.

AVIS

La qualité de cette microfiche dépend grandement de la qualité de la thèse soumise au microfilmage. Nous avons tout fait pour assurer une qualité supérieure de reproduction.

S'il manque des pages, veuillez communiquer avec l'université qui a conféré le grade.

La qualité d'impression de certaines pages peut laisser à désirer, surtout si les pages originales ont été dactylographiées à l'aide d'un ruban usé ou si l'université nous a fait parvenir une photocopie de qualité inférieure.

Les documents qui font déjà l'objet d'un droit d'auteur (articles de revue, examens publiés, etc.) ne sont pas microfilmés.

La reproduction, même partielle, de ce microfilm est soumise à la Loi canadienne sur le droit d'auteur, SRC 1970, c. C-30. Veuillez prendre connaissance des formules d'autorisation qui accompagnent cette thèse.

**THIS DISSERTATION
HAS BEEN MICROFILMED
EXACTLY AS RECEIVED**

**LA THÈSE A ÉTÉ
MICROFILMÉE TELLE QUE
NOUS L'AVONS REÇUE**

SUPERPOSED QUADRATURE AMPLITUDE MODULATION (SQAM).
- A SPECTRAL AND POWER EFFICIENT MODULATION TECHNIQUE -

by

JONGSOO, SEO

A THESIS
PRESENTED TO THE SCHOOL OF GRADUATE STUDIES AND RESEARCH
AT THE UNIVERSITY OF OTTAWA
IN PARTIAL FULFILLMENT OF THE
REQUIREMENTS FOR THE DEGREE OF
MASTER OF APPLIED SCIENCE
IN
ELECTRICAL ENGINEERING

OTTAWA, ONTARIO, 1984

© Jongsoo Seo, OTTAWA, Canada, 1984.

The University of Ottawa requires the signatures of all persons using or photocopying this thesis. Please sign below, and give address and date.

ABSTRACT

A spectral and power efficient modulation technique, - Superposed Quadrature Amplitude Modulation (SQAM) is introduced.

At first, the SQAM baseband signal encoder, using both the pulse overlapping concept and the nonlinear switching filter (NLSF) technique, is described. Experimental and simulation results of eye patterns, state space diagrams and envelope fluctuations of SQAM signals are presented. The spectral characteristics and probability of error performance of SQAM signals, in an additive white Gaussian noise (AWGN) single-channel environment, are analyzed and compared to constant envelope modulation schemes such as MSK and TFM. These results indicate that our SQAM systems have comparable spectral properties, exhibit better $P(e)$ performance and are easier to implement than TFM.

Then the performance of the SQAM system, in a nonlinearly amplified multichannel environment, in the presence of AWGN, intersymbol-interference (ISI), adjacent channel-interference (ACI) and/or cochannel interference (CCI), is investigated and compared to those of OQPSK, MSK and IJF-OQPSK (or SQORC) systems. The effects of ACI and CCI on the performance of the SQAM system are investigated by

simulation under different channel conditions , namely , (1) different channel frequency separation, (2) filter bandwidth(B) and symbol duration(T_s) product (BT_s) , (3) flat fade depth and (4) different values of amplitude parameter(A) in the SQAM signal. In the simulation , the earth station high power amplifiers (HPA), operating in saturation mode, are approximated by ideal hardlimiters. As a result of the performance evaluation , it has been found that the SQAM system outperforms QPSK , MSK and IJF-QPSK systems. Further, we illustrate that the $P(e)$ performance degradation due to the ACI or CCI can be minimized by appropriately choosing the modulation technique, type of filters (transmit and receive) and their BT_s values.

For future research , an application of the SQAM signal encoding technique to the premodulation filters , in digital FM or continuous phase frequency shift keying (CPFSK) scheme, is suggested . To attain even higher spectral efficiency , a duo-binary SQAM technique is also suggested and its power spectrum is studied.

These desirable performance characteristics, combined with the simple hardware implementations of SQAM modem may lead to numerous satellite and terrestrial radio system applications.

ACKNOWLEDGEMENTS

The author would like to express grateful thanks to his supervisor , Dr. Kamilo Feher , for his generous encouragement , guidance and constructive criticism throughout this work , without which this thesis would not have been possible.

Appreciations are also expressed to all of his colleagues in the Digital Communication Group for their helpful discussions.

Special thanks are due to his wife HyunSun, Lee for the typing and encouragement during this work.

LIST OF FIGURES.

<u>Fig.</u>		<u>Page</u>
2.1	SQAM signal encoder using double-interval pulse overlapping concept	10
2.2	Encoded SQAM output signal eye pattern using the NLSF technique	13
2.3	Block diagram of SQAM signal encoder	13
2.4	Circuit diagram of SQAM baseband signal processor	14
2.5	Measured baseband waveshape and eye pattern	15
2.6 (a)-(g)	Phase transitions of MSK, SQAM and IJF-OQPSK	17,18,19
2.6(h)	Phase transitions of MSK, TFM and CCPSK	19
2.7	Normalized PSD of SQAM signals in linear channel	23
2.8(a)	Power spectra of SQAM, MSK and TFM in linear channel	24
2.8(b)	Power spectra of SQAM and TFM	25
2.8(c)	Power spectra of SQAM, MSK and TFM in nonlinear channel	26
2.9	Measured power spectra of SQAM	27
2.10(a)	Out-of-band to total power ratios of SQAM and MSK in linear channel	29

<u>Fig.</u>		<u>Page</u>
2.10(b)	Out-of-band to total power ratios of SQAM and MSK in non-linear channel	30
3.1	Block diagram of SQAM modem	34
3.2	SQAM signal encoding progress	35
3.3	Eye patterns of SQAM signal in linear channel	37
3.4	Eye patterns of SQAM signal in hardlimited channel	38
3.5	SQAM signal space diagrams	39
3.6	Envelope fluctuations of SQAM signals	40
3.7	Composite waveforms of SQAM signal	42
3.8	Configuration of correlation receiver for SQAM	43
3.9	SQAM linear baseband model	44
3.10	Simulation model of SQAM modem	46
3.11	Eye patterns of SQAM signal after postdetection LPF in linear channel	48,49
3.12	Eye patterns of SQAM signal after postdetection LPF in hardlimited channel	50,51
3.13	Eye patterns of MSK signal after postdetection LPF in linear channel	52
3.14	Eye patterns of MSK signal after postdetection LPF in hardlimited channel	52

<u>Fig.</u>		<u>Page</u>
3.15(a)	P(e) performance of SQAM modem in linear channel	54
3.15(b)	P(e) performance of SQAM modem in nonlinear channel	55
3.16	P(e) performance degradations of SQAM, MSK and TFM	56
3.17	Experimental set-up of SQAM modem	58
3.18	Measured eye patterns of SQAM signal	59
3.19	Baseband and modulated SQAM signals	59
3.20	Measured SQAM signal space diagram	60
3.21	Measured power spectra of SQAM signals	60
4.1	Block diagram of multi-channel modem	63
4.2	Simulation model of multi-channel system	70
4.3	Frequency allocation for multichannel system	70
4.4	P(e) performance of SQAM modem in hardlimited multi-channel system (vs. 'A')	73-76
4.5	P(e) performance of SQAM modem in hardlimited multichannel system (vs. f_{3dB})	78-80
4.6	P(e) performance of SQAM modem in hardlimited multichannel system (vs. ΔF)	82,83

<u>Fig.</u>		<u>Page</u>
4.7	P(e) performance of SQAM modem in hardlimited multichannel system (vs. F.D)	86,87
4.8	E_b/N_o degradation vs. fading depth	88,89
4.9	Eye patterns of MSK, IJF-OQPSK and SQAM in hardlimited multichannel	90
4.10	Simulation model of co-channel system	92
4.11	Frequency allocation for co-channel system	92
4.12	P(e) performance of SQAM modem in hardlimited co-channel (vs. C/I)	93
4.13	E_b/N_o degradation vs. C/I ratio in hardlimited co-channel (vs. f_{3dB})	94
4.14	E_b/N_o degradation of OQPSK, MSK, IJF-OQPSK and SQAM in hardlimited co-channel	95
5.1	Impulse response of TFM premodulation filter	97
5.2	Block diagram of TFM transmitter	97
5.3	Digital FM transmitter combined with SQAM signal encoder	98
5.4	Block diagram of Duo-binary SQAM encoder	99
A.1	Double-interval raised-cosine pulse and its derivatives	103
A.2	Weighted single-interval raised-cosine pulse and its derivatives	106
B.1	Block diagram of Duo-binary encoder	109

<u>Fig.</u>		<u>Page</u>
B.2	Impulse response of Duo-binary SQAM encoder	110
B.3	Normalized PSD of Duo-binary SQAM signals	112

LIST OF TABLES.

<u>Table.</u>		<u>Page</u>
2.1	Encoded SQAM output signals	12
3.1	Maximum envelope fluctuations of SQAM signals	40
3.2	Probability of error for SQAM signals	45
3.3	Filtering strategies for different modems	57
4.1	Filtering strategies for different modems (multichannel system.)	84

CONTENTS

ABSTRACT	iv
ACKNOWLEDGEMENTS	vi

<u>Chapter</u>	<u>page</u>
I. INTRODUCTION	1
Thesis Outline	3
II. A CLASS OF POWER AND SPECTRAL EFFICIENT SQAM SIGNALS	5
Generation of SQAM Signals	6
SQAM Signal Encoder Using Pulse Overlapping Concept	6
SQAM Signal Encoder Using the NLSF Technique.	11
Phase Transitions of SQAM Signals.	16
Spectral Analysis of SQAM signals.	20
III. PERFORMANCE OF SQAM IN AWGN SINGLE-CHANNEL ENVIRONMENT	31
SQAM Modem	31
Eye pattern, Space diagram and Envelope fluctuation	36
Probability of Error Performance of SQAM Systems	41
Optimum Receiver for SQAM	41
Optimum P(e) Performance of the SQAM Modem	44
Simulation of the P(e) Performance of SQAM System	46
Experimental Results	57
IV. PERFORMANCE OF SQAM MODEM IN NONLINEAR MULTICHANNEL	61
Analysis of Probability of Error in Multichannel	61
Probability of Error in Adjacent Channel Interference	61

Probability of Error in Co-Channel Interference	66
Simulation on P(e) Performance of Multichannel SQAM	68
Assumptions Used in the Simulations	71
Effects of the Amplitude Parameter(A) in SQAM	72
Effects of the Receive Filter Bandwidth.	77
Effects of Channel Frequency Separation (Spacing)	81
Effects of Fade Depth on the Desired Signal	84
Effects of CCI on P(e) Performance of SQAM Modems	91
V. RECOMMENDED FURTHER RESEARCH	96
VI. CONCLUSION	100

<u>Appendix</u>	<u>page</u>
A.. DERIVATION OF THE PSD OF SQAM SIGNAL	102
B. POWER SPECTRUM OF DUOBINARY SQAM	109
Duo-binary Encoder	109
Power Spectrum of Duo-binary SQAM signals	110
C. PROGRAMS TO SIMULATE PERFORMANCE OF SQAM MODEM	113
REFERENCES	143

Chapter I

INTRODUCTION

In order to improve the power and spectral efficiency of digital communication systems, various filtering and baseband signal processing techniques have been studied. To attain high spectral efficiency, the power spectrum of the signal should have a narrow mainlobe and a fast spectral roll-off. To attain high power efficiency, the transmit high power amplifier (HPA) should be operated in a saturated (nonlinear) mode.

As the presently used RF spectrum becomes highly congested, many satellite systems tend to employ higher frequency bands such as 14/11 or 30/20 GHz. At these frequencies, not only up- and down-link thermal noise, but also up- and down-link fades, caused by rain attenuations, are quite important. To minimize the impact of the uplink signal fade, the satellite traveling wave tube amplifiers (TWTA) may be overdriven into the nonlinear region. To maximize the earth station power efficiency, the earth station HPAs must be operated in the saturation region. An ideal hardlimiter presents a good first-order approximation of saturated amplifiers.[1,10].

Quadrature-phase-shift-keying (QPSK) modulation technique is widely used because of its simple hardware implementation and good $P(e)$ performance in a linearly amplified channel. However, when a QPSK signal is filtered and then amplified by HPA near saturation region, the spectral sidelobes at the output of HPA regrow due to the nonlinear amplification. These regrown spectral sidelobes cause significant interference into the adjacent channels, and degrade the probability of error performance.

In PSK-type modulation schemes, multi-interval pulse overlapping techniques have been introduced to achieve higher spectral efficiency compared to the conventional QPSK, OQPSK and MSK signals. A class of intersymbol interference and jitter-free (IJF) -OQPSK scheme studied by Feher et al. [1,4,10,11] also retains a compact mainlobe and low spectral spreading after nonlinear amplification.

In this thesis, we introduce a new class of power and spectral efficient modulation technique - Superposed Quadrature Amplitude Modulation (SQAM) which produces a fast spectral roll-off, a low out-of-band energy, and shows good $P(e)$ performance.

1.1 THESIS OUTLINE

Following this introductory chapter, in Chapter 2, two methods of generation of SQAM baseband signals are presented, namely, (1) the pulse overlapping concept and (2) the nonlinear switching filter (NLSF) technique. The NLSF method is used for our low-speed hardware prototype. For higher speed applications, binary transversal filter (BTF) implementations may be preferable [10]. The power spectral densities of SQAM signals are analyzed and compared to those of QPSK (or OQPSK), MSK, IJF-OQPSK (or SQORC) and TFM signals [1,4,6].

Chapter 3 illustrates the properties of SQAM signals, including eye patterns, signal state-space diagrams and envelope fluctuations. The probability of error performance of the SQAM modem, in an AWGN single-channel environment, is studied and compared to some well-known, constant envelope modulation schemes, such as MSK and TFM.

In Chapter 4, the performance of SQAM modem, in a nonlinearly amplified multi-channel environment, in the presence of additive white Gaussian noise (AWGN), intersymbol-interference (ISI), adjacent channel interference (ACI) and/or co-channel interference (CCI), is

investigated by computer simulation, and compared to the performance of OQPSK, MSK and IJF-OQPSK modems. The effects of ACI and CCI on the performance of SQAM modem are investigated under different channel conditions, such as different channel frequency separation, filter bandwidth and symbol duration product (BT_s) and flat fade depth of the desired signal. In this computer simulation, cascaded nonlinear satellite systems are simplified to a back-to-back mode (i.e., no channel input filter or TWTA), and earth station HPAs, operating in saturation mode, are approximated by the ideal hardlimiters.

Chapter 5 contains recommended further research, where applications of the SQAM signal processing technique to digital FM or duo-binary schemes are suggested.

Chapter 6 contains final conclusions.

Chapter II

A CLASS OF POWER AND SPECTRAL EFFICIENT SQAM SIGNALS

It has been demonstrated [4,6,10] that overlapping baseband pulses, where each pulse duration is wider than one symbol interval (T_s), have spectral advantages over non-overlapping pulses. Smooth and correlated phase transitions are required to attain good spectral properties, and low envelope fluctuations (or constant envelope) of modulated signals are preferable to attain good power efficiency.[3,20,26].

In this chapter, a new class of signals, for applications in a power and spectral efficient system, is introduced and studied. The SQAM baseband signals can be generated by using either the pulse overlapping concept or the NLSF technique.[5,10]. Conceptually, both implementations lead to identical results. For our relatively low-speed (128 kb/s) prototype hardware design, we used the NLSF method. The phase transitions and power spectrum of the SQAM signals are analyzed and compared to other modulation schemes.

2.1 GENERATION OF SQAM SIGNALS

2.1.1 SQAM Signal Encoder Using Pulse Overlapping Concept

Fig.2.1 shows the SQAM signal encoder using a double-interval pulse overlapping concept [4,6,10]. The input signal $x(t)$ to the encoder is given by :

$$x(t) = \sum_{n=-\infty}^{\infty} a_n h(t-nT_S) \quad (2.1)$$

where

$a_n = \pm 1$ with probability $1/2$

$$h(t-nT_S) = \begin{cases} 1 & \text{for } t=nT_S \\ 0 & \text{otherwise} \end{cases} \quad (2.2)$$

and T_S is a data symbol duration.

Let the SQAM signal encoder have an impulse response $s(t)$, which is a double-interval ($2T_S$) raised-cosine pulse, superimposed with another weighted single-interval (T_S) raised-cosine pulse, i.e.,

$$s(t) = \frac{1}{2} \left(1 + \cos \frac{\pi t}{T_S} \right) + d(t) \quad (2.3)$$

where

$$d(t) = -\frac{1-A}{2} \left(1 - \cos \frac{2\pi t}{T_S} \right) \quad (2.4)$$

$$0.5 \leq A \leq 1.5$$

$$-T_S \leq t \leq T_S$$

and A is an amplitude parameter of the SQAM signal. The encoded signal $y(t)$ is obtained by the convolution of the input signal $x(t)$ with the impulse response of the encoder $s(t)$, and is given by :

$$y(t) = \sum_{n=-\infty}^{\infty} a_n s(t-nT_S) \quad (2.5)$$

In order to obtain an intersymbol-interference and jitter-free (IJF) signal $y(t)$, the double-interval pulse $s(t)$ must satisfy the following IJF conditions.[1].

$$s(t)^e = s(-t) \quad \text{for} \quad -T_S \leq t \leq T_S \quad (2.6.a)$$

$$s(T_S) = s(-T_S) = 0 \quad (2.6.b)$$

From (2.3) and (2.4), it can be readily proven that SQAM signals meet the IJF conditions. Since the input signal duration is T_S second and $s(t)$ has a $2T_S$ second duration, the encoded signal can be obtained by the superposition of double-interval pulses $s(t-nT_S)$ and $s(t-(n+1)T_S)$. Therefore, the encoded signal can be rewritten as :

$$y(t) = \sum_{n=-\infty}^{\infty} y_m(t-nT_S) \quad (2.7)$$

where $m=1,2,3,4$.

$$\begin{aligned}
 y_1(t-nT_S) &= -s(t-nT_S) - s(t-(n+1)T_S) \quad \text{for } a_n = a_{n+1} = -1 \\
 y_2(t-nT_S) &= s(t-nT_S) - s(t-(n+1)T_S) \quad \text{for } a_n = 1 \text{ and } a_{n+1} = -1 \\
 y_3(t-nT_S) &= -s(t-nT_S) + s(t-(n+1)T_S) \quad \text{for } a_n = -1 \text{ and } a_{n+1} = 1 \\
 y_4(t-nT_S) &= s(t-nT_S) + s(t-(n+1)T_S) \quad \text{for } a_n = a_{n+1} = 1
 \end{aligned}
 \tag{2.8}$$

For the illustrative impulse sequence shown in Fig.2.1(c), with input symbols $a_0 = a_1 = 1$, the encoded SQAM signal, in the interval $[0, T_S]$, is given by :

$$\begin{aligned}
 y_4(t) &= s(t) + s(t-T_S) \\
 &= \left[\frac{1}{2}(1 + \cos \pi t/T_S) + d(t) \right] \\
 &\quad + \left[\frac{1}{2}(1 + \cos \pi (t-T_S)/T_S) + d(t-T_S) \right] \\
 &= 1 + 2d(t) \\
 &= A + (1-A)\cos 2\pi t/T_S
 \end{aligned}
 \tag{2.9}$$

In the interval $[T_S, 2T_S]$, with input symbols $a_1 = 1$ and $a_2 = -1$, the encoded SQAM signal is given by :

$$\begin{aligned}
 y_2(t-T_S) &= s(t-T_S) - s(t-2T_S) \\
 &= \left[\frac{1}{2}(1 + \cos \pi (t-T_S)/T_S) + d(t-T_S) \right] \\
 &\quad - \left[\frac{1}{2}(1 + \cos \pi (t-2T_S)/T_S) + d(t-2T_S) \right] \\
 &= -\cos \pi t/T_S
 \end{aligned}
 \tag{2.10}$$

In the interval $[2T_S, 3T_S]$, with input symbols $a_2 = -1$ and $a_3 = 1$, the encoded SQAM signal is given by :

$$\begin{aligned}
 y_3(t-2T_S) &= -s(t-2T_S) + s(t-3T_S) \\
 &= -\left[\frac{1}{2}(1 + \cos \pi(t-2T_S)/T_S) + d(t-2T_S)\right] \\
 &\quad + \left[\frac{1}{2}(1 + \cos \pi(t-3T_S)/T_S) + d(t-3T_S)\right] \\
 &= \cos \pi t/T_S \qquad (2.11)
 \end{aligned}$$

Applying the same concept with input symbols $a_n = a_{n+1} = -1$, the encoded signal is given by :

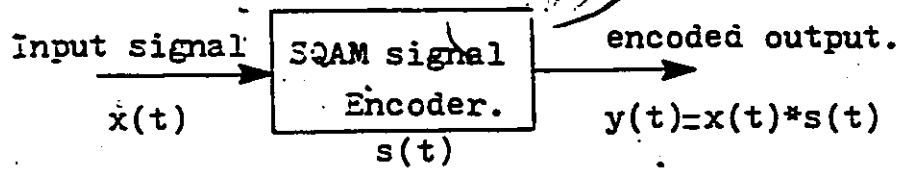
$$\begin{aligned}
 y_1(t-nT_S) &= -s(t-nT_S) - s(t-(n+1)T_S) \\
 &= -1 - 2d(t) \\
 &= -A - (1-A) \cos 2\pi t/T_S \qquad (2.12)
 \end{aligned}$$

and also

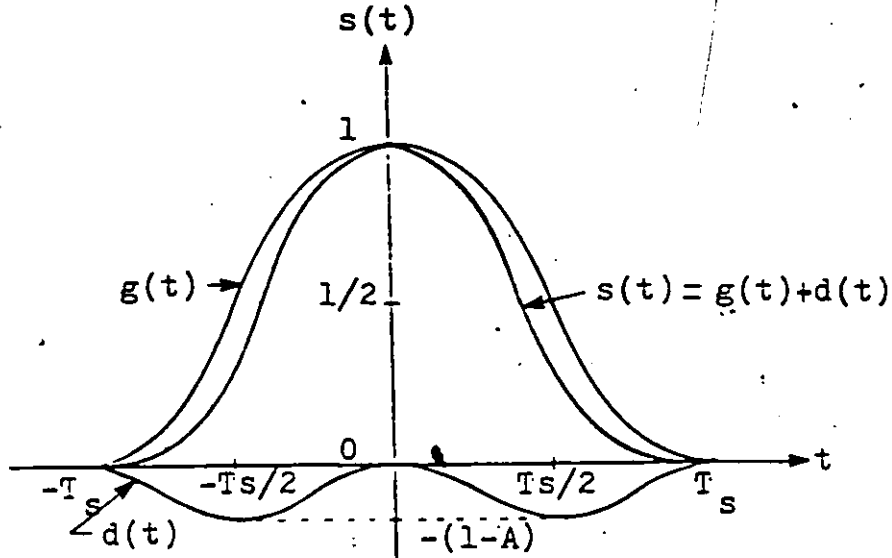
$$y_4(t-nT_S) = -y_1(t-nT_S) \qquad (2.13)$$

$$y_3(t-nT_S) = -y_2(t-nT_S) \qquad (2.14)$$

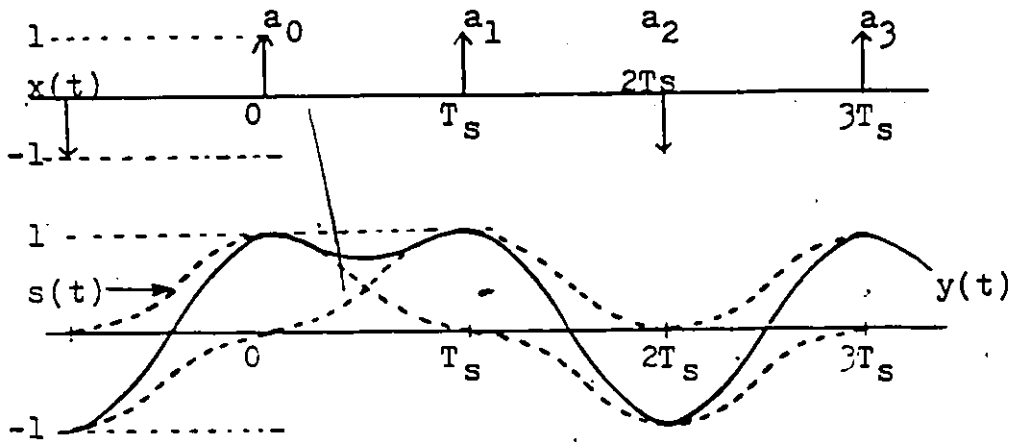
Thus, the pulse overlapped SQAM signal, in any signaling interval, is a function of two consecutive input symbols, a_n and a_{n+1} .



(a) SQAM signal encoder having an impulse response $s(t)$.



(b) An example of SQAM double-interval pulse.



(c) SQAM signal encoding process using pulse overlapping concept.

Fig.2.1. SQAM signal encoder using double-interval pulse overlapping concept.

2.1.2 SQAM Signal Encoder Using the NLSF Technique.

In this section, the SQAM baseband signal encoder, using the nonlinear switching filter (NLSF) technique [5,10], is described. We have defined four SQAM encoded signals in the $0 \leq t \leq T_s$ interval in (2.9) ... (2.12). (See Table 2.1.) Fig.2.2 shows the encoded SQAM signal eye pattern using the NLSF technique. For each consecutive T_s symbol interval, one of these signals is switched to the transmission system. The required switching function is achieved in the channel multiplex (MUX) unit, which is controlled by a logic control unit. The selection of the $y_1(t-nT_s) \dots y_4(t-nT_s)$ signal states depends upon the states of two consecutive input symbols. In Fig.2.3, the corresponding hardware block diagram is shown, while in Fig.2.4 the detailed circuit diagram of the SQAM baseband signal processor is shown. In Fig.2.4, U1 ... U7 consist a logic control unit, which provides 2 bit control signals to a 4 channel MUX(U10). A monostable multivibrator(U6) compensates the time delay caused by the logic control unit. Using a 128kHz input clock pulse, U8,9 generate 64kHz sine(or cosine) components $y_2(t)$ and $y_3(t)$. (See Fig.2.2.) U13,14 generate weighted and d.c biased (i.e., $0.5 \leq A \leq 1.5$) 128kHz sine components $y_1(t)$ and $y_4(t)$. U12 compensates a time delay between the output components $y_1(t) \dots y_4(t)$. Fig.2.5 illustrates the measured waveshape and eye pattern of the SQAM signal.

Table 2.1 Encoded SQAM output signals.

NRZ input data		SQAM output signal
a_{n+1}	a_n	$y(t)$
-1	-1	$y_1(t)$
-1	1	$y_2(t)$
1	-1	$y_3(t)$
1	1	$y_4(t)$

SQAM output signals $y_1(t)$ to $y_4(t)$ are defined as follows.

$$y_1(t) = -A - (1-A) \cos(2\pi t/T_S)$$

$$y_2(t) = -\cos(\pi t/T_S)$$

$$y_3(t) = \cos(\pi t/T_S)$$

$$y_4(t) = A + (1-A) \cos(2\pi t/T_S)$$

where

$$0.5 \leq A \leq 1.5$$

$$0 \leq t \leq T_S$$

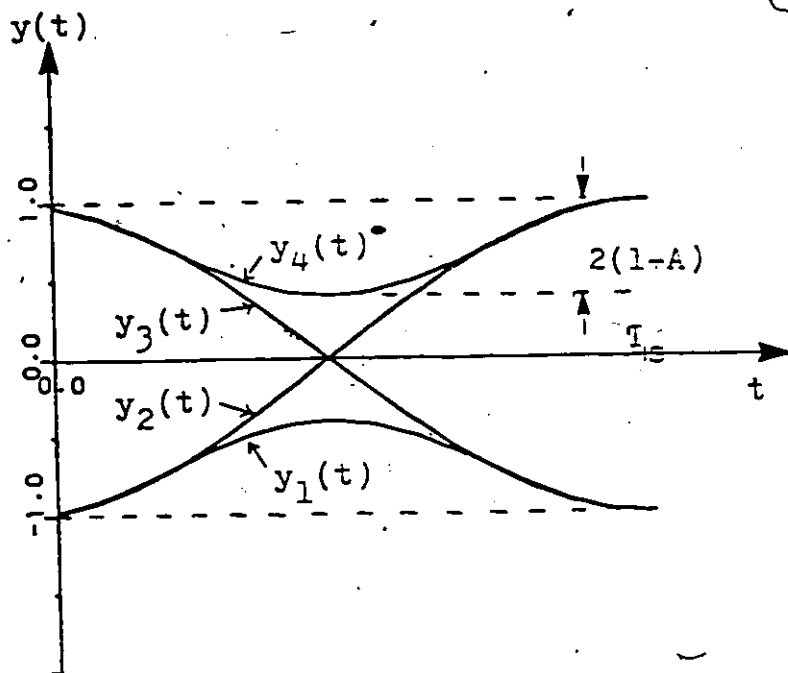


Fig.2.2 Encoded SQAM output signal eye pattern using the NLSF technique.

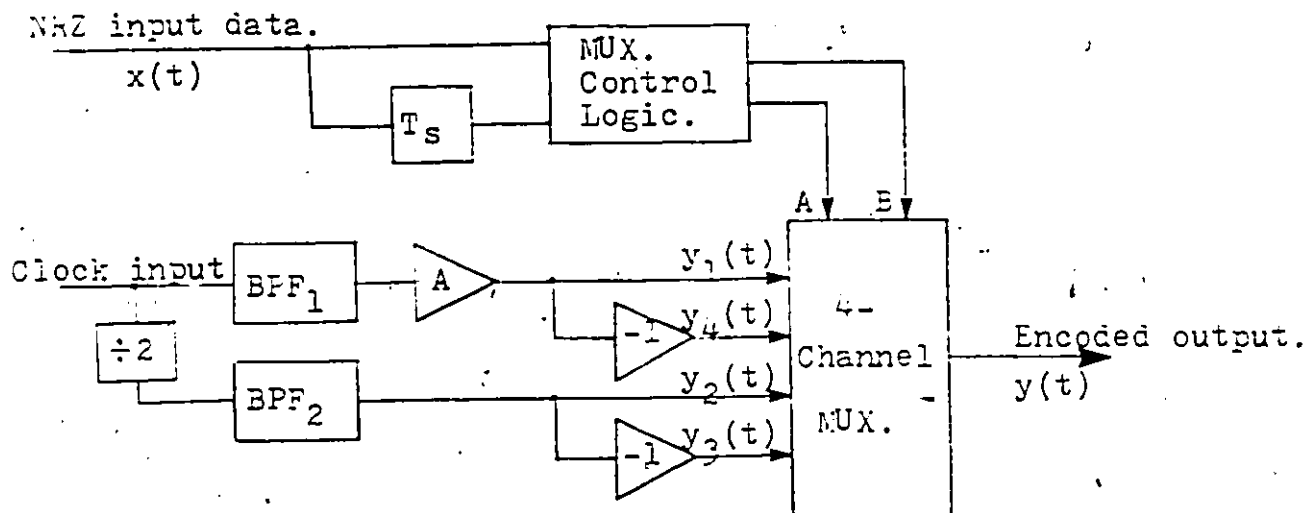


Fig.2.3 Block diagram of SQAM signal encoder using the NLSF technique.

DATE July 1983
 DESSINE ORGC BY J.S. Seo
 VÉRIFIÉ CMKD BY

SUJET SUBJECT
 SQAM Baseband Signal Processor.

FEUILLE SHEET 1 DE OF 2
 NO REF. JOB NO.
 ECHELLE SCALE

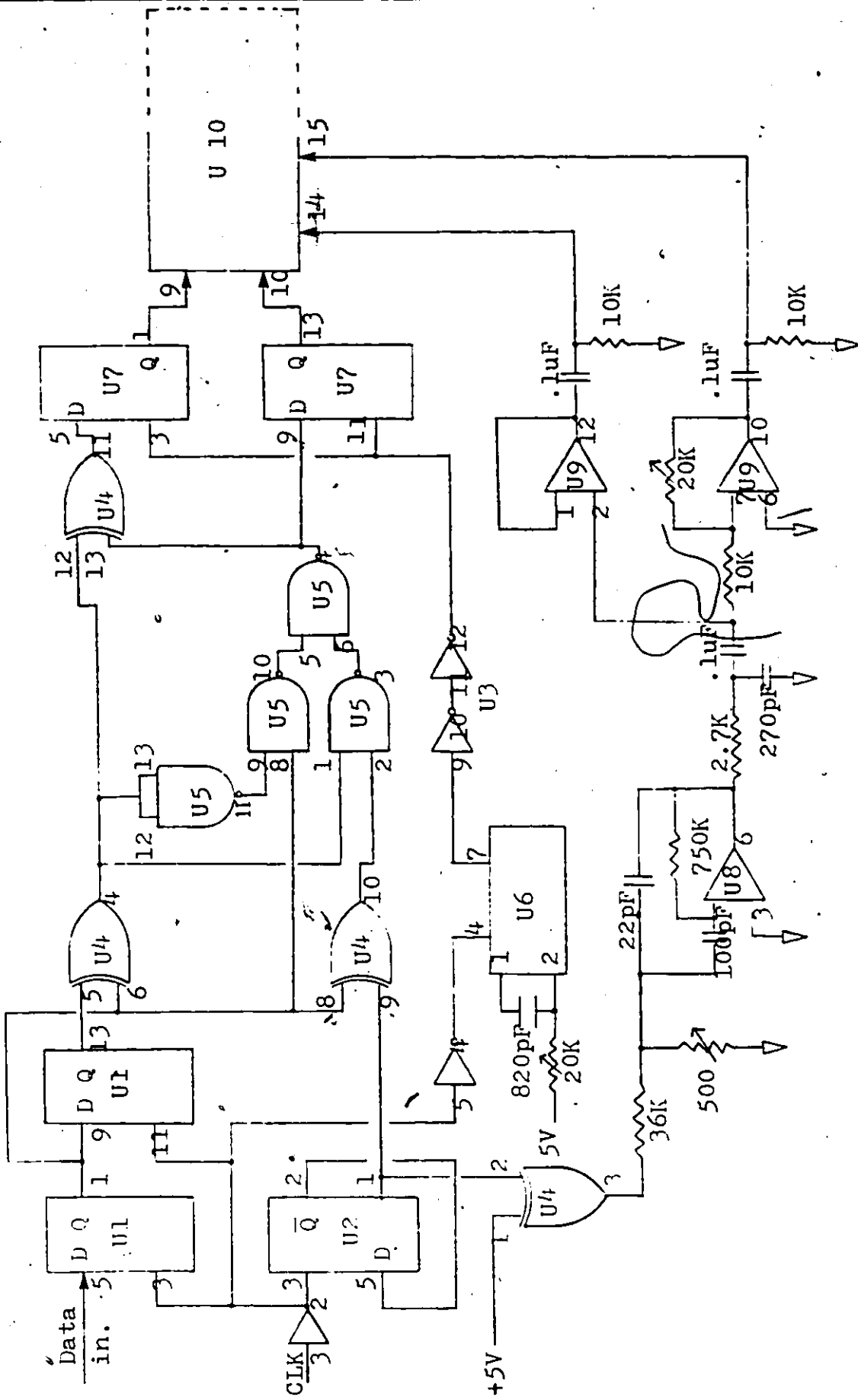


Fig.2.4 Circuit diagram of SQAM baseband signal processor based on the NLSF concept. [1,5]

DATE July 1983	SUJET SQUAM Baseband Signal Processor.	FEUILLE 2 DE 2
DESSINE ORRG BY J.S. Seo		NO REF. JOB NC
VERIFIE CAKD BY		ECHELLE SCALE

★ Legend

Part No.	Spec.
U1,2,7	CD4013
U3	CD4049
U4	CD4070
U5	CD4011
U6,12	CD4098
U8,11,13	CA3100
U9	uA 747
U10	CD4052
U14	uA4136

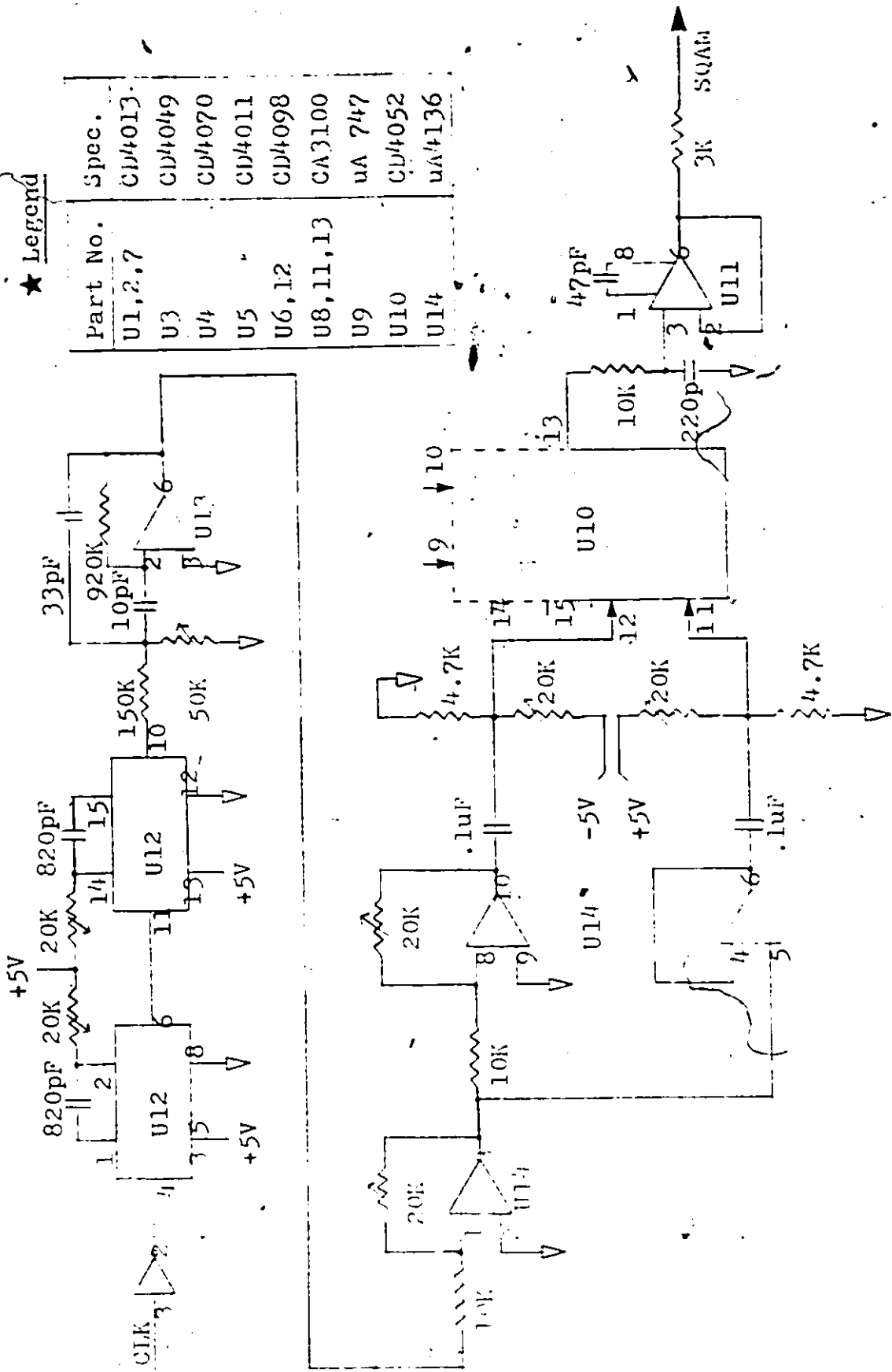
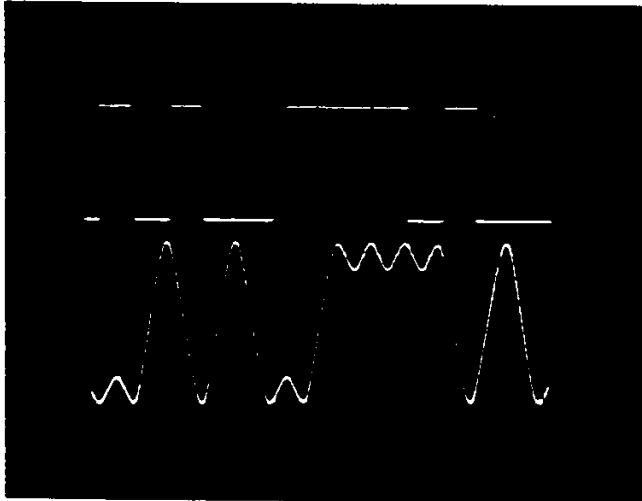
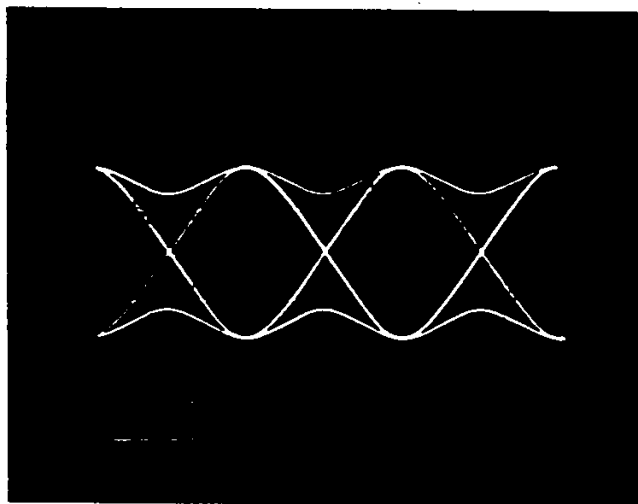


FIG. 2.4 Circuit diagram of SQUAM baseband signal processor.



{ Vert. : 2.5 volt/div.
 { Hori. : 10.4 us./div.

(a). Measured wavelshape.(I-channel)



{ Vert. : 2.5 volt/div.
 { Hori. : 2.2 us. /div.

(b). Measured eye pattern. (I-channel)

Fig.2.5 Measured baseband wavelshape and eye pattern of
 a $f_s = 64$ kbaud SQAM signal.(Q-channel eye pattern
 is identical to I-channel.)
 Amplitude parameter, $A = 0.6$.

Note the IJF condition is fully satisfied.

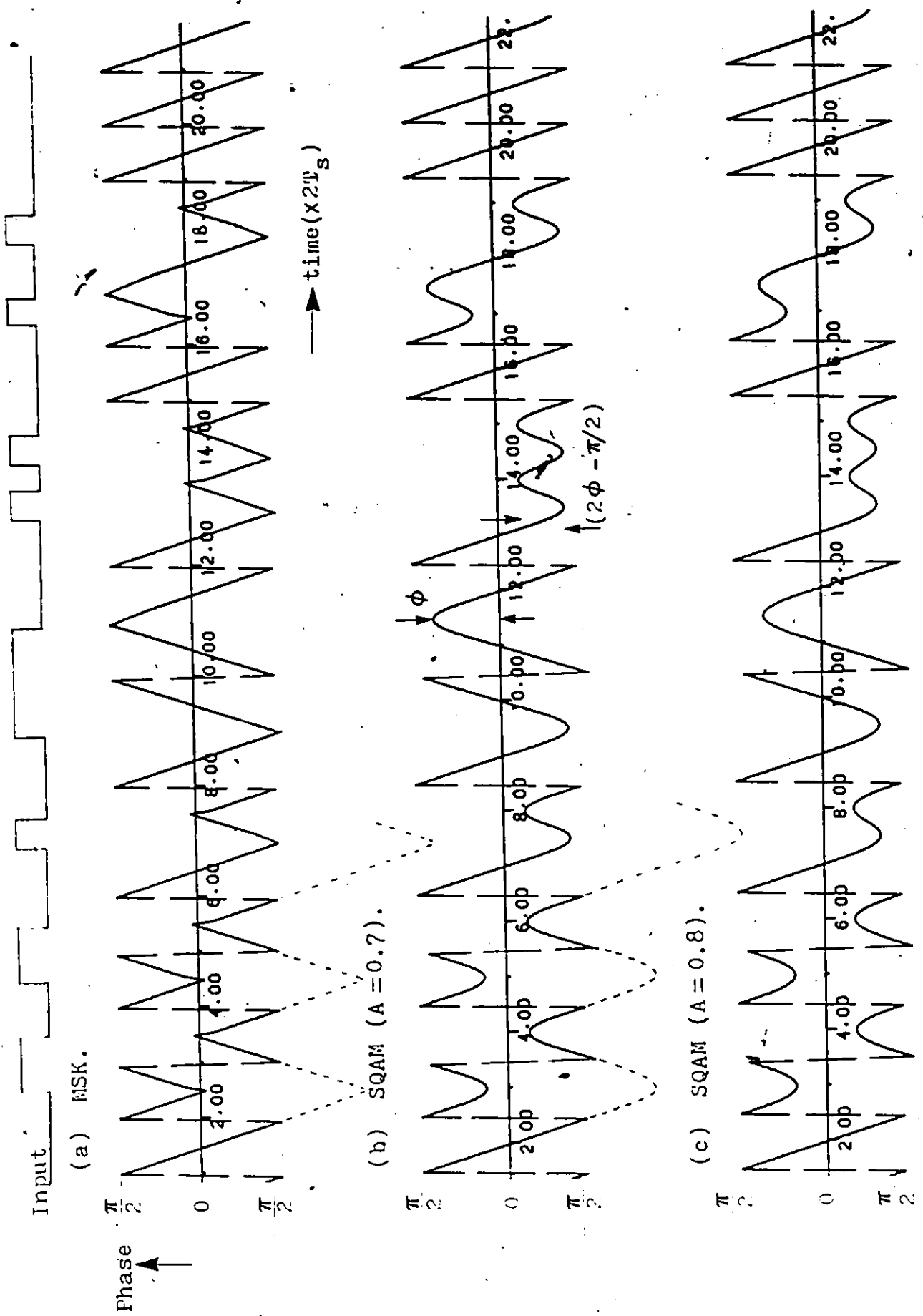
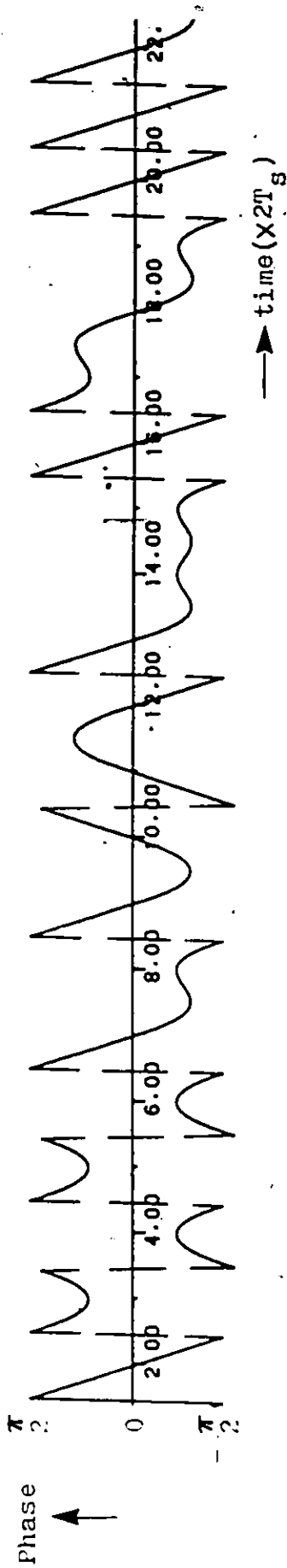
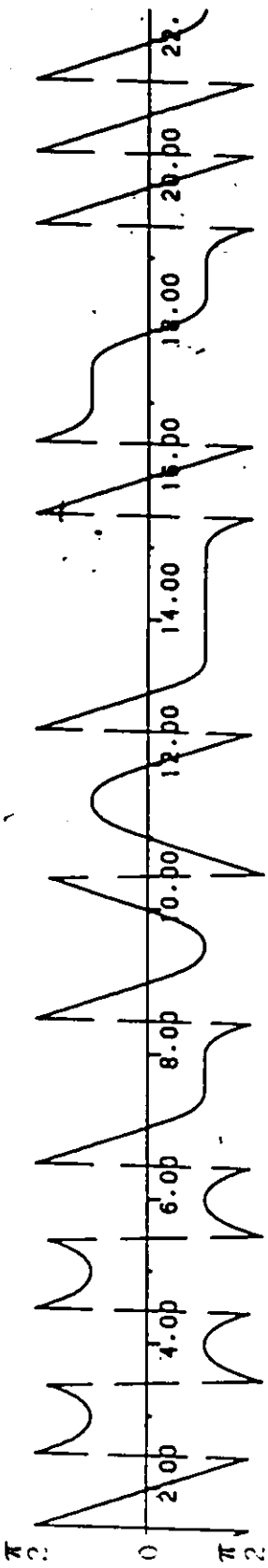


Fig.2.6 Phase transitions of MSK, SQAM and IJF-OQPSK(A=1.0).

(d) SQAM (A=0.9)



(e) SQAM (A=1.0, IJF-OQPSK)



(f) SQAM (A=1.1)

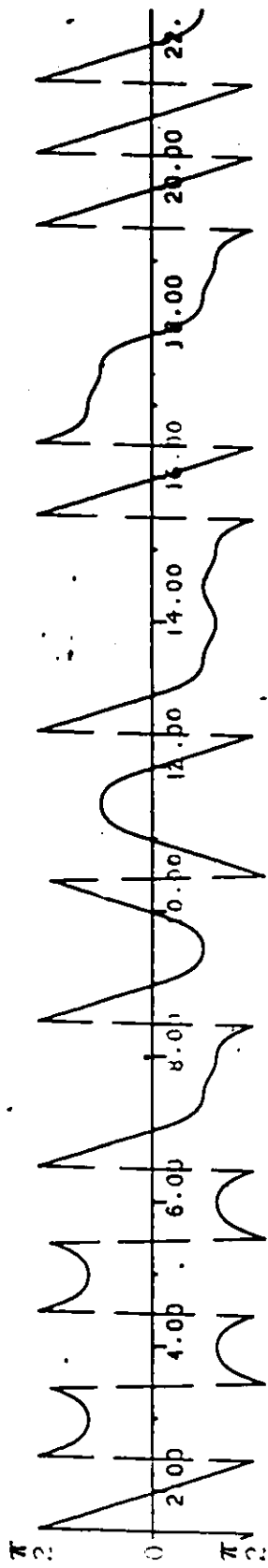


Fig.2.6 Phase transitions of MSK, SQAM and IJF-OQPSK (A=1.0).

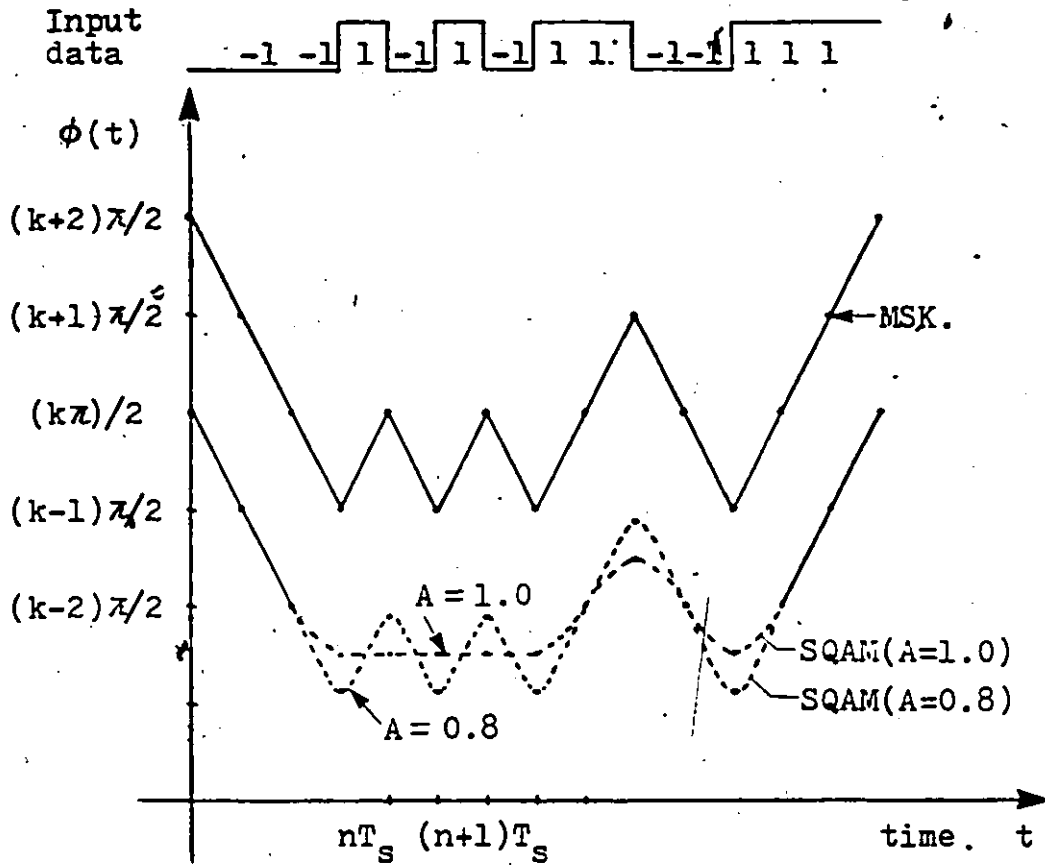


Fig.2.6(g) Phase transitions of MSK and SQAM(A=0.8 and 1.0).

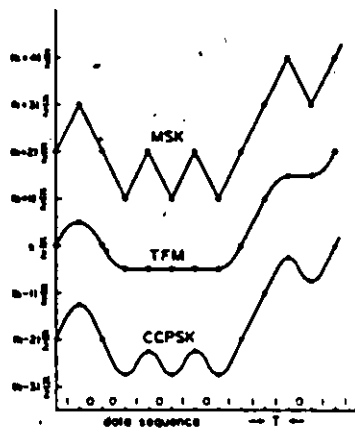


Fig.2.6(h) Phase transitions of MSK, TFM and CCPSK.

2.3 SPECTRAL ANALYSIS OF SQAM SIGNALS.

In this section , the power spectral density (PSD) of SQAM signals is derived and compared with the PSD of some other well-known signals. The PSD function of the SQAM signal is derived by using the Impulse method [20] and the Fourier transforms of the SQAM double-interval pulse. From (2.3) and (2.4) , the SQAM double-interval pulse is expressed as :

$$s(t) = g(t) + d(t) \quad (2.15)$$

where

$$g(t) = \frac{1}{2}(1 + \cos \pi t/T_s) \quad (2.16)$$

The frequency spectrum of the SQAM signal is :

$$S(f) = G(f) + D(f) \quad (2.17)$$

where $S(f)$, $G(f)$ and $D(f)$ are Fourier transforms of $s(t)$, $g(t)$ and $d(t)$ respectively, and are readily obtained as :

$$G(f) = F[g(t)] = \frac{T_s}{1-4T_s^2 f^2} \cdot \frac{\sin 2\pi f T_s}{2\pi f T_s} \quad (2.18)$$

and

$$D(f) = F[d(t)] = \frac{(A-1)T_s}{1-T_s^2 f^2} \cdot \frac{\sin 2\pi f T_s}{2\pi f T_s} \quad (2.19)$$

Therefore

$$S(f) = T_S \left(\frac{1}{1-4T_S^2 f^2} + \frac{A-1}{1-T_S^2 f^2} \right) \frac{\sin 2\pi f T_S}{2\pi f T_S} \quad (2.20)$$

and

$$S(0) = AT_S \quad (2.21)$$

Thus, the normalized PSD function of the SQAM signal $s(t)$ is given by :

$$\left| \frac{S(f)}{S(0)} \right|^2 = \frac{1}{A^2} \left(\frac{1}{1-4T_S^2 f^2} + \frac{A-1}{1-T_S^2 f^2} \right) \left(\frac{\sin 2\pi f T_S}{2\pi f T_S} \right)^2 \quad (2.22)$$

(See Appendix A. for the detailed derivation of eq.(2.22).)

Fig.2.7 shows the computed power spectra of equiprobable random SQAM baseband signals for different values of the amplitude parameter 'A'. We note that a decrease of 'A' leads to a faster spectral roll-off at higher frequencies, but at the expense of a wider main-lobe. Depending on particular system applications, desirable SQAM signals may be selected, based on the trade-off between the main-lobe occupancy and side-lobe roll-off. In Figs.2.8(a) ... (c), the power spectra of SQAM signals are compared with those of

other constant envelope modulation schemes, such as MSK and TFM, for linear and nonlinear channels [1,3,10]. The detailed computer simulation program is listed in Appendix C. From the results, we note that the SQAM signals have significant spectral advantages over QPSK and MSK signals, and comparable spectral properties to TFM signals. (The spectral region of practical interest is between 0 dB and -35 dB for most applications.) Figs.2.9(a) ... (c) show measured power spectra of the SQAM signals with amplitude parameters $A = 0.8, 0.9$ and 1.0 in a linear channel. In this experiment, we used a random 128 kb/s equiprobable NRZ signal. The experimental, computer simulation and theoretical results indicate a close agreement. We note that the SQAM signal, designated with $A=1.0$, is identical with the conventional overlapped raised-cosine (QORC) signal and also the IJF-QPSK (subclass $n=1$) signal.[1,6].

SQAM POWER SPECTRUM

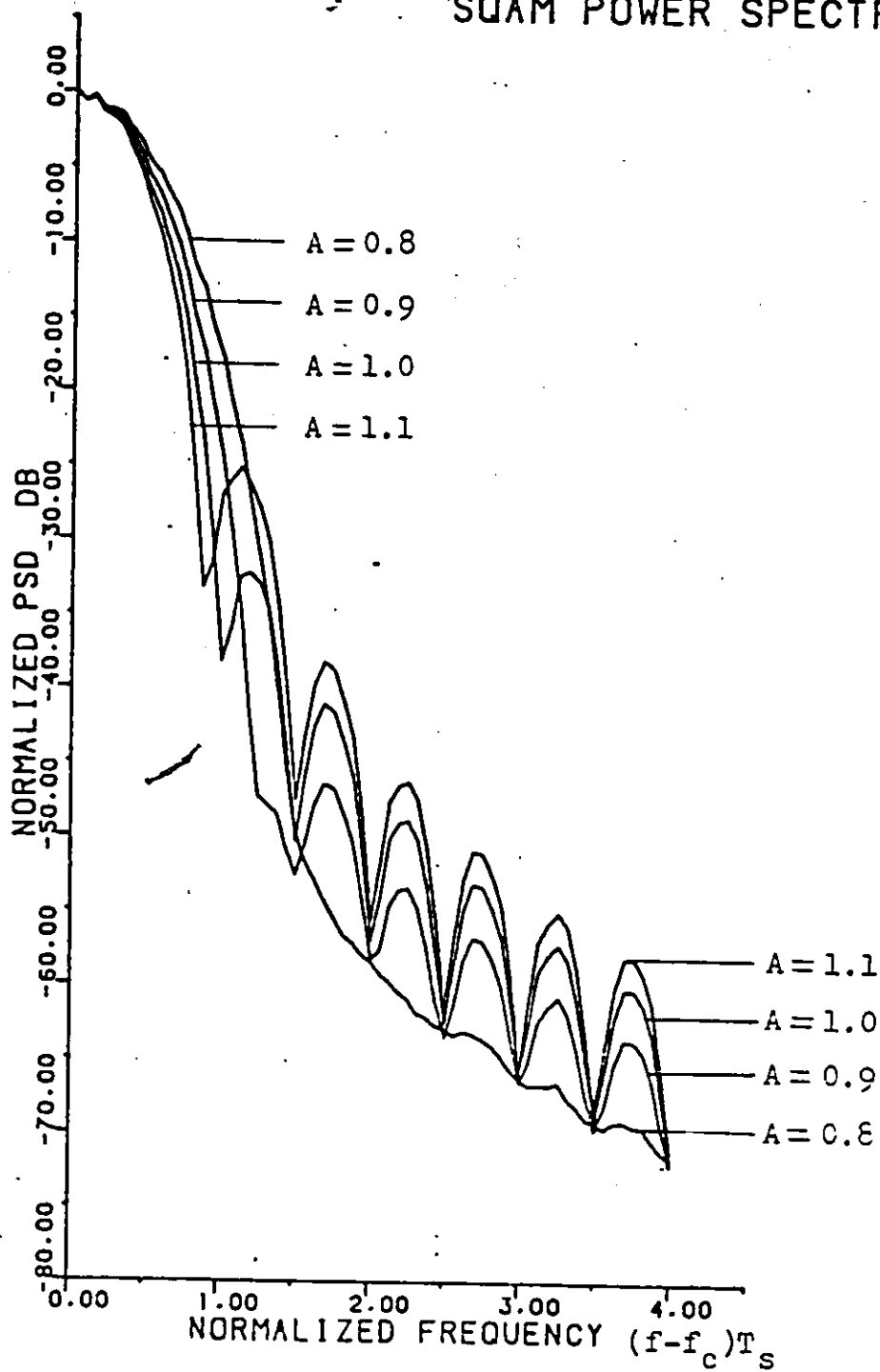


Fig.2.7. Normalized power spectral densities of SQAM signals in a linear channel.(computations based on equation (2.22).)

SQAM POWER SPECTRUM

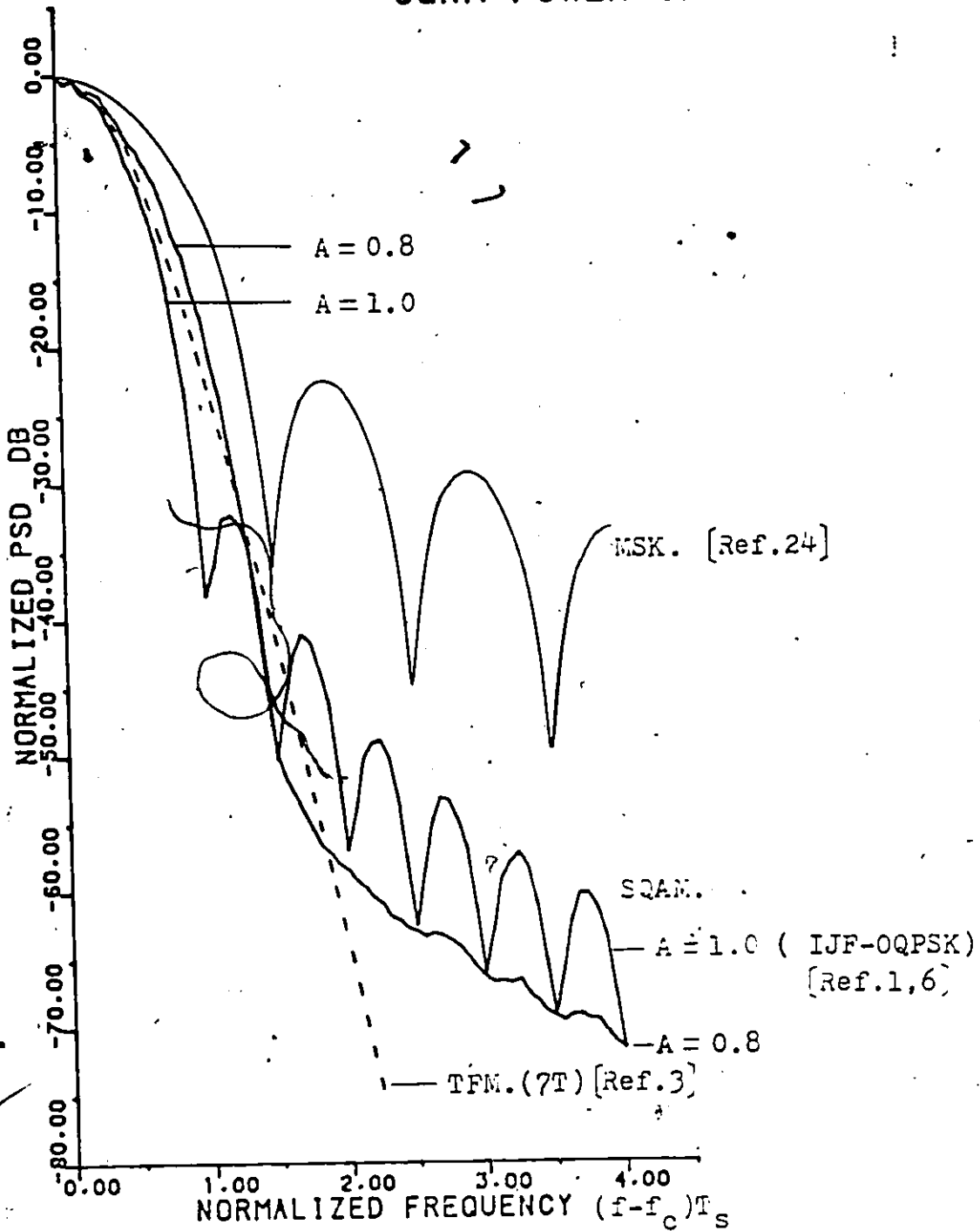


Fig.2.8(a). Power spectra of SQAM, MSK and TFM signals in a linear channel. (The $A=1.0$ case is identical to IJF-QQPSK($n=1$) described in [1,11] or QORC [6].)

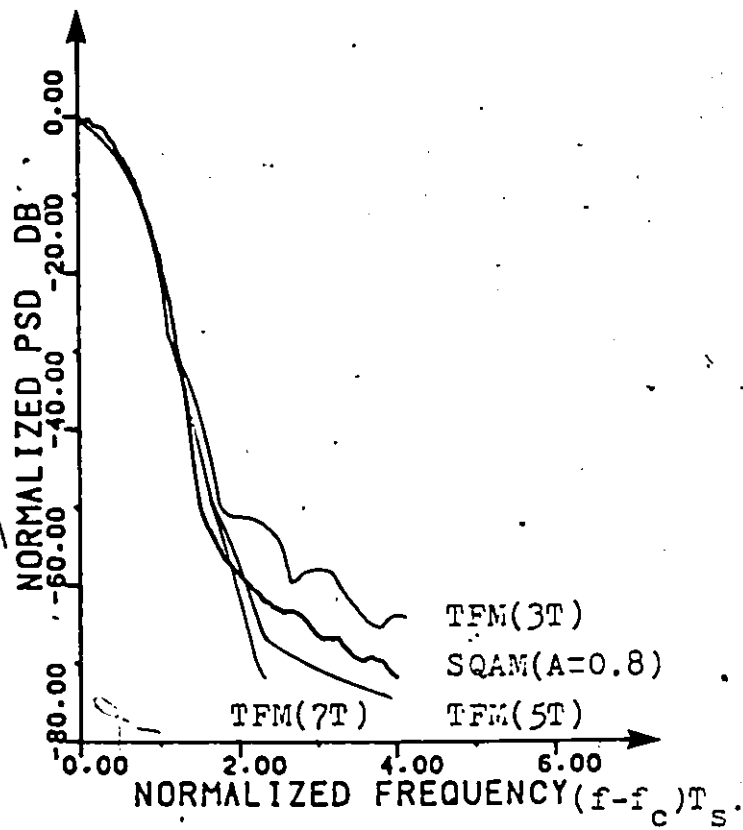


Fig.2.8(b). Power spectra of SQAM and TFM(with truncation length 3T, 5T and 7T) in a linear channel.

SQAM POWER SPECTRUM

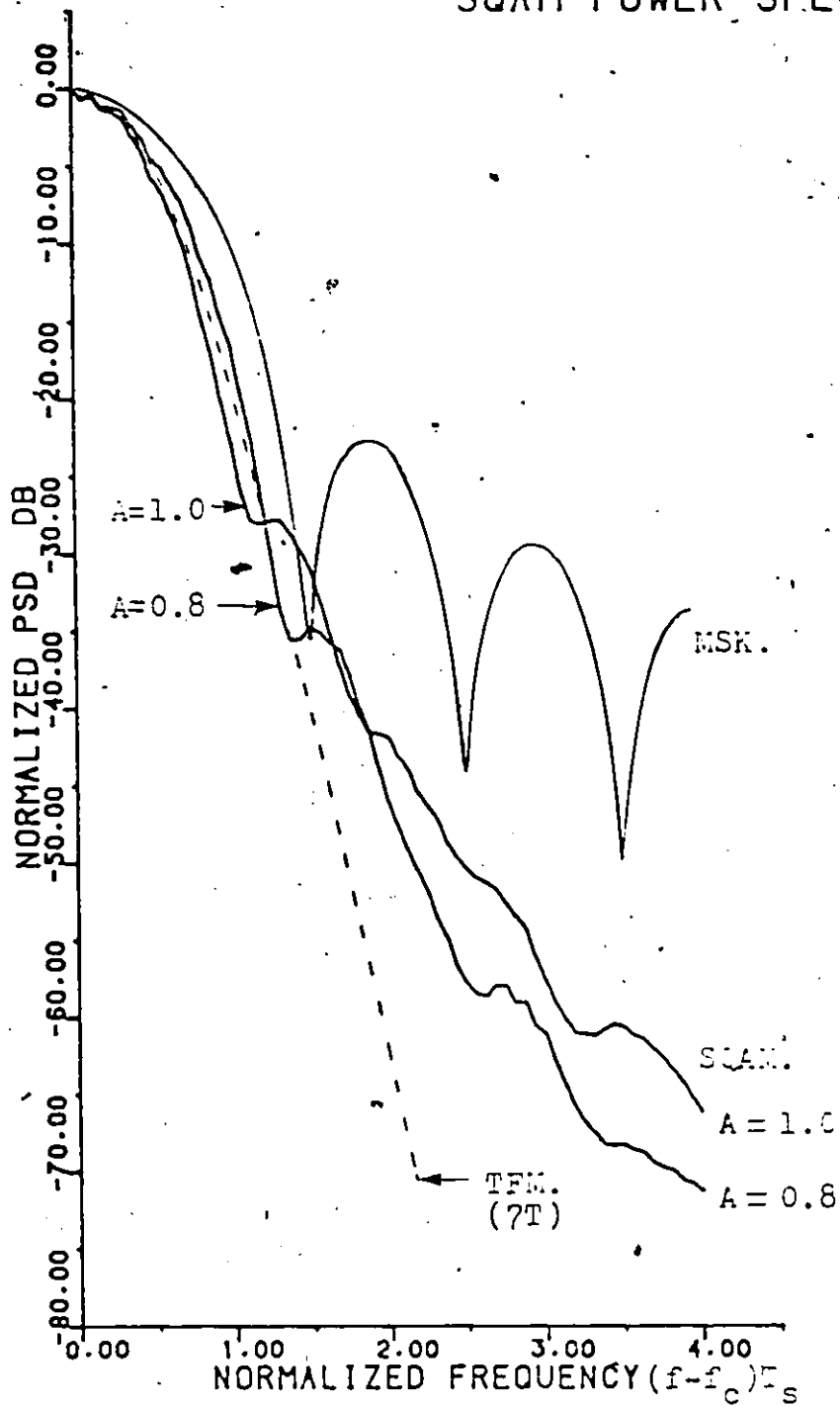
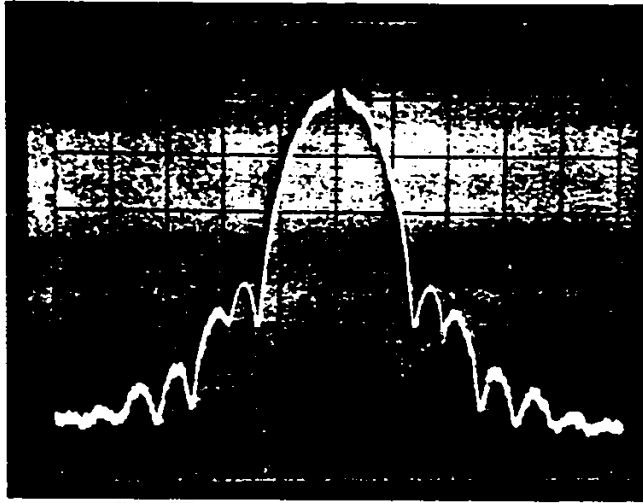
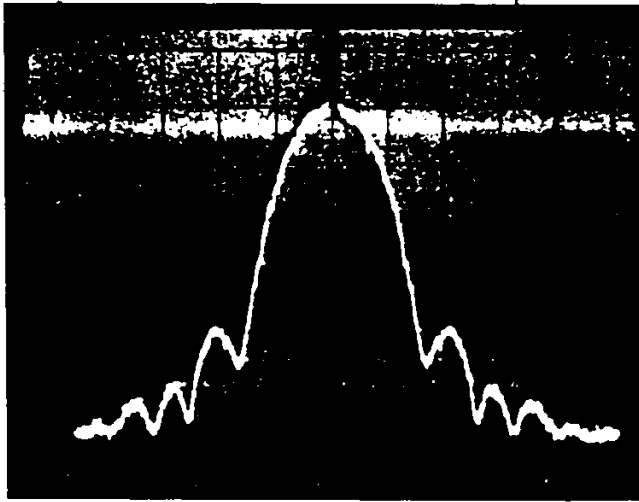


Fig.2.8(c). Power spectra of SQAM, MSK and TFM signals in a nonlinear (hardlimited) channel.

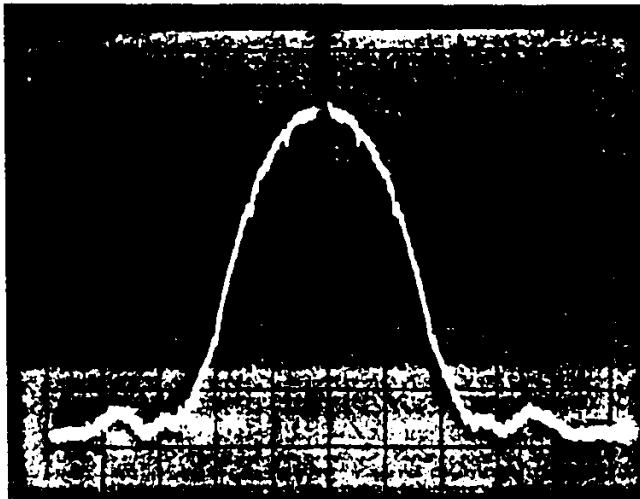


Vert. : 10dB/div.
Hori. : 50kHz/div.

(a) $A=1.0$



(b) $A=0.9$



(c) $A=0.8$

Fig.2.9. Measured power spectra of $f_s=64\text{kHz}$ ($f_b=128\text{kHz}$) SQAM signals in a linear channel.

A useful measure of a spectral compactness can be obtained from the fractional out-of-band power P_{ob} , defined as :

$$P_{ob} = 1 - \left[\int_{-B}^B S'(f) df / \int_{-\infty}^{\infty} S'(f) df \right] \quad (2.23)$$

where

$$S'(f) = \left| \frac{S(f)}{S(0)} \right|^2 \quad (2.24)$$

and B is a channel bandwidth normalized to the data symbol rate (i.e., $(f-f_c)/f_s$). Figs.2.10(a) and (b) show the computed out-of-band to total power ratios of SQAM and MSK signals for linear and nonlinear channels. It is noticed that SQAM signals have a sharper spectral roll-off and lower out-of-band energy, compared to MSK signal. Also note that in the SQAM system, for normalized frequencies $(f-f_c)T_s > 1.0$, the out-of-band energy for $A < 1.0$ is lower than that for $A \geq 1.0$.

SQAM POWER SPECTRUM

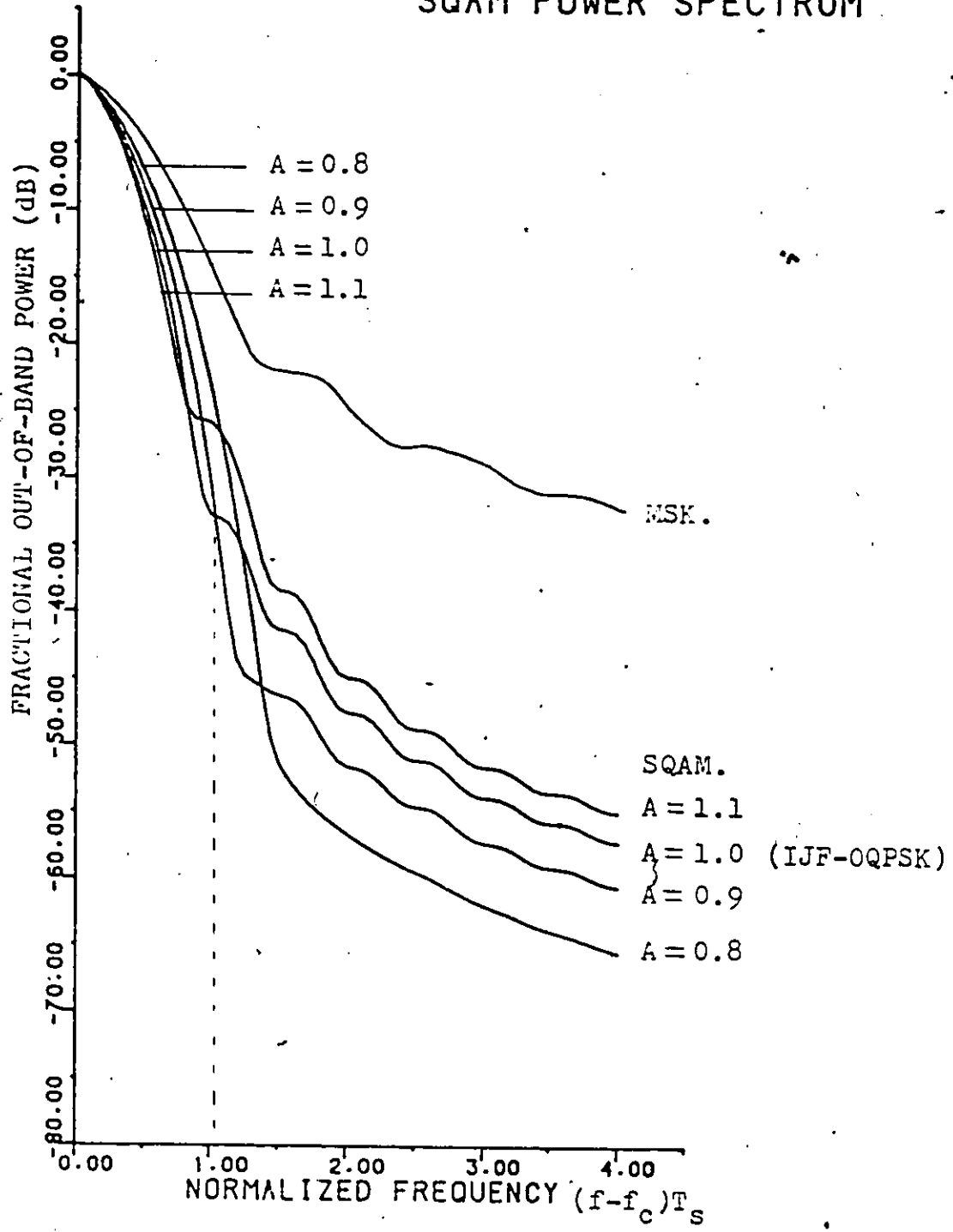


Fig.2.10(a). Out-of-band to total power ratios of SQAM and MSK signals in a linear channel.

SQAM POWER SPECTRUM

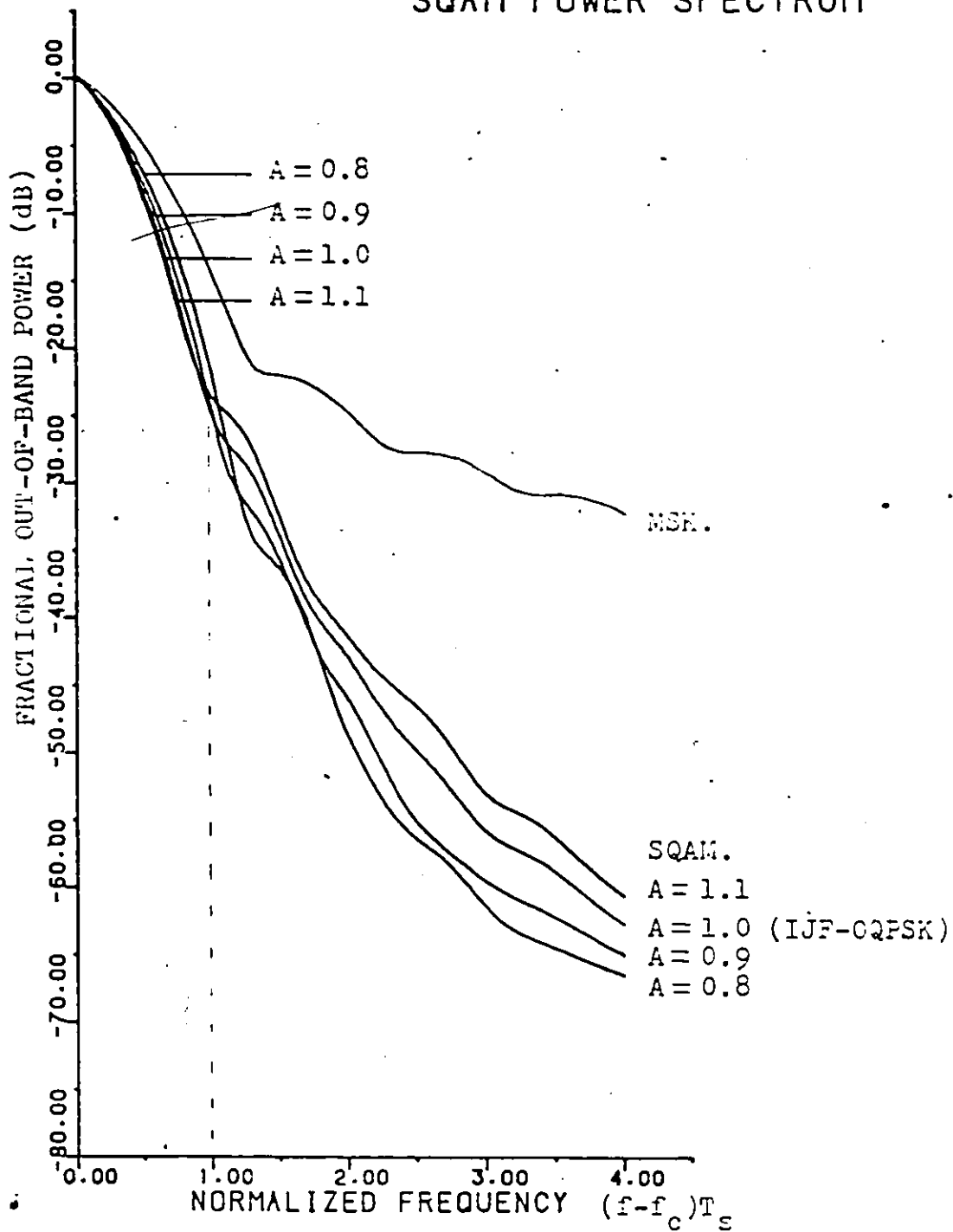


Fig.2.10(b). Out-of-band to total power ratios of SQAM and MSK signals in a nonlinear (hardlimited) channel.

Chapter III

PERFORMANCE OF SQAM IN AWGN SINGLE-CHANNEL ENVIRONMENT

3.1 SQAM MODEM

The block diagram of a SQAM modem is shown in Fig.3.1. The SQAM modulator consists of SQAM signal encoders and a conventional Offset-QPSK modulator structure. For this modulator, we do not require additional spectral shaping filters. Two encoded (i.e., in-phase and quadrature) SQAM baseband signals $y_{I_m}(t)$ and $y_{Q_m}(t)$ are quadrature-modulated. The modulated SQAM signals, prior to the hardlimiter, can be expressed as :

$$\begin{aligned} z(t) &= y_{I_m}(t) \cos \omega_c t + y_{Q_m}(t) \sin \omega_c t \\ &= E_m(t) \cos[\omega_c t + \phi_m(t)] \end{aligned} \quad (3.1)$$

where $E_m(t)$ and $\phi_m(t)$ are the envelope and phase of the SQAM quadrature-modulated signals, that is,

$$E_m(t) = [y_{I_m}^2(t) + y_{Q_m}^2(t)]^{1/2} \quad (3.2)$$

and

$$\phi_m(t) = - \tan^{-1} \frac{y_{Qm}(t)}{y_{Im}(t)} \quad (3.3)$$

The SQAM demodulator is the same as a conventional OQPSK demodulator. In our computer simulation and experimental set-up, we used fourth-order Butterworth low pass filters (LPF) at the demodulator. (As we found that a 4th order Butterworth LPF yields the best P(e) performance in a single-channel environment.) For the nonlinearly amplified SQAM modem, an ideal hardlimiter presents a good first-order approximation to the saturated HPA.[1,10]. Note that the hardlimited SQAM signal $z'(t)$ has a constant envelope.

As the SQAM modem operates with an offset (staggered) logic (i.e., a $T_b = T_s/2$ delay-line is inserted in the Q-channel), we obtain the following 16 combinations for the I and Q-channel output signals :

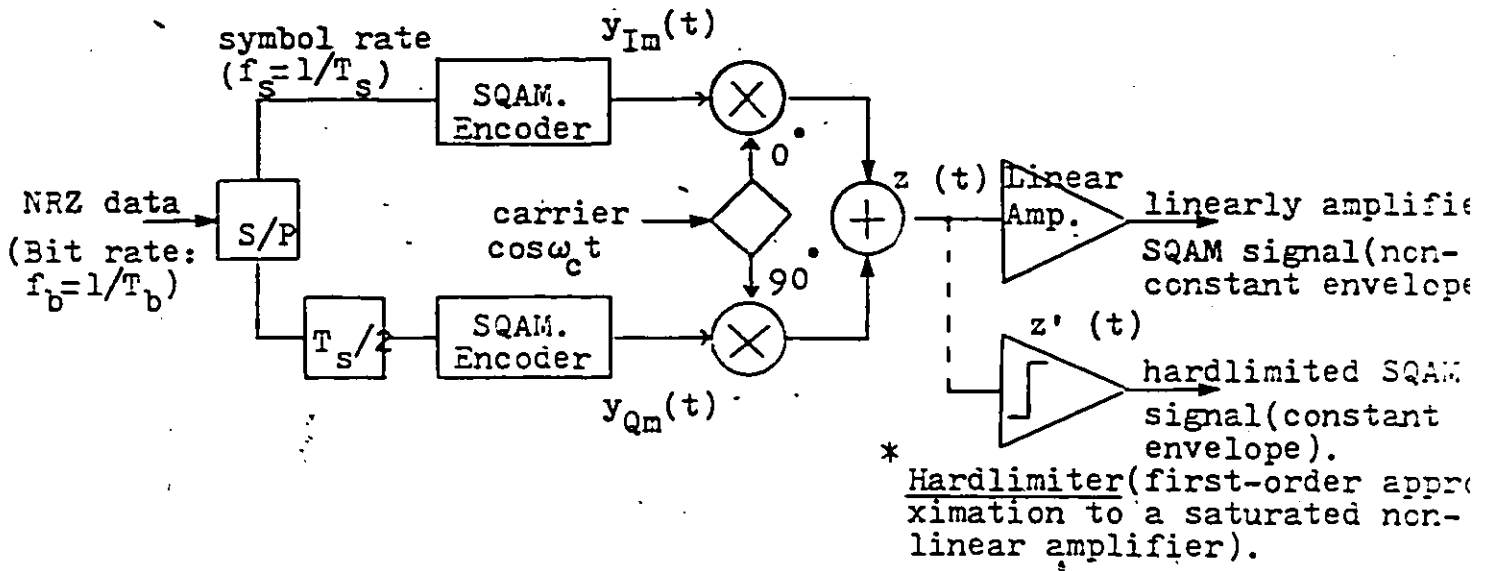
I-Channel Output Signals	Q-Channel Output Signals
$\pm y_1(t - nT_s)$	$\pm y_1(t - T_s/2 - nT_s)$
$\pm y_1(t - nT_s)$	$\pm y_2(t - T_s/2 - nT_s)$
$\pm y_2(t - nT_s)$	$\pm y_1(t - T_s/2 - nT_s)$
$\pm y_2(t - nT_s)$	$\pm y_2(t - T_s/2 - nT_s)$

where

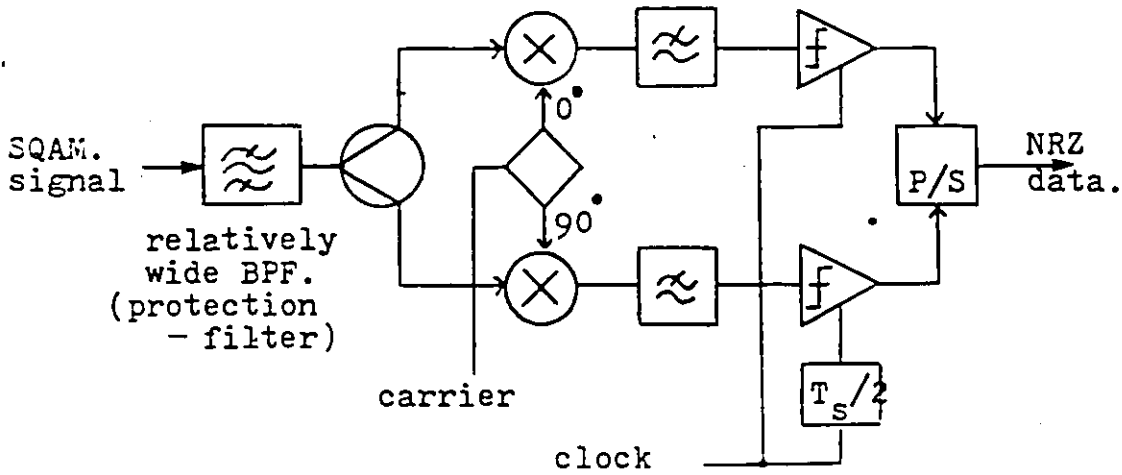
$$y_1(t - T_S/2 - nT_S) = -A + (1-A)\cos(2\pi t/T_S) \quad (3.4)$$

$$y_2(t - T_S/2 - nT_S) = -\sin(\pi t/T_S) \quad (3.5)$$

The value of the amplitude parameter A , in the I and Q -channel signals respectively, is selected to control the envelope fluctuations of the modulated signal. (However, the parameter A should be same for both the channels.) We note that the IJF- OQPSK signal described in [1,10,11] is a special case of the SQAM signals for $A=1.0$. An example of the SQAM signal encoding process, for the in-phase and quadrature baseband channels of the SQAM modulator, is illustrated in Fig.3.2.



(a). SQAM modulator.

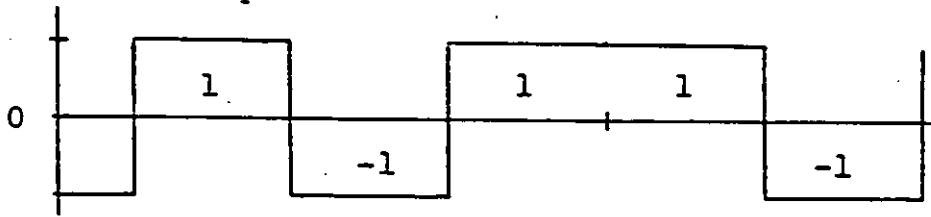


(b). SQAM demodulator.

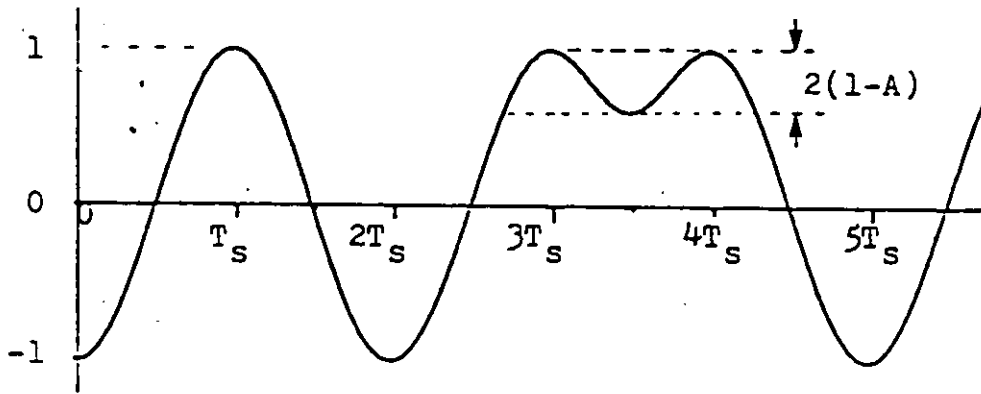
Fig.3.1 The block diagram of a SQAM modem.
(Both linearly amplified and hardlimited SQAM signal transmitters are illustrated.)

(a) I-channel.

NRZ input data.

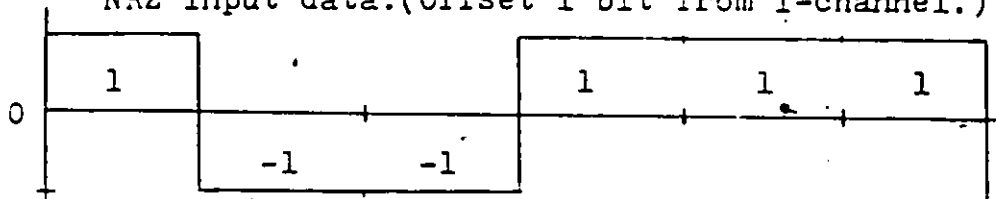


Encoded SQAM signal.



(b) Q-channel.

NRZ input data. (Offset 1 bit from I-channel.)



Encoded SQAM signal.

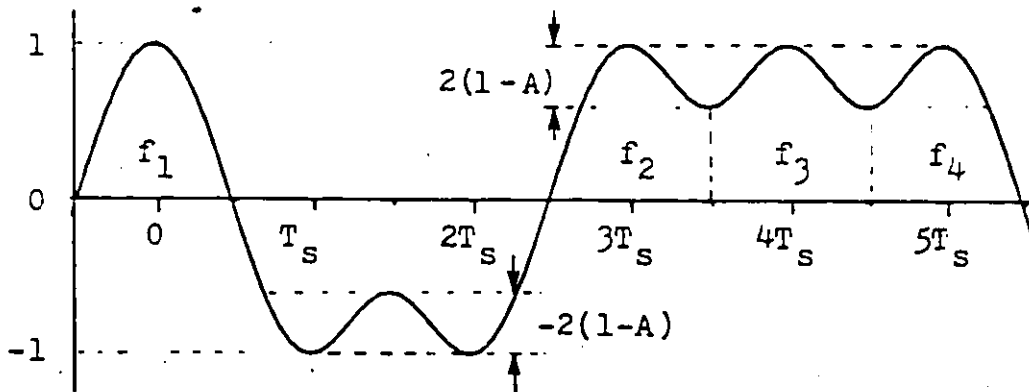


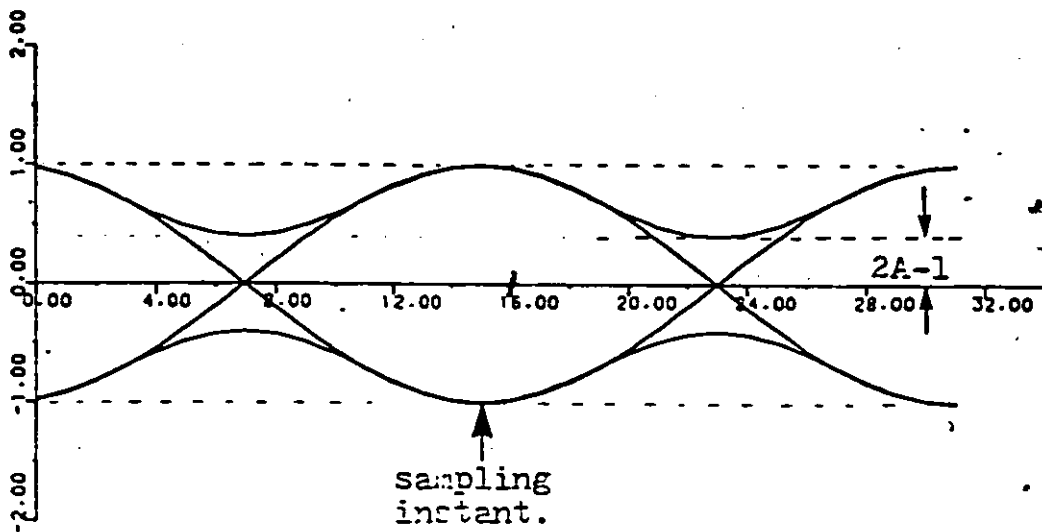
Fig.3.2 SQAM I and Q-channel signal encoding process.

3.2 EYE PATTERN, SPACE DIAGRAM AND ENVELOPE FLUCTUATION

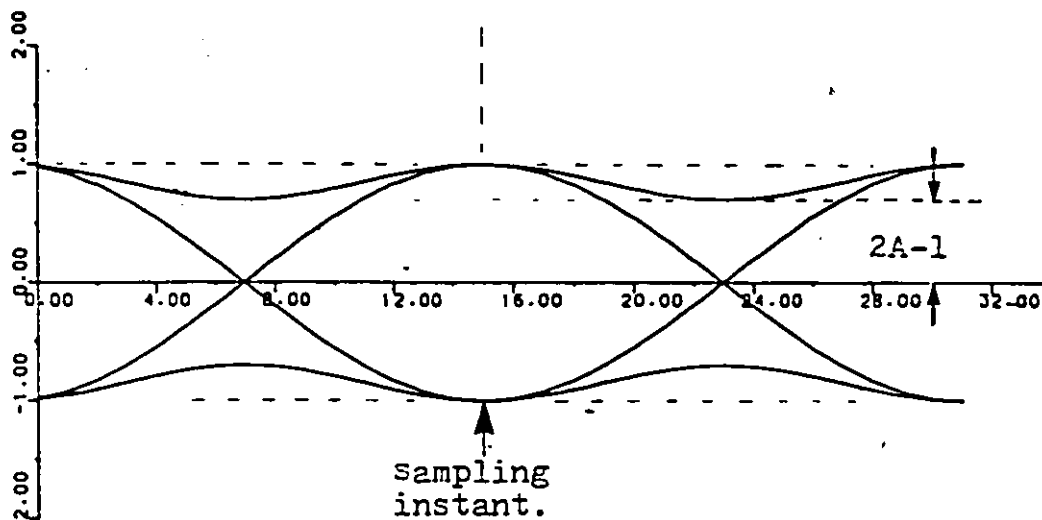
Fig.3.3 and 3.4 show the computer simulated eye patterns of the demodulated SQAM baseband signals with amplitude parameter $A=0.7$, 0.85 and 1.0 , for linear and nonlinear (hardlimited) channels. The eye patterns of these SQAM signals, for a linearly amplified case, indicate that the vertical eye opening (VEO), for different values of A , have full amplitudes at every sampling instant, thus the SQAM signals would suffer negligible intersymbol interference (ISI) and $P(e)$ performance degradation. In a nonlinearly amplified system, the VEO for $A < 1.0$ is wider than that for $A \geq 1.0$, hence we can expect that the $P(e)$ performance for $A < 1.0$ will be better than that for $A \geq 1.0$. (See also demodulated and filtered SQAM eye patterns in Fig.3.10 and 3.11.) Fig.3.5 shows the simulated signal space diagrams of the SQAM signals with amplitude parameters $A=0.7$, 0.85 and 1.0 . The maximum envelope fluctuations of the SQAM signals with amplitude parameters $A=0.7$ to 1.0 are shown in Table 3.1 and Fig.3.6. Note that the maximum envelope fluctuation changes from 0.7 dB (for $A=0.7$) to 3.0 dB (for $A=1.0$), depending on the amplitude parameter.

SQAM EYE DIAGRAM

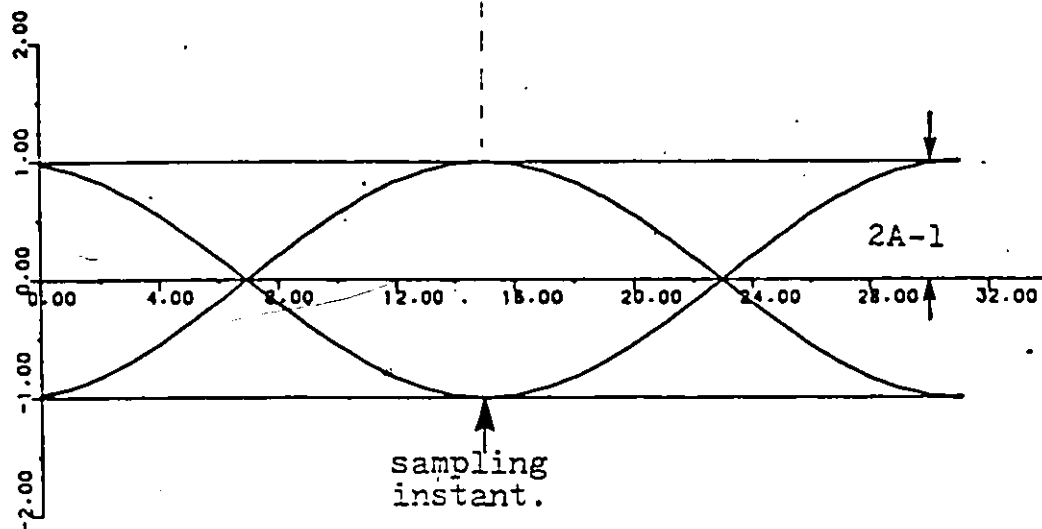
37 .



(a) $A = 0.7$



(b) $A = 0.85$

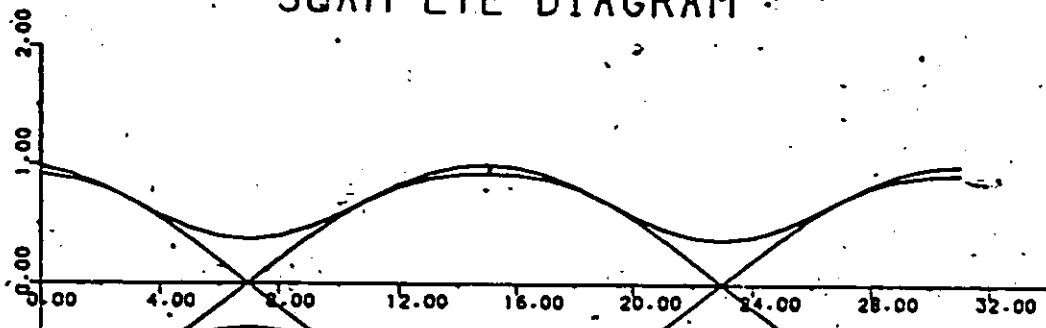


(c) $A = 1.0$

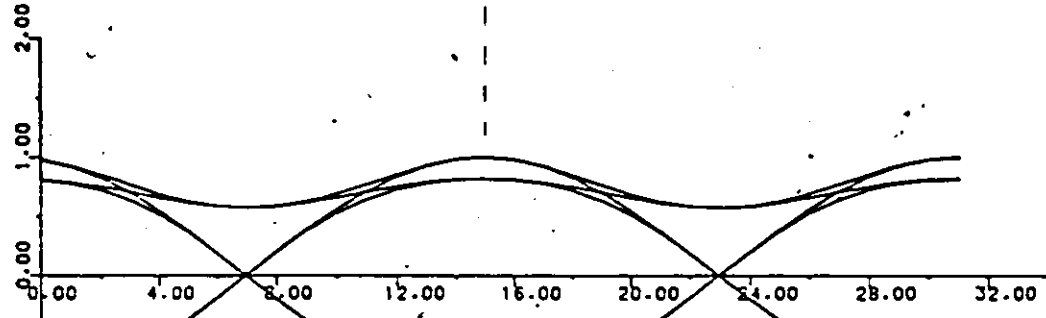
Fig. 3.3 Simulated eye patterns of the SQAM baseband signals for linear channel. Note: The $A=1.0$ case is the same as the IJF-QPSK [1,11] or the QORC [6].

SQAM EYE DIAGRAM

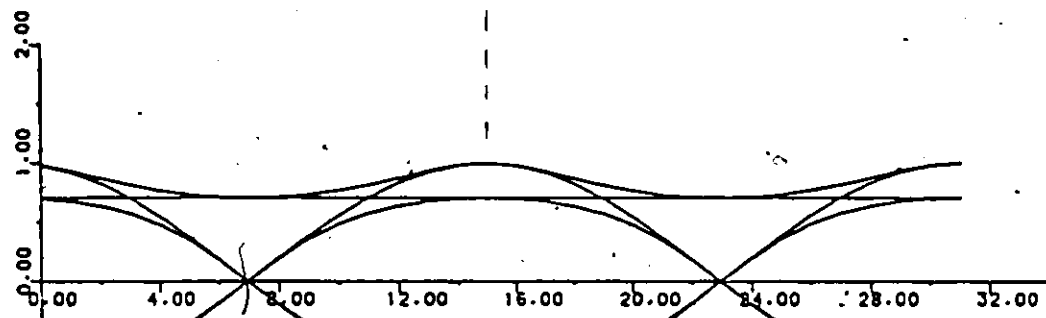
38



(a) $A = 0.7$



(b) $A = 0.85$



(c) $A = 1.0$

Fig.3.4 Simulated eye patterns of the SQAM baseband signals for hardlimited channel.

SPACE DIAGRAM

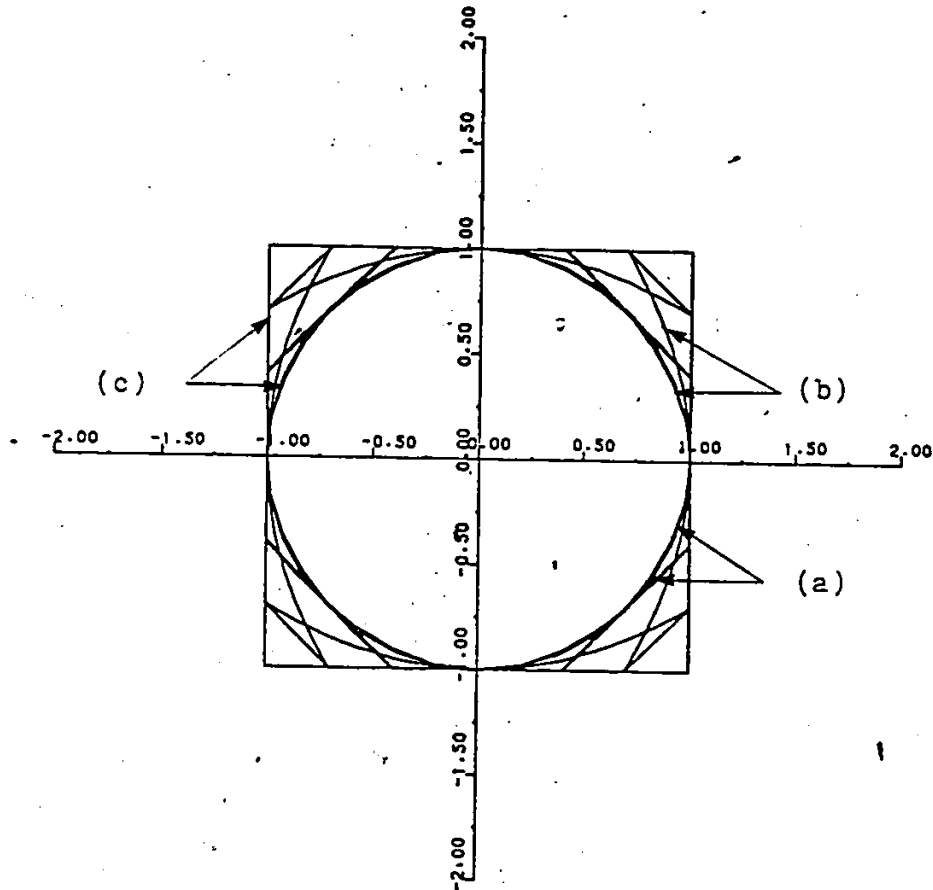


Fig.3.5. Simulated signal space diagrams of SQAM signals.

- (a) $A = 0.7$ (Max. envelope fluctuation = 0.7dB)
- (b) $A = 0.85$ (Max. envelope fluctuation = 1.7dB)
- (c) $A = 1.0$ (Max. envelope fluctuation = 3.0dB)

Table 3.1. Computed maximum envelope fluctuations of the SQAM signals.

A	Max. signal amplitude.	Min. signal amplitude.	Max. envelope fluctuation.(dB)
0.7	1.075	0.987	0.7
0.8	1.165	1.0	1.3
0.9	1.280	1.0	2.1
1.0	1.414	1.0	3.0

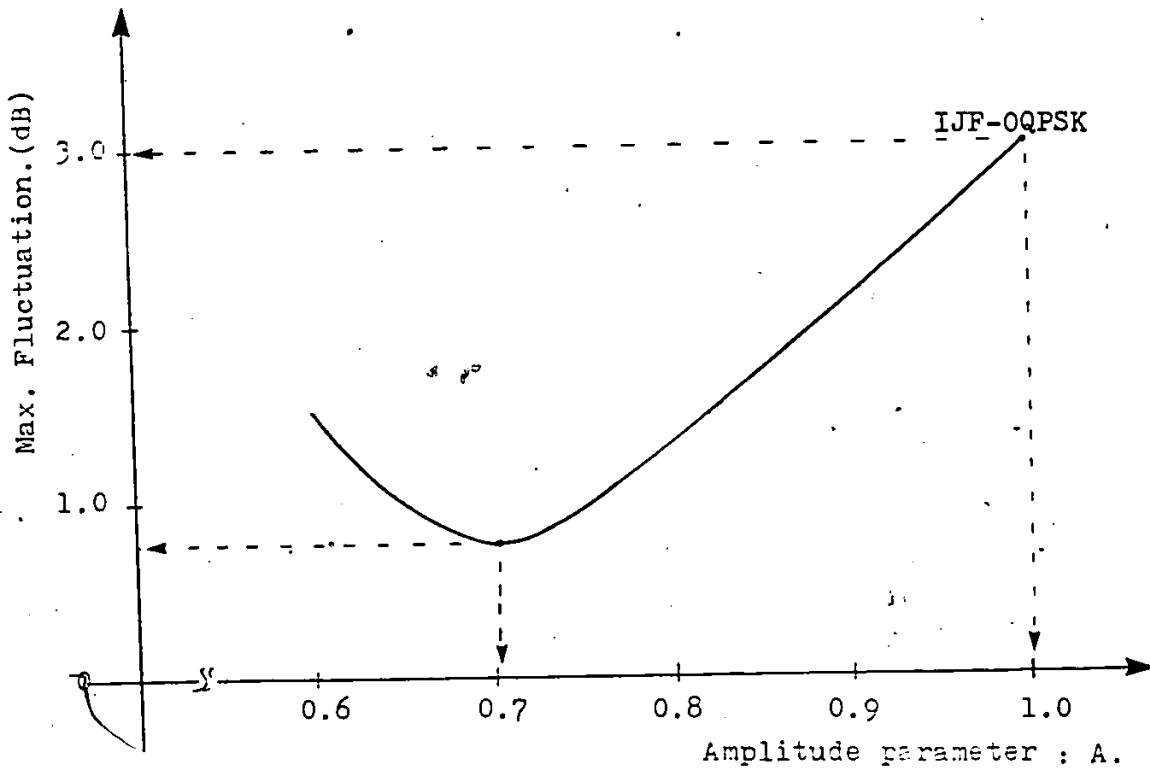


Fig.3.6. Envelope fluctuation of the SQAM signals.

3.3 PROBABILITY OF ERROR PERFORMANCE OF SQAM SYSTEMS

In this section, we investigate an optimum receiver for the SQAM, and derive an optimum $P(e)$ performance of the SQAM system. Then the $P(e)$ performance of the SQAM modem, in the presence of an AWGN, is evaluated by computer simulation, for linear and nonlinear (hardlimited) channels.

3.3.1 Optimum Receiver for SQAM

Referring to Fig.3.2, the signals taken at every sampling instant nT_s , over the interval of $[\pm T_s/2]$, form a set of 8 waveforms and are shown in Fig.3.7. The remaining four not shown in Fig.3.7 are the negative symmetricals of the ones shown.

In general, the optimum correlation receiver maximizes the signal energy at its output, and minimizes the equivalent noise bandwidth. An optimum receiver for the SQAM must be equivalent to a coherent detector in which the receiver input signal, disturbed by interference and noise, is correlated with replicas of the transmitted signal.

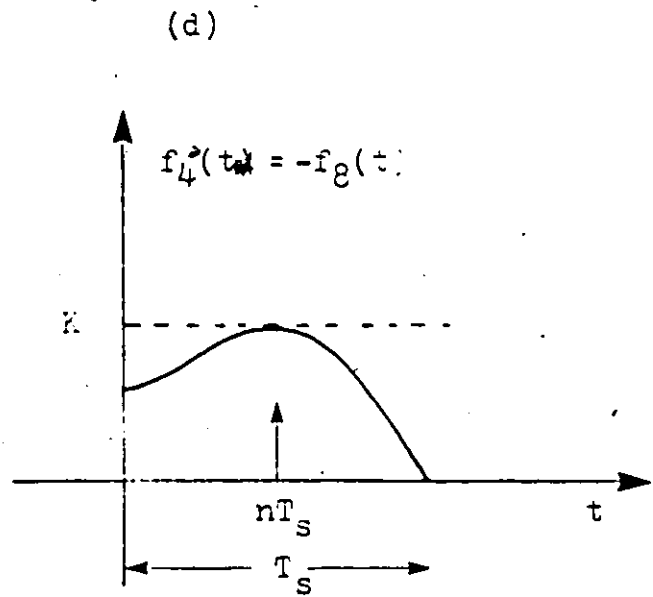
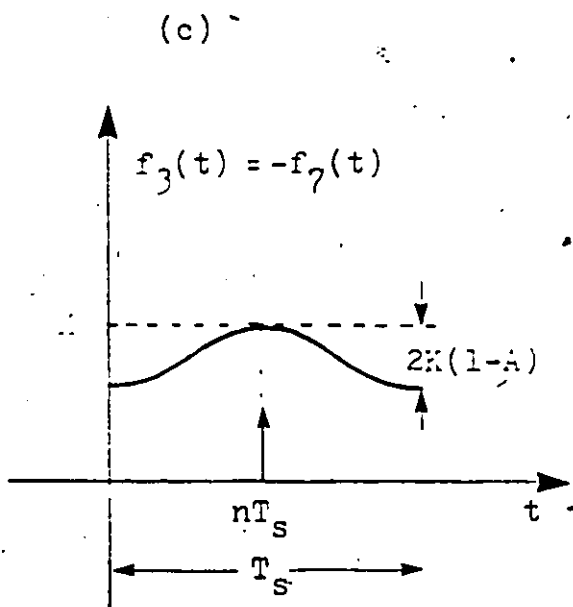
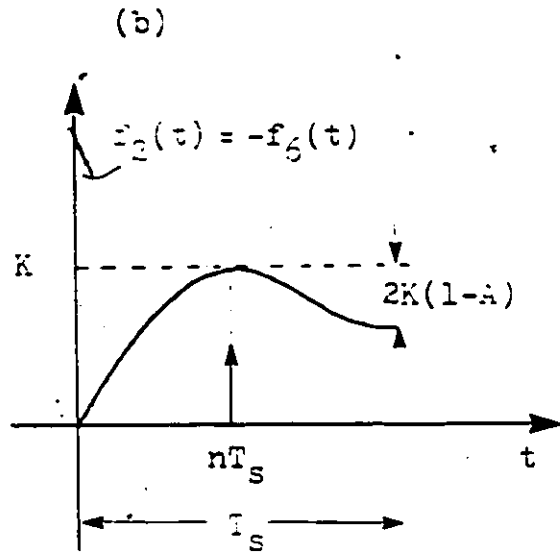
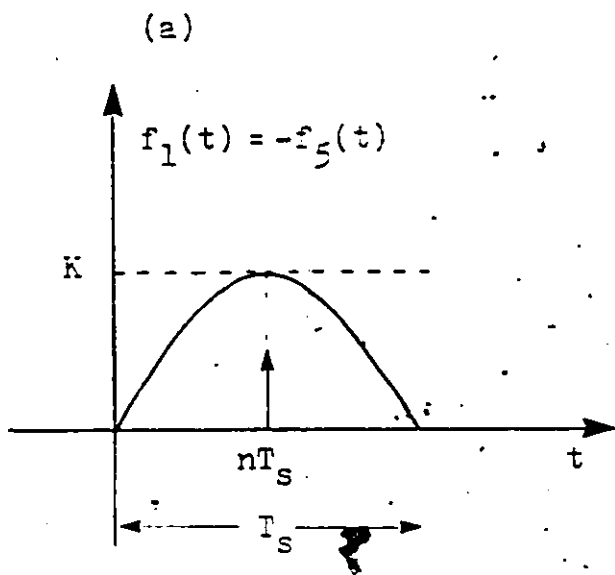


Fig.3.7 Composite waveforms of SQAM signal ,
at center duration T_s .

Fig.3.8 shows the configuration of a basic correlation receiver, which consists of multipliers followed by integrators and sampling detectors.

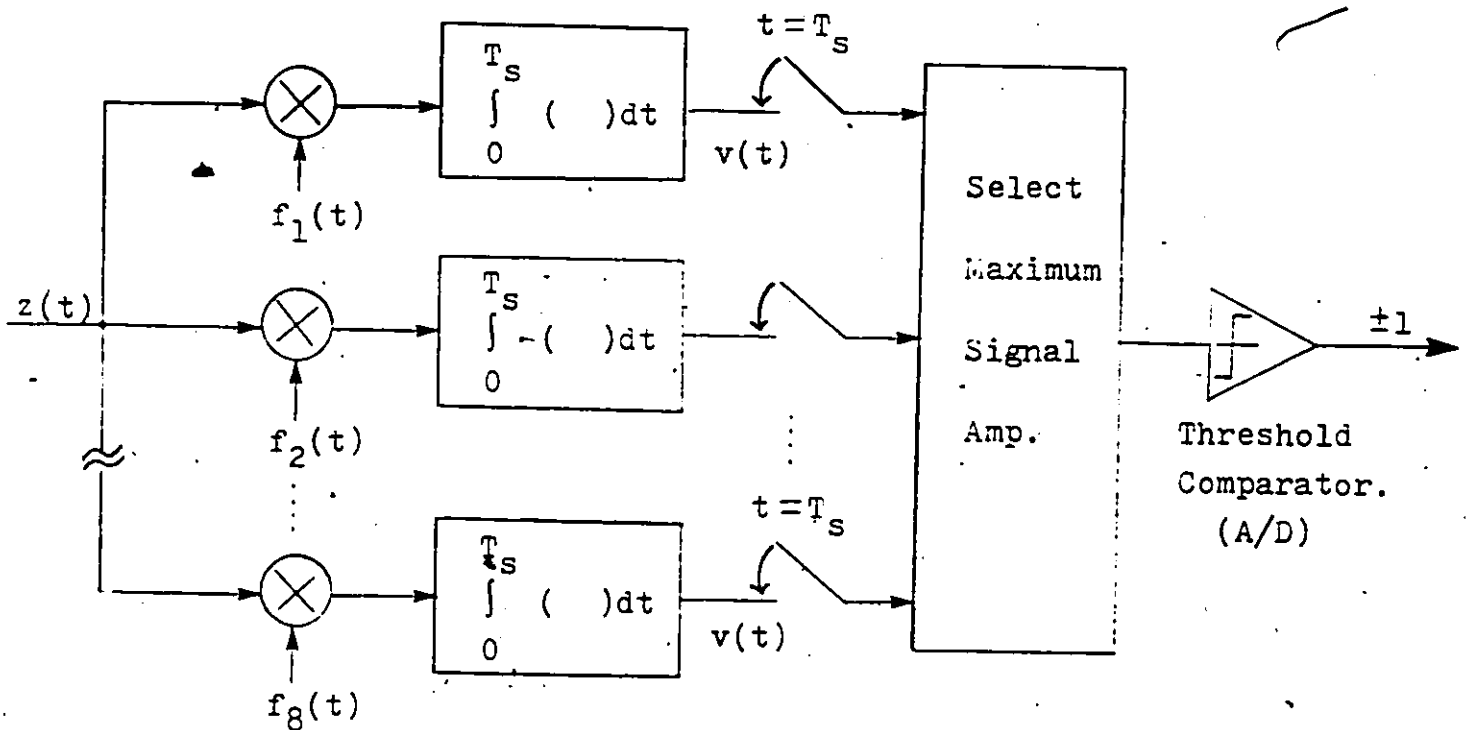


Fig.3.8 Configuration of a correlation receiver for SQAM.

The output of the correlation receiver, at the sampling instant $t=T_s$, is obtained as :

$$v(T_s) = \int_0^{T_s} z(t) f_j(t) dt \quad (3.6)$$

where $j = 1, 2, \dots, 8$.

3.3.2 Optimum $P(e)$ Performance of the SQAM Modem

Fig.3.9 shows the equivalent baseband model of a SQAM system.

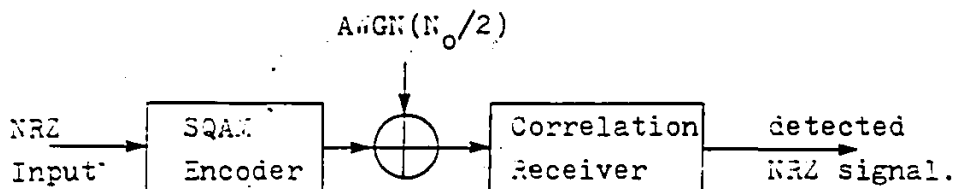


Fig.3.9 SQAM linear baseband model.

As the NRZ input data is an equiprobable random signal, the probability of occurrence of any SQAM output signal is identical. At every sampling instant, the signal amplitude of any output signal is equal to 'K'. (In (2.9) and (2.12), the value of K is normalized to 1.0). Therefore, the probability of error in any case is given by

$$P_1 = P_2 = P_3 = P_4 = 0.5 \operatorname{erfc}(K/\sigma\sqrt{2}) \quad (3.7)$$

where σ is the RMS value of noise power. (See Table 3.2.)

Table 3.2. Probability of error for SQAM signals.

NRZ input data		Encoded SQAM output signal	Probability of occurrence	Probability of error
a_{n+1}	a_n			
-1	-1	$y_1(t)$	1/4	$P_1 = 0.5 \operatorname{erfc}(K/\sigma\sqrt{2})$
-1	1	$y_2(t)$	1/4	$P_2 = 0.5 \operatorname{erfc}(K/\sigma\sqrt{2})$
1	-1	$y_3(t)$	1/4	$P_3 = 0.5 \operatorname{erfc}(K/\sigma\sqrt{2})$
1	1	$y_4(t)$	1/4	$P_4 = 0.5 \operatorname{erfc}(K/\sigma\sqrt{2})$

Therefore, the overall probability of error is given by :

$$\begin{aligned}
 P &= 1/4 (P_1 + P_2 + P_3 + P_4) \\
 &= 1/2 \operatorname{erfc}(K/\sigma\sqrt{2}) \qquad (3.8)
 \end{aligned}$$

An ideal (optimum) curve of the SQAM $P(e)$ performance is shown in Fig.3.14.

3.3.3 Simulation of the P(e) Performance of SQAM System

Fig.3.10 shows the computer simulation model, used to evaluate the P(e) performance of the SQAM modem, for linear and nonlinear (hardlimited) channels. Additive white Gaussian noise (AWGN) is added to the modulated, hardlimited signal. The SQAM baseband signal processor is the only spectral shaping element in the transmitter. The receiver is modeled as a conventional coherent OQPSK demodulator having signal shaping 4th order Butterworth LPFs with $f_{3dB} = 1.1 f_N$ ($f_N = f_s / 2 =$ Nyquist frequency). In our simulation, we frequently used $f_b = 120\text{Mb/s}$ rate, thus in this case, the 3dB bandwidth (f_{3dB}) is equal to 33MHz.

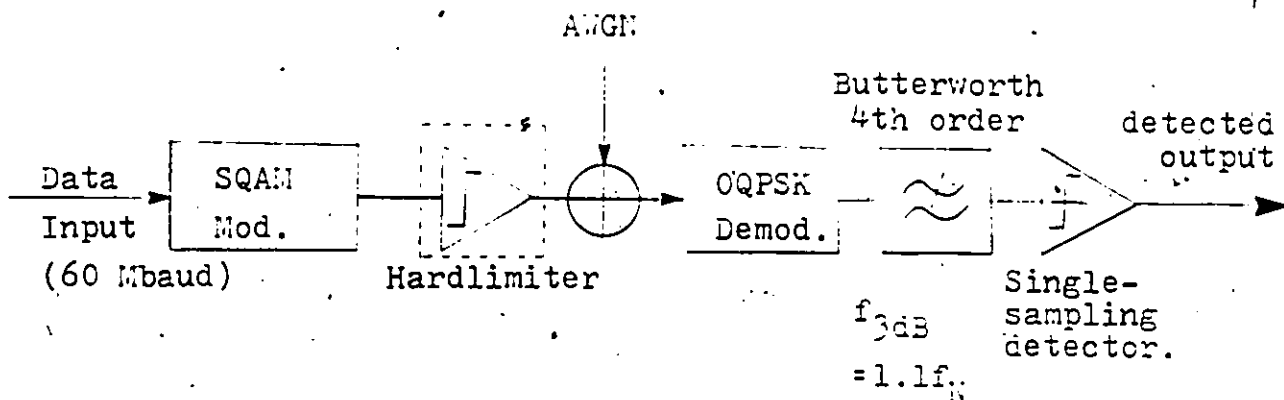
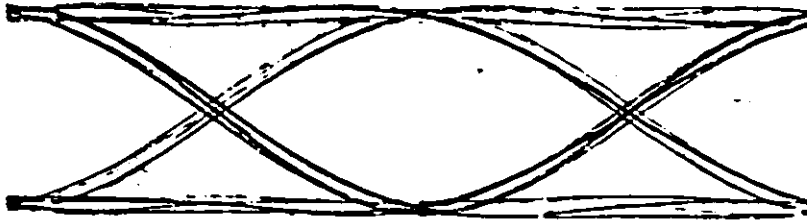


Fig.3.10 Simulation model of the SQAM modem.

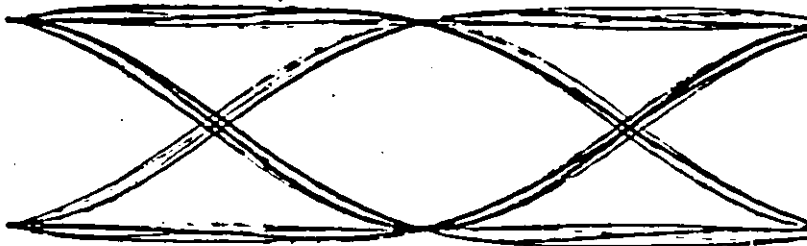
Computer simulated eye patterns of the SQAM signals, after the postdetection LPF (or before the sampling detector), are shown in Figs.3.11 and 3.12 for linear and hardlimited channels. These eye patterns show that the SQAM signal with amplitude parameter $A=0.8$ results in the best eye opening and the least intersymbol-interference (ISI) at the sampling instant, both in linear and hardlimited channels. For comparison purpose, eye patterns of the MSK signal, after the postdetection LPF, are also shown in Figs.3.13 and 3.14 for linear and hardlimited channels. Note that the SQAM signal with $A=0.8$ has better eye patterns than MSK signal in linear and nonlinear channels.

SQAM EYE DIAGRAM

(a) $A = 0.7$



(b) $A = 0.8$



(c) $A = 0.9$

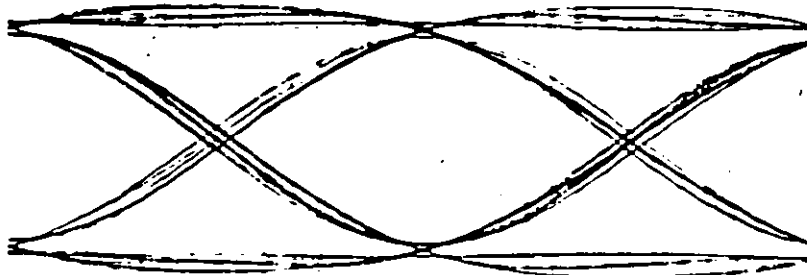
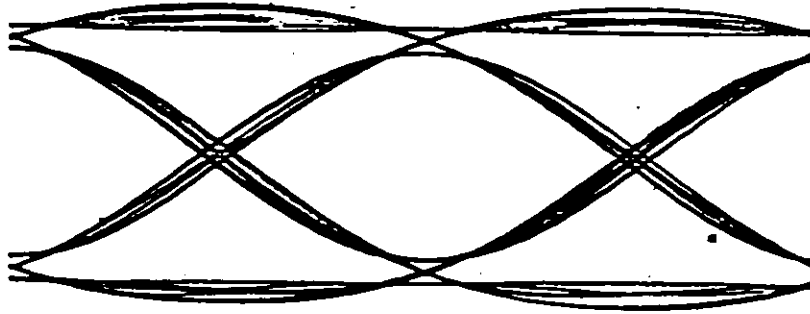


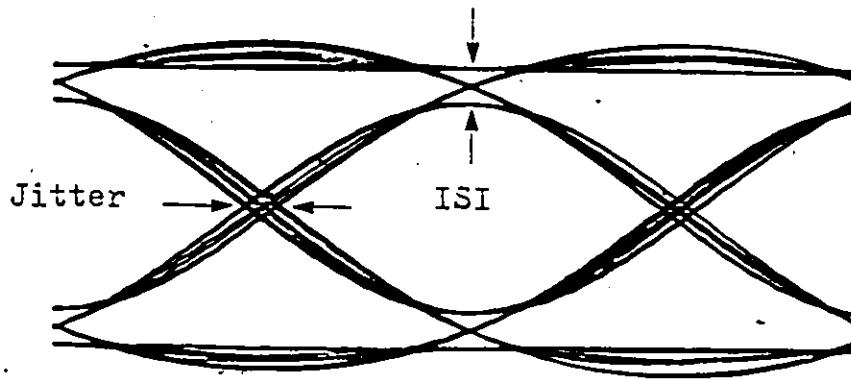
Fig.3.11 Eye patterns of the SQAM signals after postdetection LPF in a linear channel (I or Q-channel).

SQAM EYE DIAGRAM

(d) $A=1.0$



(e) $A=1.1$



(f) $A=1.2$

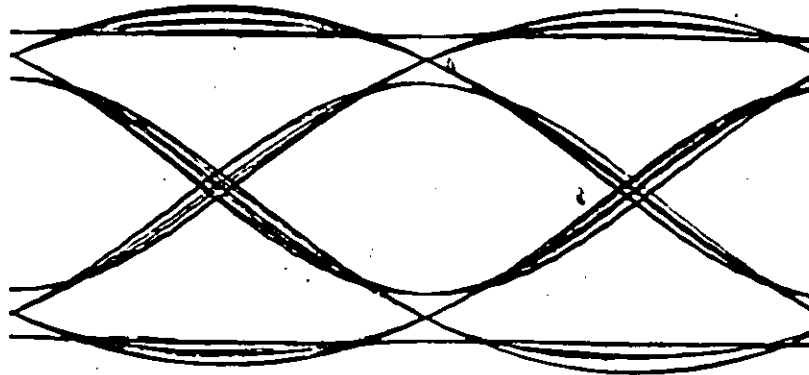
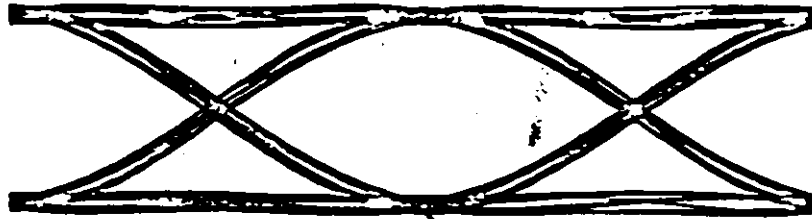


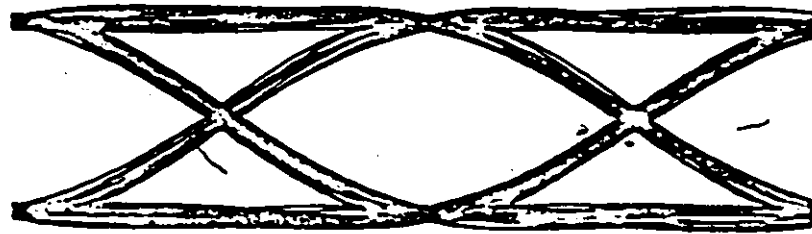
Fig.3.11 Eye patterns of the SQAM signals after postdetection LPF in a linear channel.

SQAM EYE DIAGRAM

(a) $A = 0.7$



(b) $A = 0.8$



(c) $A = 0.9$

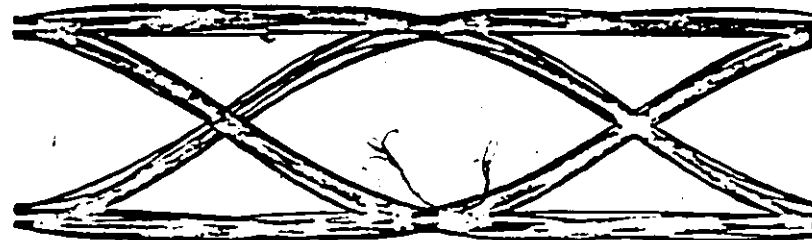
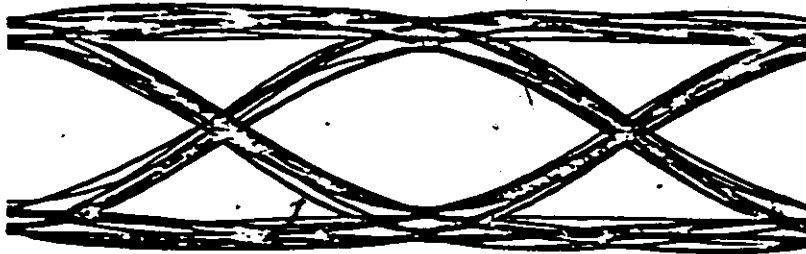


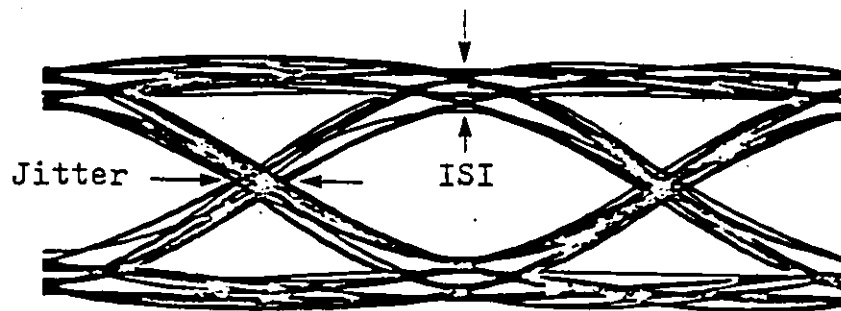
Fig. 3.12 Eye patterns of the SQAM signals after postdetection LFF in a hardlimited channel.

SQAM EYE DIAGRAM

(d) $A=1.0$



(e) $A=1.1$



(f) $A=1.2$

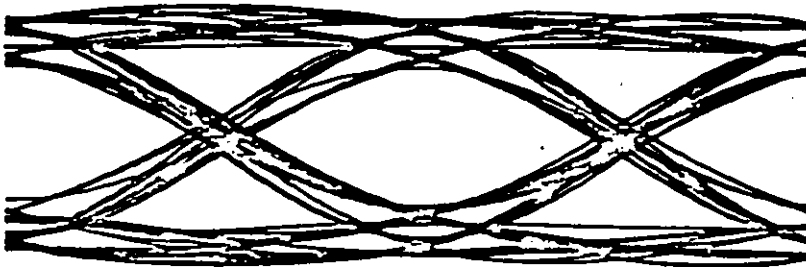
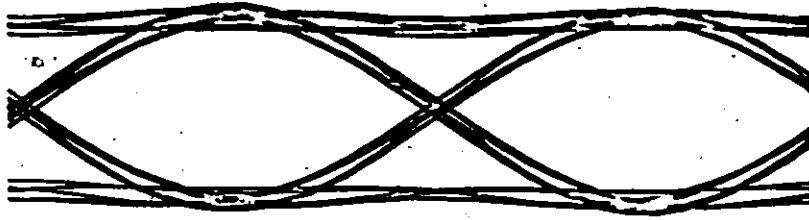


Fig.3.12 Eye patterns of the SQAM signals after postdetection LPF in a hardlimited channel.

(a) With receive filter only.



(b) With transmit and receive filters.

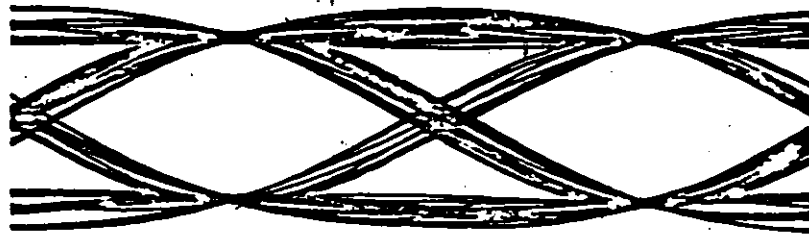
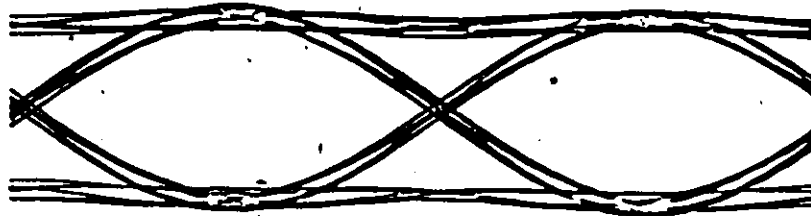


Fig.3.13 Eye patterns of the MSK signal after postdetection LPF in a linear channel.

(a) With receive filter only.



(b) With transmit and receive filters.

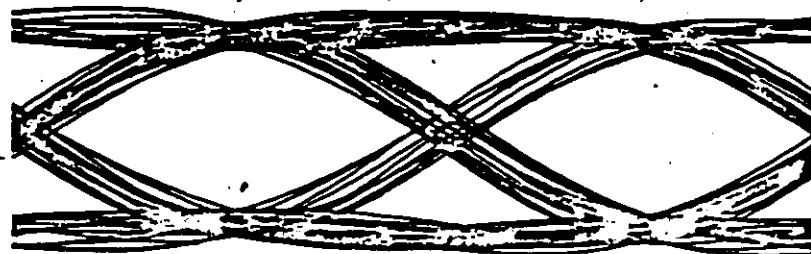


Fig.3.14 Eye patterns of the MSK signal after postdetection LPF in a hardlimited channel.

Figs.3.15(a) and (b) show the simulated $P(e)$ performance results of the SQAM modem for linear and nonlinear channels. For the illustrative case, a data bit rate of 120 Mb/s (60 Mbaud) was assumed. We obtained the best performance for $A=0.8$ in linearly and nonlinearly amplified channels. Figs.3.16(a) and (b) illustrate the $P(e)$ performance degradation, that is, the increased E_b/N_0 requirement of this SQAM system to maintain $P(e)=10^{-4}$. The performance of SQAM is degraded by 0.3 dB (for $A=0.8$) in a linear channel, and 0.5 dB (for $A=0.8$) in a saturated (hard-limited) channel. To facilitate the comparison with the performance of MSK and TFM, the increased E_b/N_0 requirements of these systems are also shown in Figs.3.16(a) and (b). [3]. The filtering strategies, which have been used for the generation of these results, are summarized in Table 3.3. Note that SQAM ($A=0.8$) outperforms MSK by 0.5dB in a linear channel, and by 0.8dB in a hardlimited channel. SQAM ($A=0.8$) also outperforms TFM by 0.7dB in a linear channel. Further, the generation of SQAM signal is much simpler than that of TFM signal.

SQAM BER CURVE

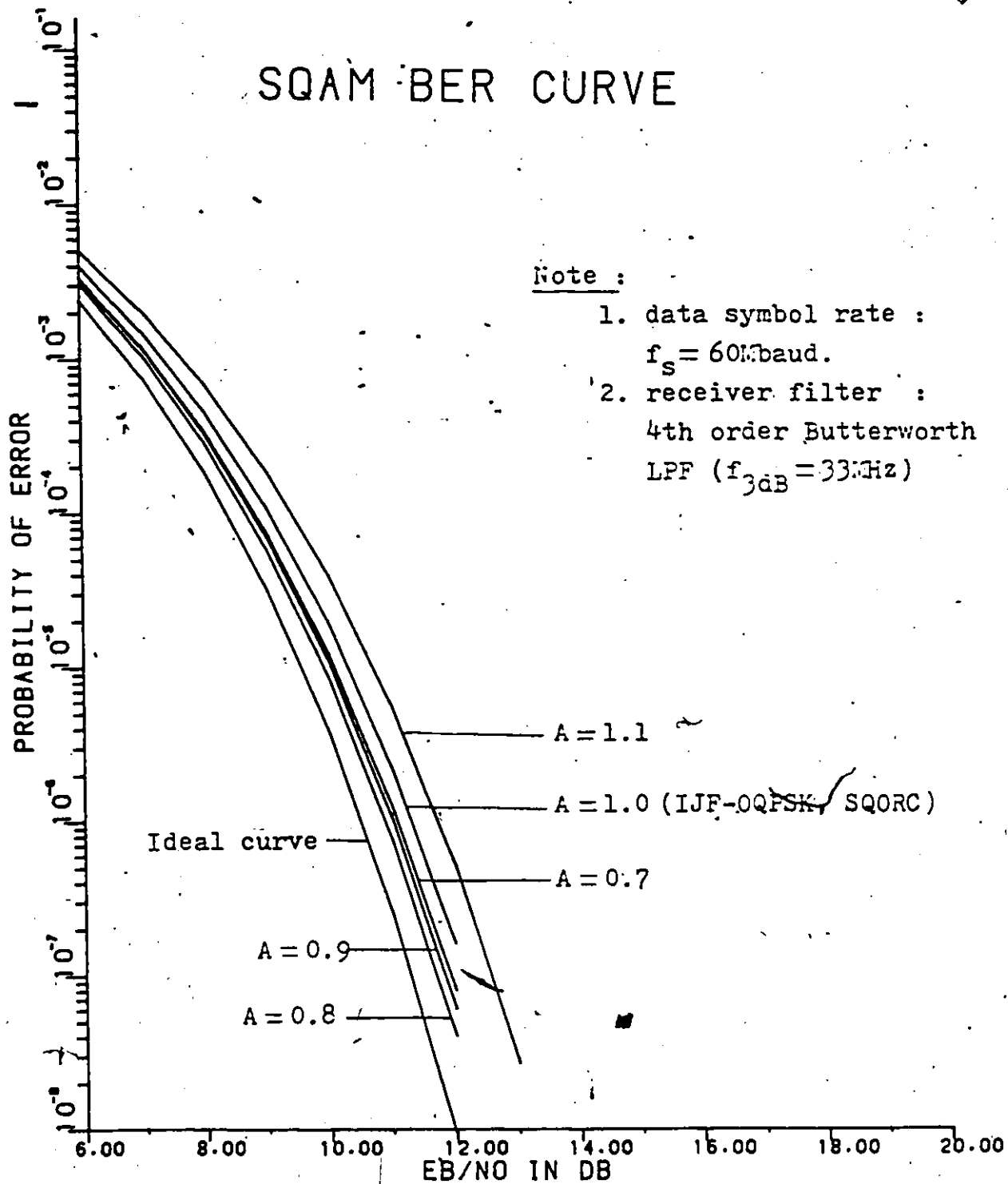


Fig.3.15(a). Simulated P_e performance of SQAM modem in a linear channel.

SQAM BER CURVE

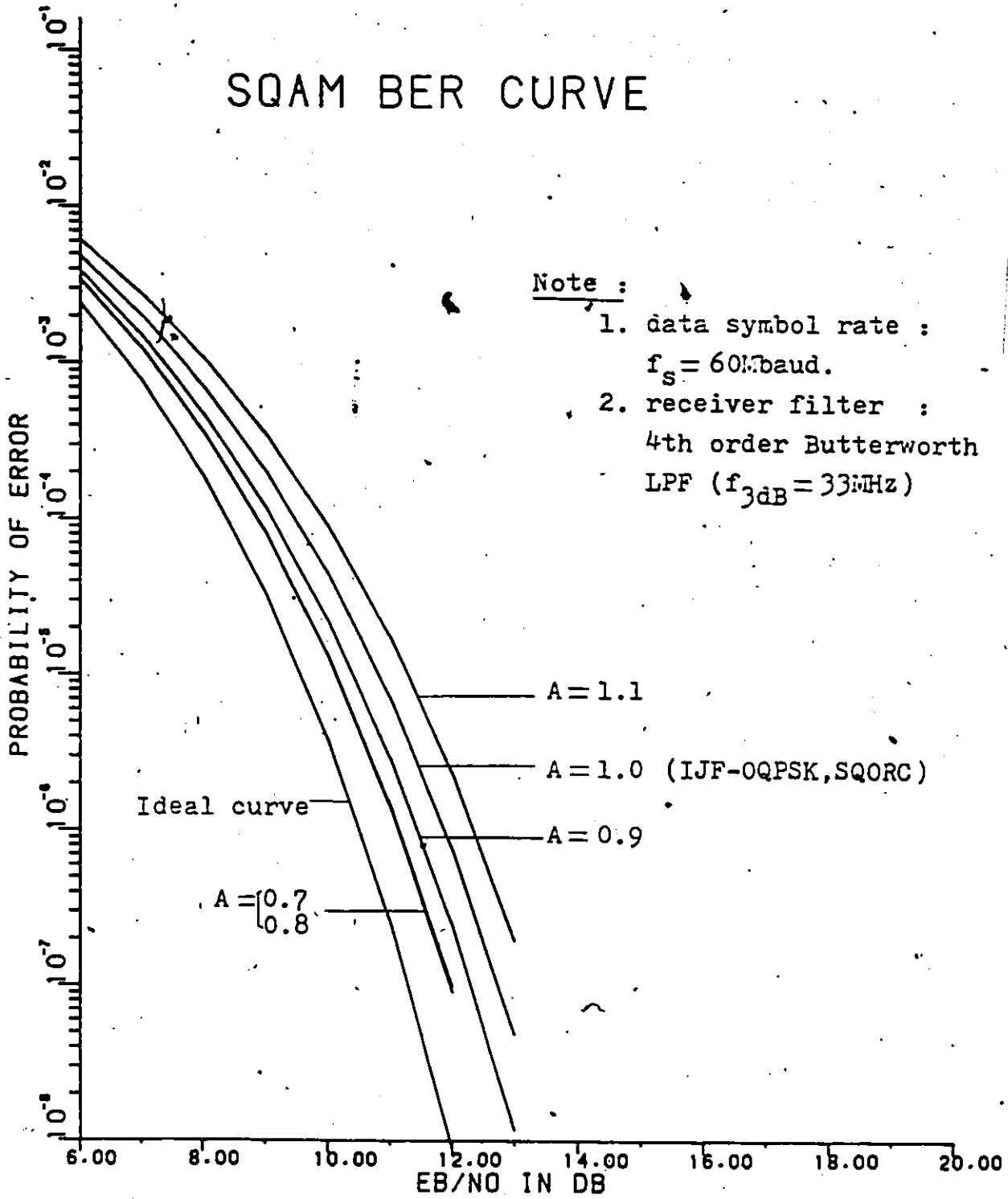
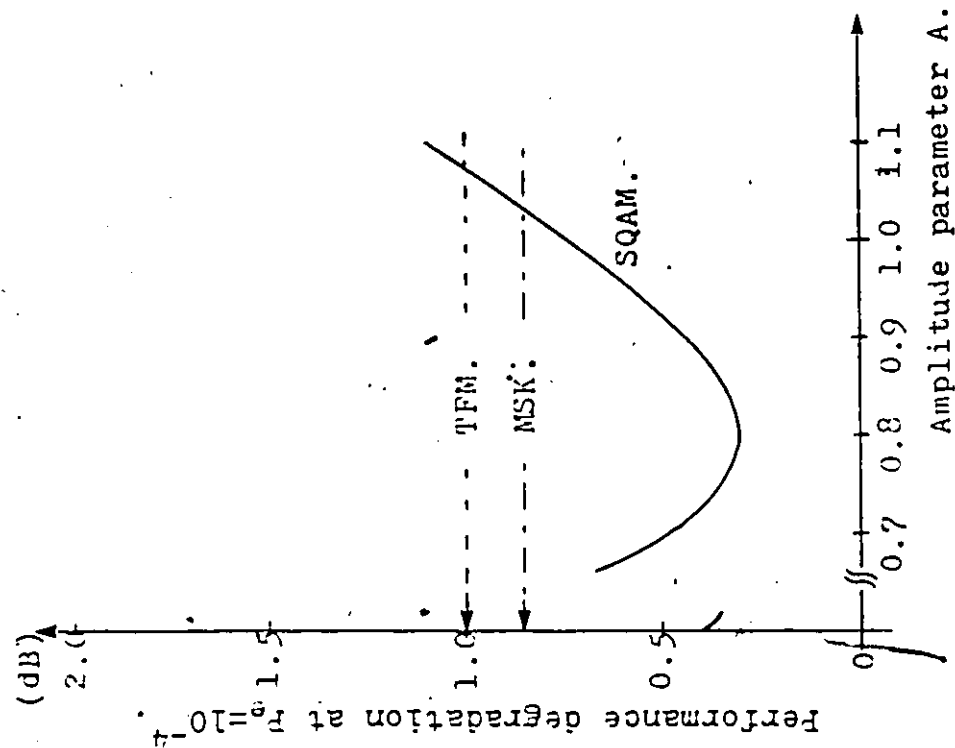
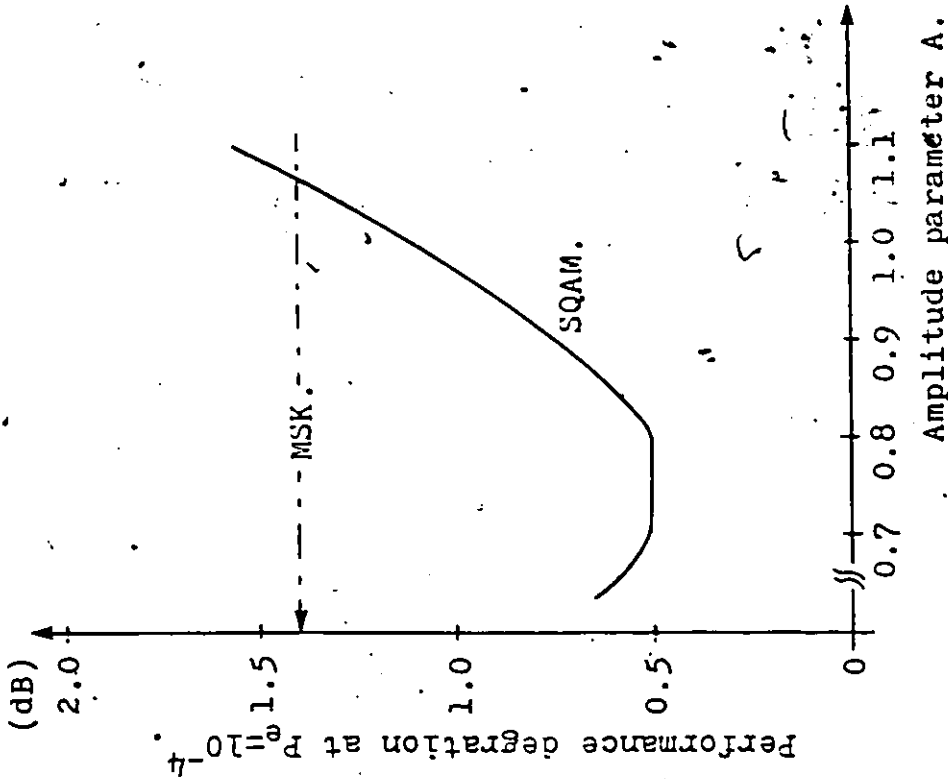


Fig.3.15(b). Simulated P_e performance of SQAM modem in a nonlinear(hardlimited) channel.



(a) linear channel.



(b) nonlinear channel.

Fig. 3.16. Required increase in E_b/N_0 (performance degradation) to maintain $P_b = 10^{-4}$ for SQAM, MSK and TFM.

Table 3.3 Filtering strategies for different modems.

Modem.	Transmit filter.	Receive filter.
MSK.	4th order Butterworth LPF. ($f_{3dB} = 33$ MHz)	4th order Butterworth LPF. ($f_{3dB} = 33$ MHz)
TFM[3]	Low pass filter :B(w)	optimum LPF for TFM:A(w)
IJF-OQPSK [1]	Nil	aperture equalized full raised-cosine filter ($\alpha = 0.4$)
SQAM	Nil	4th order Butterworth LPF. ($f_{3dB} = 33$ MHz)

3.4 EXPERIMENTAL RESULTS

The schematics of experimental set-up of SQAM modem is shown in Fig.3.17. In this set-up, a pseudo random binary sequence (PRBS) generator provides a NRZ data of 128 kb/s, and a random noise generator (20 Hz - 20 MHz) provides an AWGN. Phase equalized 4th order Butterworth LPFs ($f_{3dB} = 35.2$ kHz) are used as postdetection LPFs in the receiver. Fig.3.18 shows the measured I and Q-channel eye patterns of the SQAM signal for $A=0.8$ in a linear channel. Fig.3.19 (a) and (b) show a baseband I (or Q)-channel SQAM signal ($A=0.8$)

and a corresponding modulated (carrier frequency : $f_c = 1\text{MHz}$) I (or Q)-channel SQAM signal, respectively. Fig.3.20 (a) and (b) show measured signal space diagrams of SQAM signal ($A=0.8$) in a linear and in a hardlimited channel, respectively. Note that the hardlimited SQAM signal has a constant envelope. Fig.3.21 shows measured power spectra of SQAM signal for $A=1.0$ in a linear and in a hardlimited channel, and also for $A=0.8$ in a hardlimited channel. Note that for $A=0.8$, the spectral spreading is lower than that for $A=1.0$ in a hardlimited channel.

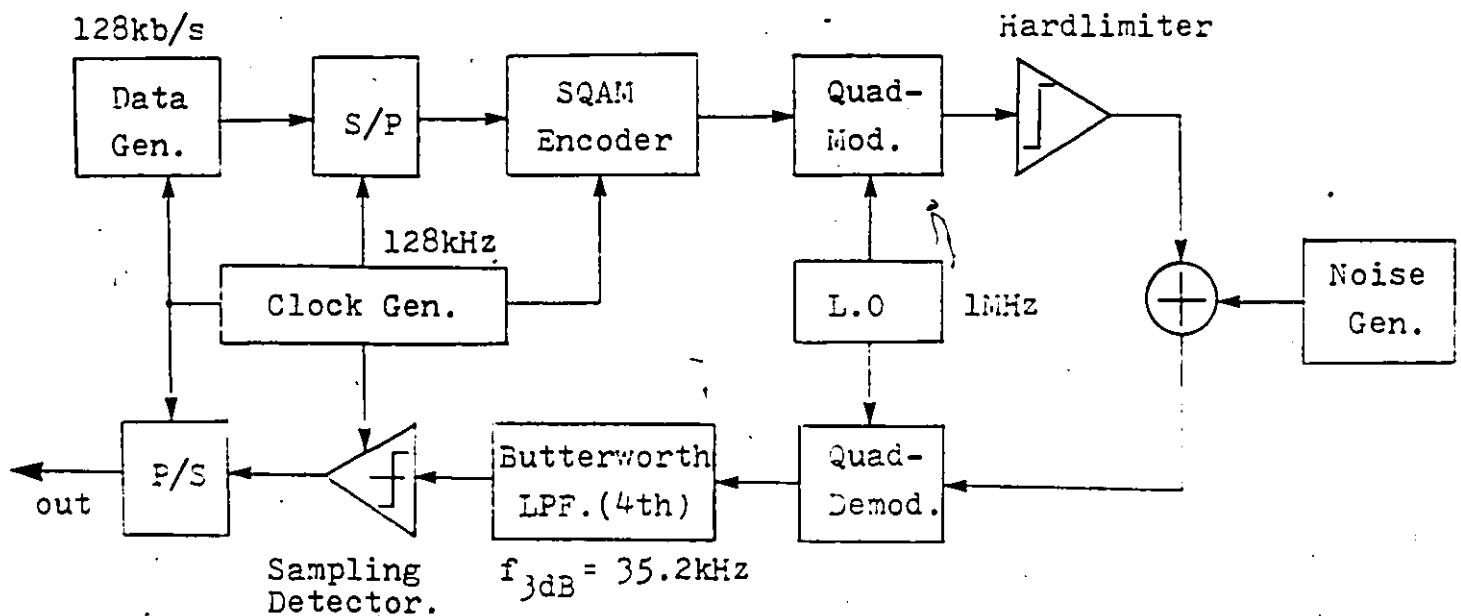
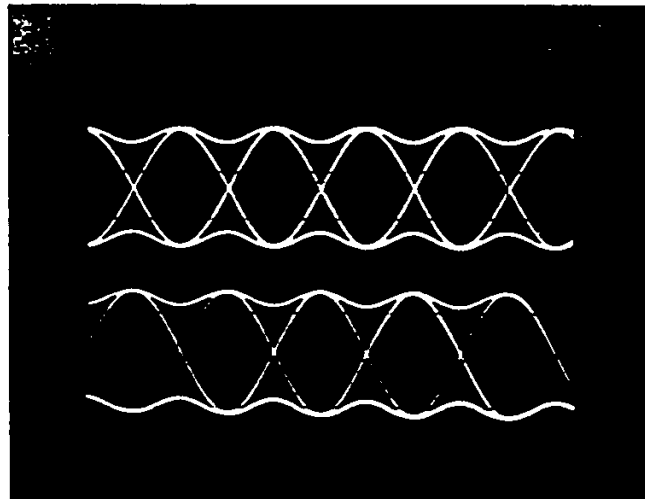


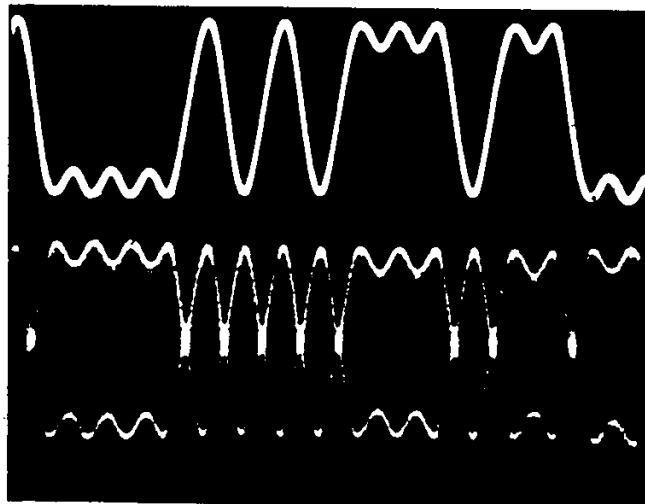
Fig.3.17 Experimental set-up of SQAM modem.



I-channel.

Q-channel.

Fig.3.18. Measured Eye-patterns of SQAM signal ($A=0.8$).



(a)

(b)

Fig.3.19. (a). I (or Q)- channel SQAM baseband signal.

(b). I (or Q)- channel modulated ($f_c=1\text{MHz}$)
SQAM signal.

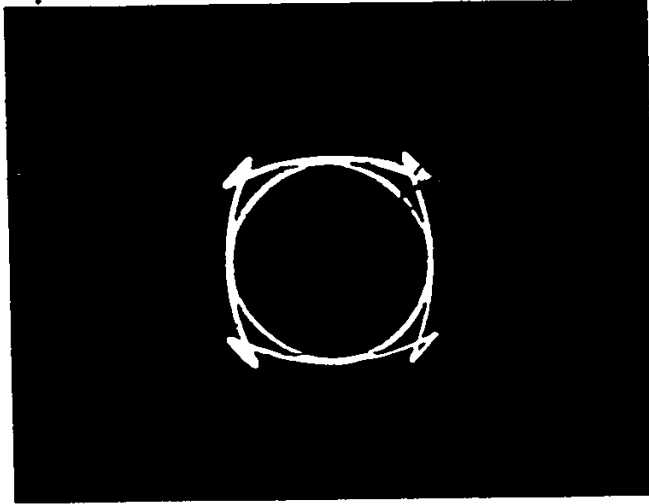
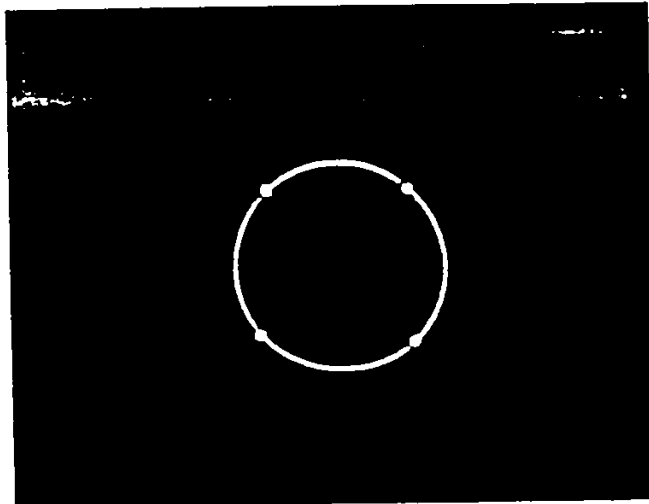


Fig.3.20.
Measured SQAM signal
($A=0.8$) space diagram.

(a). In a linear channel.



(b). In a hardlimited
channel.

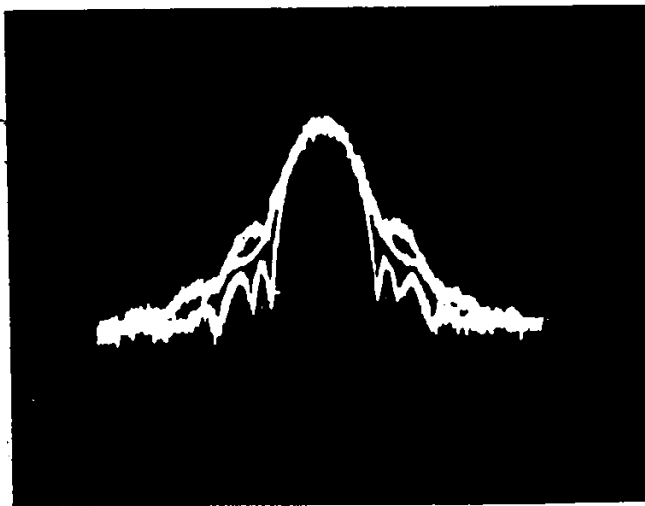


Fig.3.21.
Measured power spectra
of SQAM signals.

- (a). Upper : $A=1.0$,
hardlimited.
- (b). Middle: $A=0.8$,
hardlimited.
- (c). Lower : $A=1.0$,
linear.

Chapter IV

PERFORMANCE OF SQAM MODEM IN NONLINEAR MULTICHANNEL

4.1 ANALYSIS OF PROBABILITY OF ERROR IN MULTICHANNEL

In this section, we derive expressions for the $P(e)$ performance which include the effects of ISI, ACI [27] and/or CCI in the linearly amplified multichannel system. Based on these expressions, we also find the worst case (high bound) error probability in an ACI or CCI environment.

4.1.1 Probability of Error in Adjacent Channel Interference

The probability of error, for linearly amplified multichannel systems in the presence of AWGN, ISI and ACI, is analyzed. The block diagram of a multichannel modem is shown in Fig.4.1, where two adjacent channels (i.e., one higher frequency adjacent channel and another lower frequency adjacent channel) interfere with the main (desired) channel.

The transmitted signal is given by :

$$z_n(t) = \text{Re} [v_n(t) \exp(j2\pi f_c t)] \quad (4.1)$$

where $n = [-1, 0, 1]$, and ' $n=0$ ' represents the term due to the desired signal, and ' $n = \pm 1$ ' represent terms due to the interfering signals, and f_0 is the carrier frequency of the main channel.

The corresponding complex envelope $v_n(t)$ is given by [27] :

$$v_n(t) = K \rho_n \exp\left[\frac{j\pi}{2} \sum_{-\infty}^t a_{n,i} s(\tau - \tau_n - iT_S) d\tau + n\Delta F 2\pi t + \theta_n\right] \quad (4.2)$$

where

K = amplitude of desired signal.

ρ_n = relative signal amplitude of adjacent channel.

($\rho_0 = 1$ and F.D(fade-depth) = $20 \log(\rho_{\pm 1}/\rho_0)$.)

$s(t)$ = impulse response of a baseband signal encoder.

(For SQAM signal encoder, see (2.3) and (2.4).)

τ_n = symbol timing misalignment of adjacent channels

($\tau_0 = 0$ sec.)

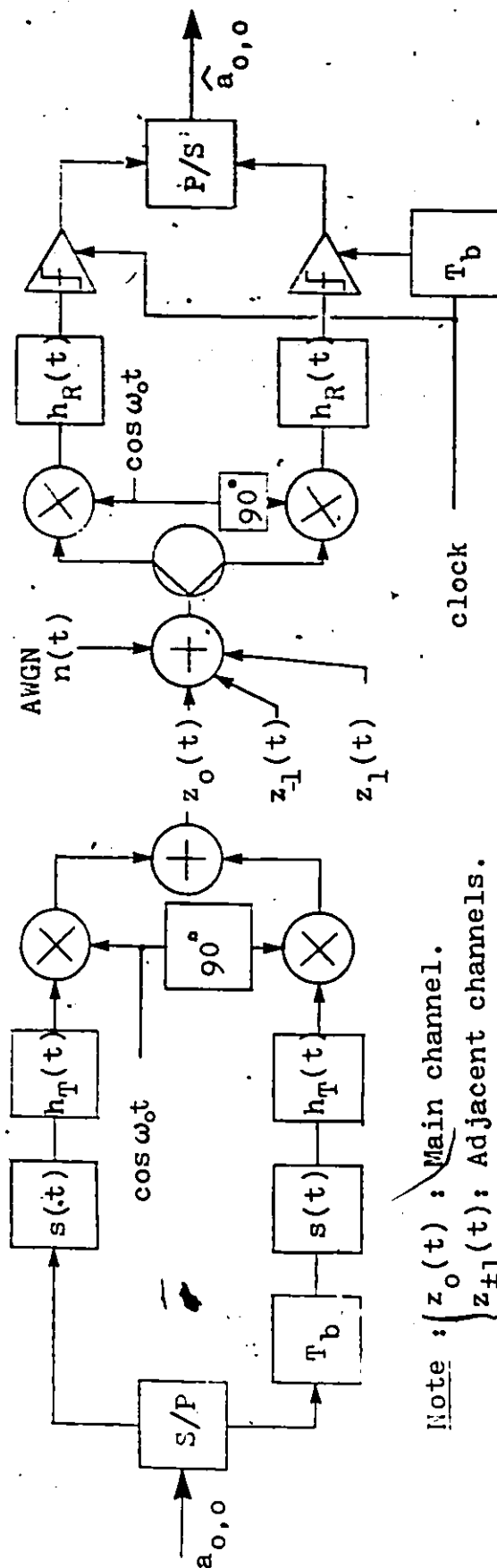
ΔF = channel spacing. (See Fig.4.3.).

θ_n = carrier phase misalignment of adjacent channels

($\theta_0 = 0$ rad.)

$a_{n,i} = \pm 1$ with equal probability. (' i ' represents terms due to intersymbol-interference.)

T_S = symbol duration.



Note : $\begin{cases} z_0(t) : \text{Main channel.} \\ z_{\pm 1}(t) : \text{Adjacent channels.} \\ h_T(t) \triangleq h_0(t) \end{cases}$

Fig.4.1 Block diagram of a modem in a multichannel interference environment.

The demodulated signal, at the output of the receive filter, is given by :

$$r(t) = x_n(t) + n(t) \quad (4.3)$$

$$x_n(t) = x_0(t) + x_1(t) + x_{-1}(t) \quad (4.4)$$

$$x_n(t) = \text{Re} [v_n * h_n(t) * h_R(t)] \quad (4.5)$$

where * denotes convolution, $h_n(t)$ and $h_R(t)$ represent the impulse response of transmit and receive filters, respectively. (Let the main-channel transmit filter have an impulse response $h_n(t) \triangleq h_0(t)$ with $n=0$.)
 $n(t)$ is a zero-mean Gaussian noise with variance

$$\sigma_n^2 = N_0/2 \int_{-\infty}^{\infty} |H_R(f)|^2 df \quad (4.6)$$

where $N_0/2$ is the double-sided PSD of AWGN, and

$$H_R(f) = F\{h_R(t)\}$$

Assuming $i=0$ and desired signal $a_{0,0}=1$, then the probability of error, at the sampling instant $t=t_0$, is expressed as :

$$P(e) = Q [(Kf(t_0) + \text{ISI} + \text{ACI}) / \sigma_n] \quad (4.7)$$

where

$$f(t) = s(t) * h_n(t) * h_R(t) \quad (4.8)$$

$$\text{ISI} = K \sum_{i \neq 0} a_{0,i} f(t_0 - iT_s) \quad (4.9)$$

$$ACI = x_1(t_0) + x_{-1}(t_0) \quad (4.10)$$

$$Q(x) = \frac{1}{\sqrt{2\pi}} \int_x^{\infty} \exp(-y^2/2) dy \quad (4.11)$$

and the bar (—) denotes the average over all random symbols contained in ISI and ACI.

In (4.9), let us assume only two intersymbol-interference components are significant, then

$$ISI = K [a_{0,1} f(t_{-1}) + a_{0,-1} f(t_1)] \quad (4.12)$$

and the worst ISI occurs when $a_{0,1} = a_{0,-1} = -1$, that is,

$$\text{worst ISI} = -K [f(t_{-1}) + f(t_1)] \quad (4.13)$$

When adjacent channel signals have opposite polarities to that of the desired signal, that is $a_{1,0} = a_{-1,0} = -1$, the worst ACI appears to be

$$\text{worst ACI} = - [|x_1(t_0)| + |x_{-1}(t_0)|] \quad (4.14)$$

The worst case (high bound) error probability can be calculated from (4.7), (4.13) and (4.14).

4.1.2 Probability of Error in Co-Channel Interference

The probability of error, in the presence of AWGN, ISI and CCI, is analyzed in this section. Using the same parameters as in the case of ACI in section 4.1.1, the transmitted signal is given by :

$$z_n(t) = \text{Re} [v_n(t) \exp(j2\pi f_0 t)] \quad (4.1)$$

where complex envelope $v_n(t)$ is given by :

$$v_n(t) = K \rho_n \exp\left[\frac{j\pi}{2} \int_{-\infty}^t a_{n,i} s(\tau - \tau_n - iT_S) d\tau + \theta_n\right] \quad (4.2)$$

(ΔF in (4.2) is set to zero in CCI environment.)

The demodulated output signal is :

$$r(t) = x_n(t) + n(t) \quad (4.3)$$

$$x_n(t) = x_0(t) + x_1(t) + \dots \quad (4.4)$$

$$x_n(t) = \text{Re} [v_n(t) * h_n(t) * h_R(t)] \quad (4.5)$$

where $n(t)$ is zero-mean Gaussian noise with variance

$$\sigma_n^2 = N_p/2 \int_{-\infty}^{\infty} |H_R(f)|^2 df \quad (4.6)$$

The probability of error is expressed as :

$$P(e) = Q \left[\frac{Kf(t_0) + \text{ISI} + \text{CCI}}{\sigma_n} \right] \quad (4.7)'$$

where

$$f(t) = s(t) * h_T(t) * h_R(t) \quad (4.8)$$

$$\text{ISI} = K \sum_{\substack{n \\ i \neq 0}} \rho_n a_{n,i} f(t_0 - iT_s) \quad (4.9)'$$

$$\text{CCI} = \sum_{n \neq 0} x_n(t_0) \quad (4.10)'$$

$$Q(x) = \frac{1}{\sqrt{2\pi}} \int_x^{\infty} \exp(-y^2/2) dy \quad (4.11)$$

$$\text{dominant ISI} = K \sum_n \rho_n [a_{n,1} f(t_{-1}) + a_{n,-1} f(t_1)] \quad (4.12)'$$

The worst ISI occurs with $a_{n,1} = a_{n,-1} = -1$, and the worst CCI occurs with $a_{n,0} = -1$ when a desired signal $a_{0,0} = 1$ is assumed.

Thus,

$$\text{worst ISI} = -K \sum_n \rho_n [f(t_{-1}) + f(t_1)] \quad (4.13)'$$

$$\text{worst CCI} = - \sum_{n \neq 0} |x_n(t_0)| \quad (4.14)'$$

where the integer 'n' will be determined depending on different applications (folds) of the frequency reuse system. The worst case (high bound) error probability can be calculated from (4.7) , (4.13) and (4.14).

However , it is quite difficult to analytically evaluate the average $P(e)$ performance of quadrature modems, in the presence of AWGN, ISI and ACI [14,16,27] or CCI [13,15,17] , especially for the nonlinearly amplified multichannel system. Therefore, in our next step, a computer simulation is employed to analyze the performance of the SQAM modem in a nonlinear multichannel environment.

4.2 SIMULATION ON $P(E)$ PERFORMANCE OF MULTICHANNEL SQAM

In this section , we describe a computer simulation approach which is employed to evaluate the performance of the SQAM modem in a nonlinear channel with ACI and CCI . We use a well established computer simulation software package called COMSIM. COMSIM is a software package (primarily based on time domain operations) used for the computer aided design and analysis of digital communication systems, and was developed at Digital Communication Group of

University of Ottawa. A simulation model of a SQAM modem with two adjacent channels is shown in Fig.4.2, while its frequency allocation is shown in Fig.4.3.

In section 4.2.1, we discuss the assumptions made for this simulation. The performance of the multichannel SQAM modem, for different values of 'A', is evaluated in section 4.2.2, under different channel conditions. In section 4.2.3 ... 4.2.6, effects of the receive filter bandwidth, channel spacing, fade depth on the desired signal, and effects of co-channel interference (CCI) on the performance of the SQAM multichannel systems are investigated and compared to those of other modems.

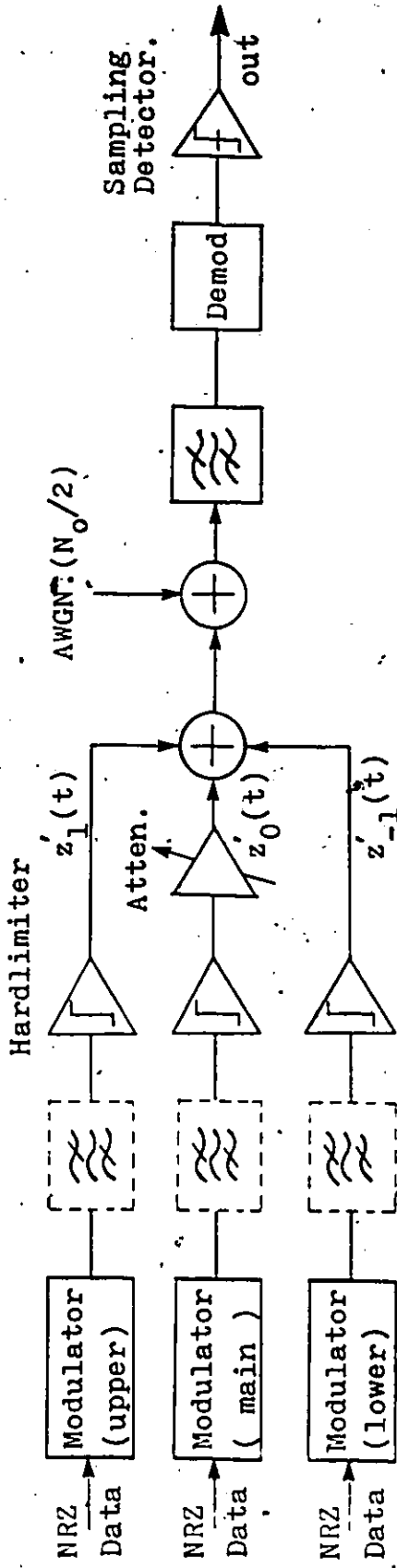
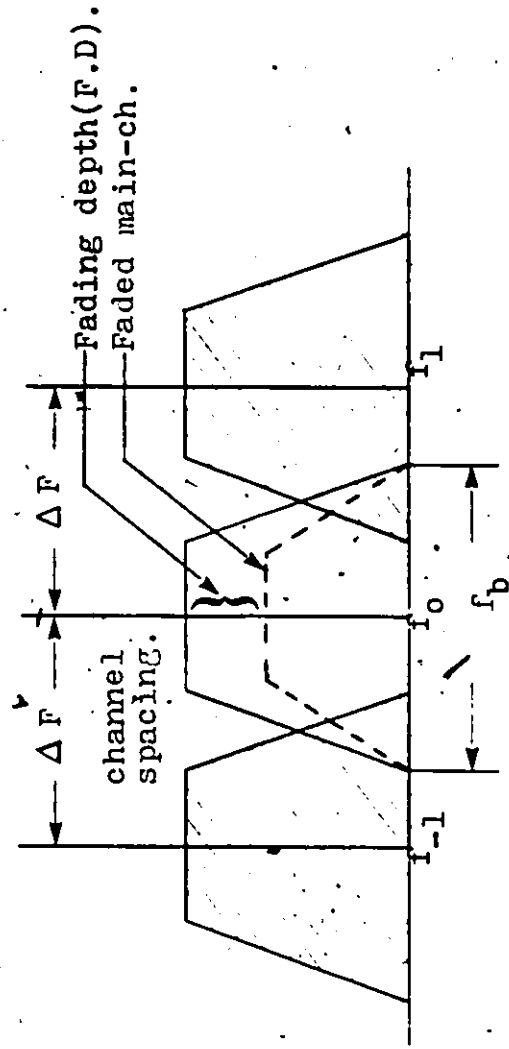


Fig.4.2 A simulation model of a multichannel system.



Lower adj-ch. Main channel. Upper adj-ch.

Fig.4.3 Frequency allocation for multi-channel system.

Note :

f_0 : main-ch. carrier freq.
 $f_{\pm 1}$: adj-ch carrier freq.
 $(f_{\pm 1} = f_0 \pm \Delta F)$

4.2.1 Assumptions Used in the Simulations

- (1). Two interfering adjacent channels are equally spaced. In Fig.4.3, the main channel has a carrier frequency f_0 , and the adjacent channels have carrier frequencies $f_{\pm 1} = f_0 \pm \Delta F$; where ΔF is the channel frequency separation (or channel spacing).
- (2). The interfering signals have the same form as the desired signal.
- (3). The carrier phase and symbol timings of the interfering signals are randomized over the interval $(0, 2\pi)$ and $(-T_S/2, T_S/2)$ respectively to avoid the coherence and synchronization between the interfering and main channels.
- (4). The earth station HPAs, operating in saturation mode, are approximated by ideal hardlimiters. (An ideal hardlimiter presents a good first-order approximation of a saturated amplifier. [1,12,13])
- (5). Only the desired signal is attenuated due to uplink flat fading.
- (6). An illustrative input data bit rate, $f_b = 120$ Mb/s (or data symbol rate $f_s = 60$ Mbaud) is used. This is a typical bit rate for a number of high speed systems.
- (7). In the SQAM modem, only receive filters are used.

4.2.2 Effects of the Amplitude Parameter(A) in SQAM

In this simulation, phase equalized 5th order Butterworth LPFs ($f_{3dB} = 30$ MHz) are used in the receiver. The P(e) performance results of the hardlimited multichannel SQAM modem for different values of 'A' are shown in Figs.4.4(a)...(d). In Figs.4.4(a) and (b), the adjacent interfering channels have the equal power as the main channel, while in Figs.4.4 (c) and (d), the main channel suffers a fading by an amount of 6 dB. Note that with low levels of fading, the SQAM modem for $A = 0.8$ shows the best performance, while with high levels of fading, the SQAM modem for $A = 0.9$ has a better performance. Hereafter, the SQAM signal for $A = 0.85$ is considered for our further evaluation on the P(e) performance of the multichannel SQAM systems.

SQAM BER CURVE

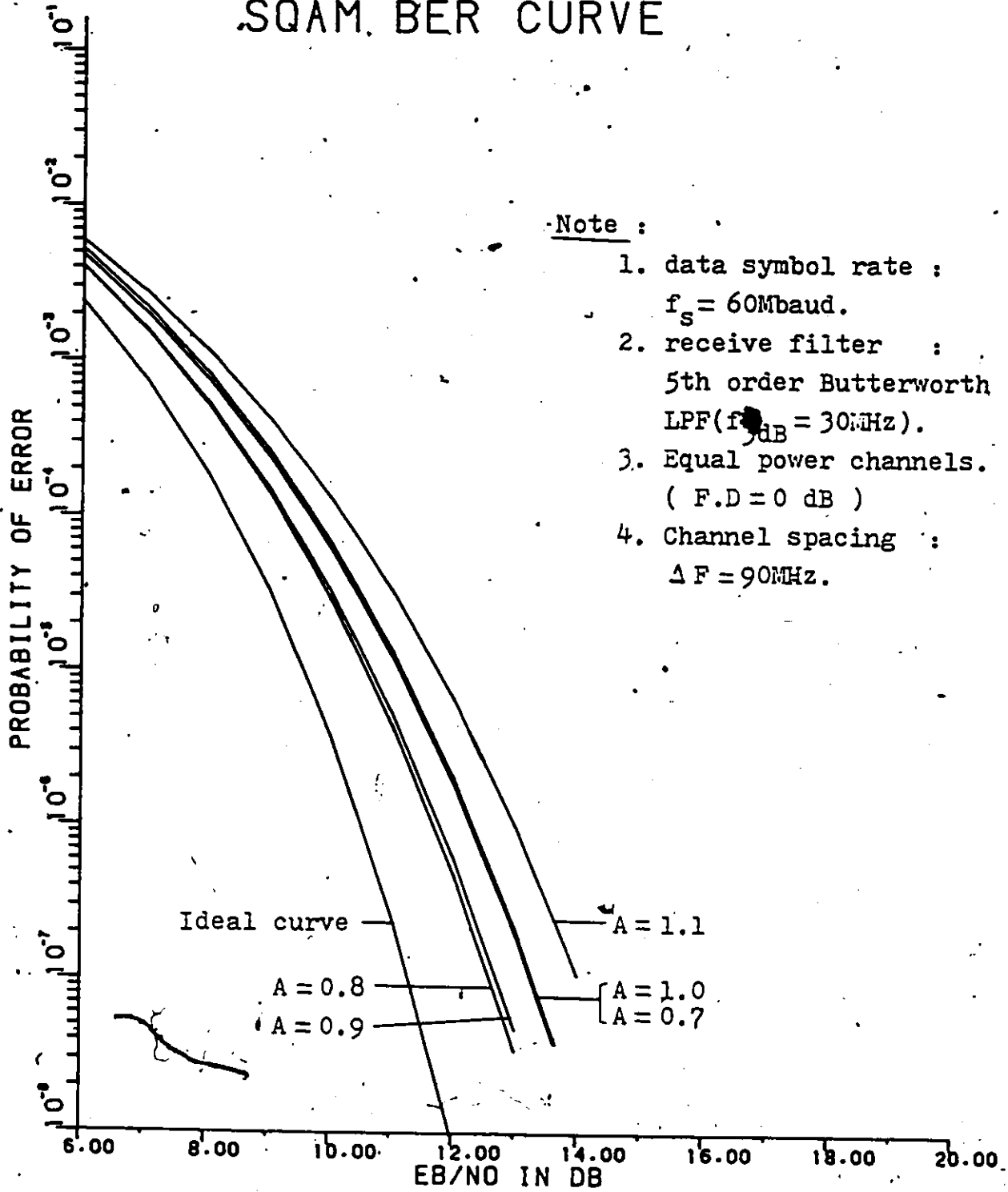


Fig.4.4(a) P_e performance of SQAM modem in a hardlimited multi-channel system (vs. 'A').

SQAM BER CURVE

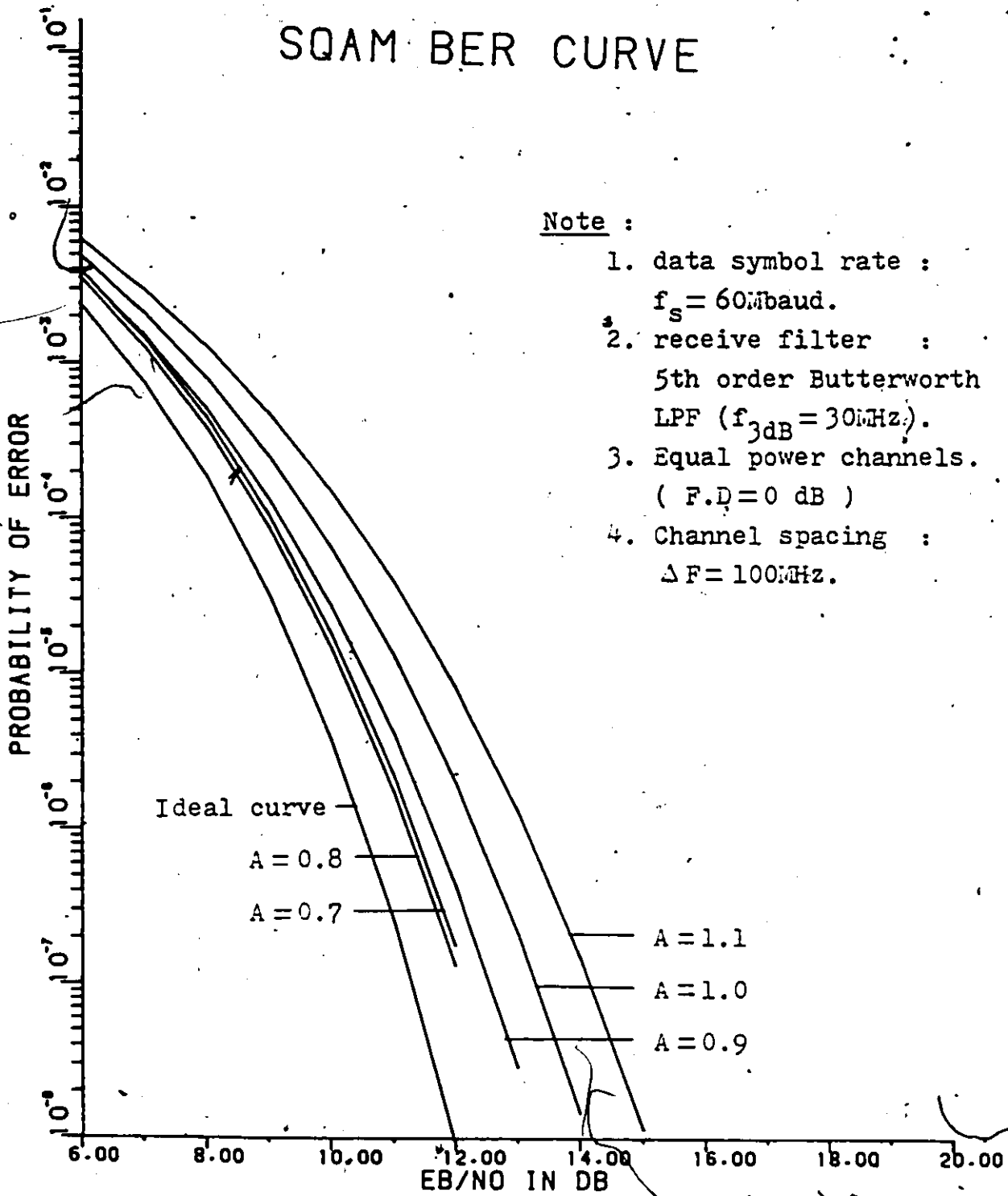


Fig.4.4(b) P_e performance of SQAM modem in a hardlimited multi-channel system (vs. 'A').

SQAM BER CURVE

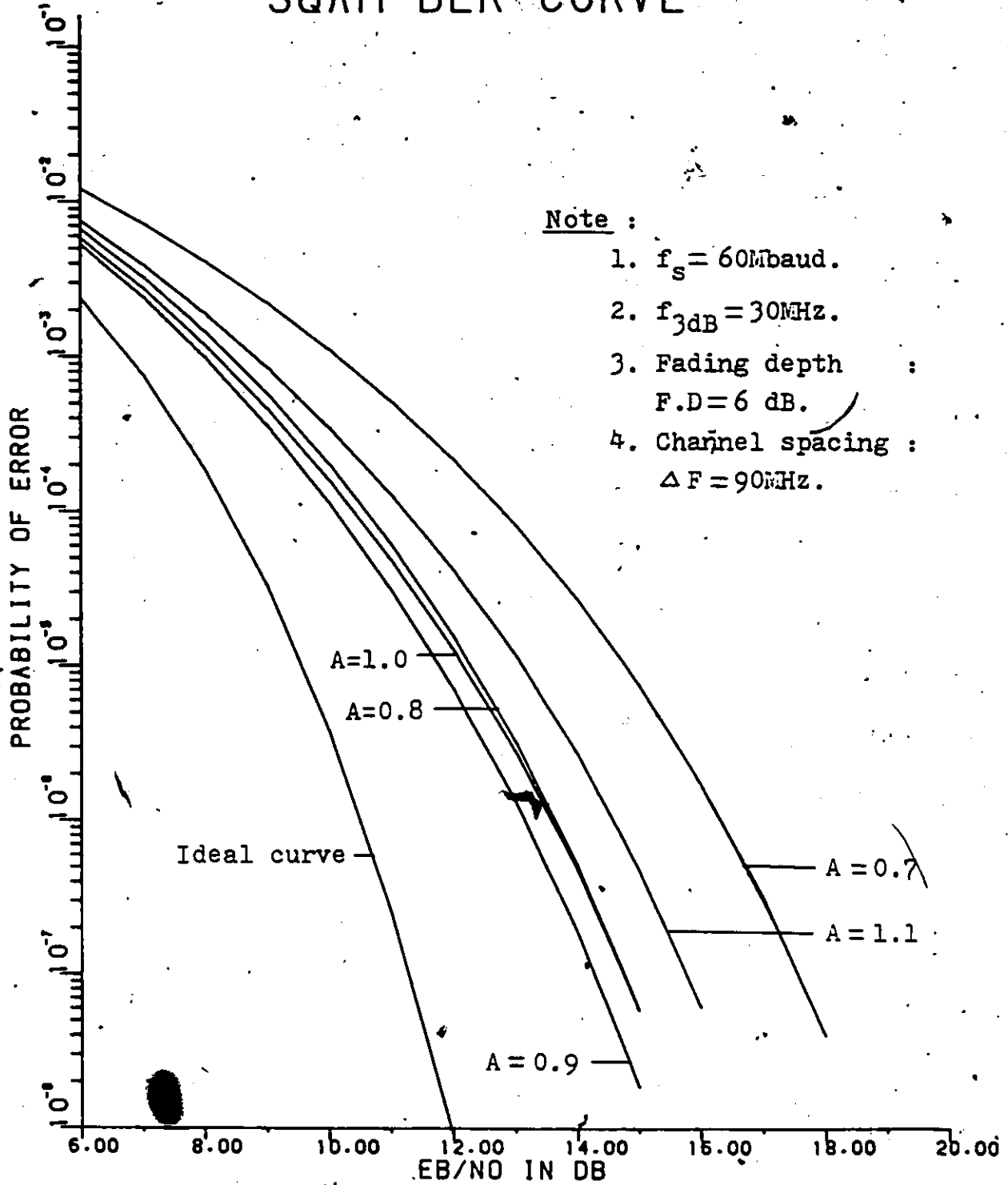


Fig.4.4(c) P_e performance of SQAM modem in a hardlimited multi-channel system (vs. 'A').

SQAM BER CURVE

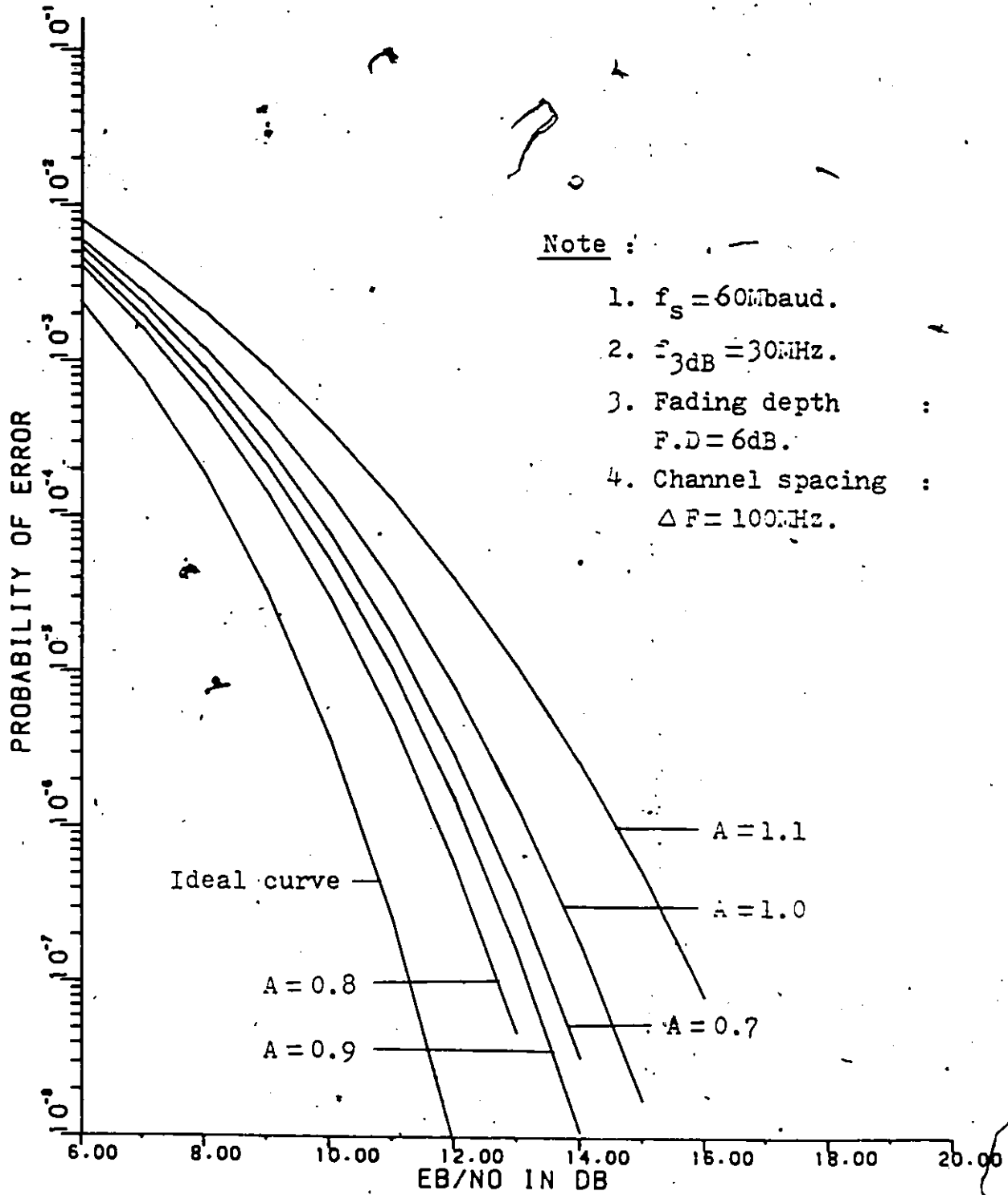


Fig. 4.4(d) P_e performance of SQAM modem in a hardlimited multi-channel system, (vs. 'A').

4.2.3 Effects of the Receive Filter Bandwidth.

In this section, we investigate effects of a receive filter bandwidth on the performance of the SQAM modem in a multichannel environment, and try to find out an optimal filter bandwidth (B) and symbol duration (T_s) product for the 5th order Butterworth LPF. In these simulations, phase-equalized 5th order Butterworth LRFs are used. The $P(e)$ performance results of the SQAM ($A=0.85$) modem for different bandwidth (f_{3dB}) of the receive filter are shown in Figs. 4.5(a) and (b), with channel spacings $\Delta F=90$ and 100 MHz respectively. The $P(e)$ performance degradation (that is, the increased E_b/N_0 requirement of this SQAM system to maintain $P(e)=10^{-4}$), as a function of BT_s product, is shown in Fig. 4.5(c), where B (or f_{3dB}) is the 3dB bandwidth of the LPF, and T_s ($=1/f_s$) is the data symbol duration. It must be noted that the filter bandwidth cannot be too large because of the thermal noise and ACI effects, and cannot be too small because of ISI effect. A trade-off exists between ISI and ACI losses, hence an optimal receive bandwidth is to be found. Using the simulation, we found that the near optimal BT_s product is about 0.5, and the major source of the performance impairment is the ACI when $BT_s > 0.5$, and the ISI when $BT_s < 0.5$. It is also noticed that the LRF optimal bandwidth increases with increasing values of channel spacing (ΔF), and decreases with increasing values of fade depth of the desired signal.

SQAM BER CURVE

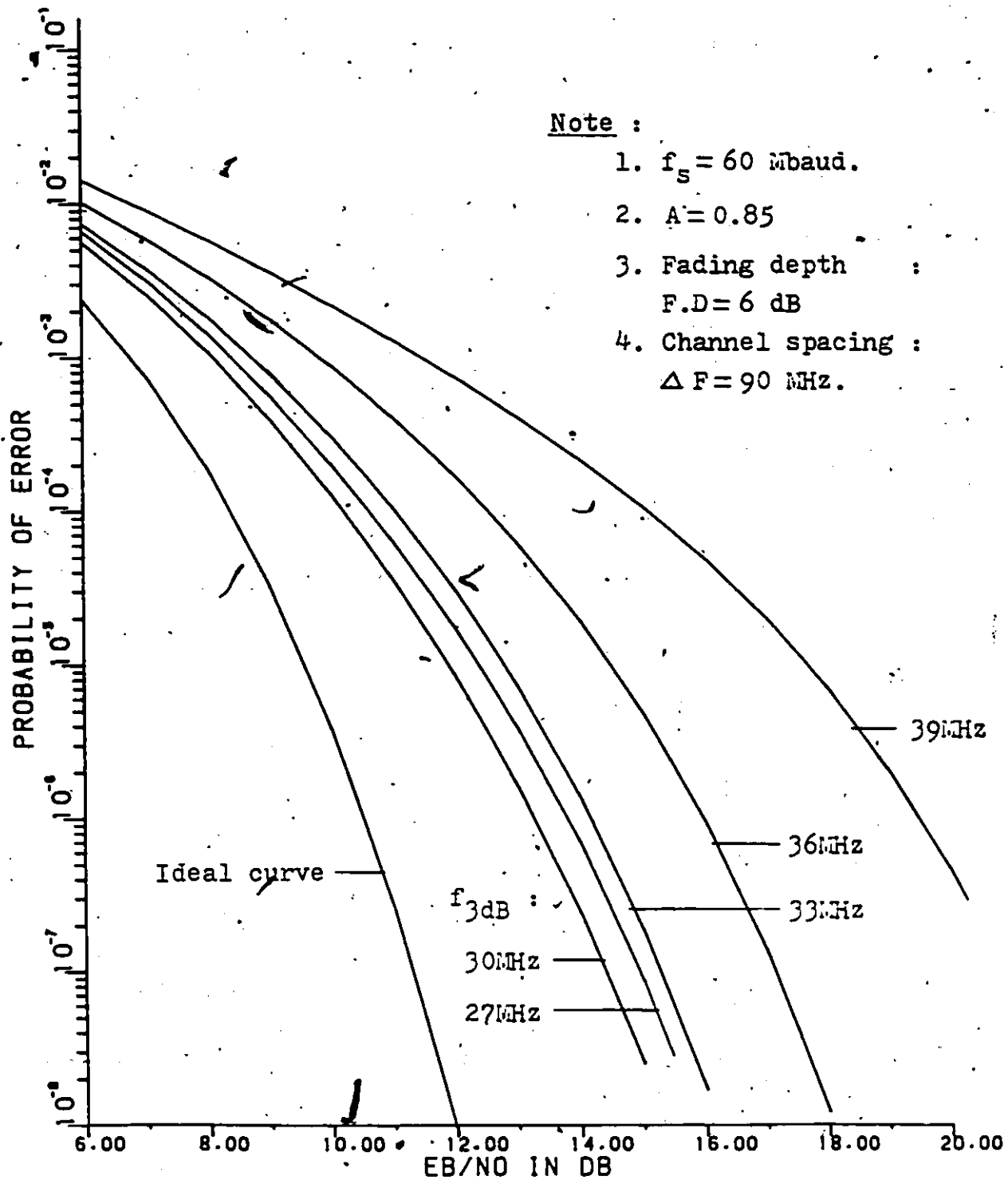


Fig.4.5(a) P_e performance of SQAM modem in a hardlimited multi-channel system (vs. f_{3dB}).

SQAM BER CURVE

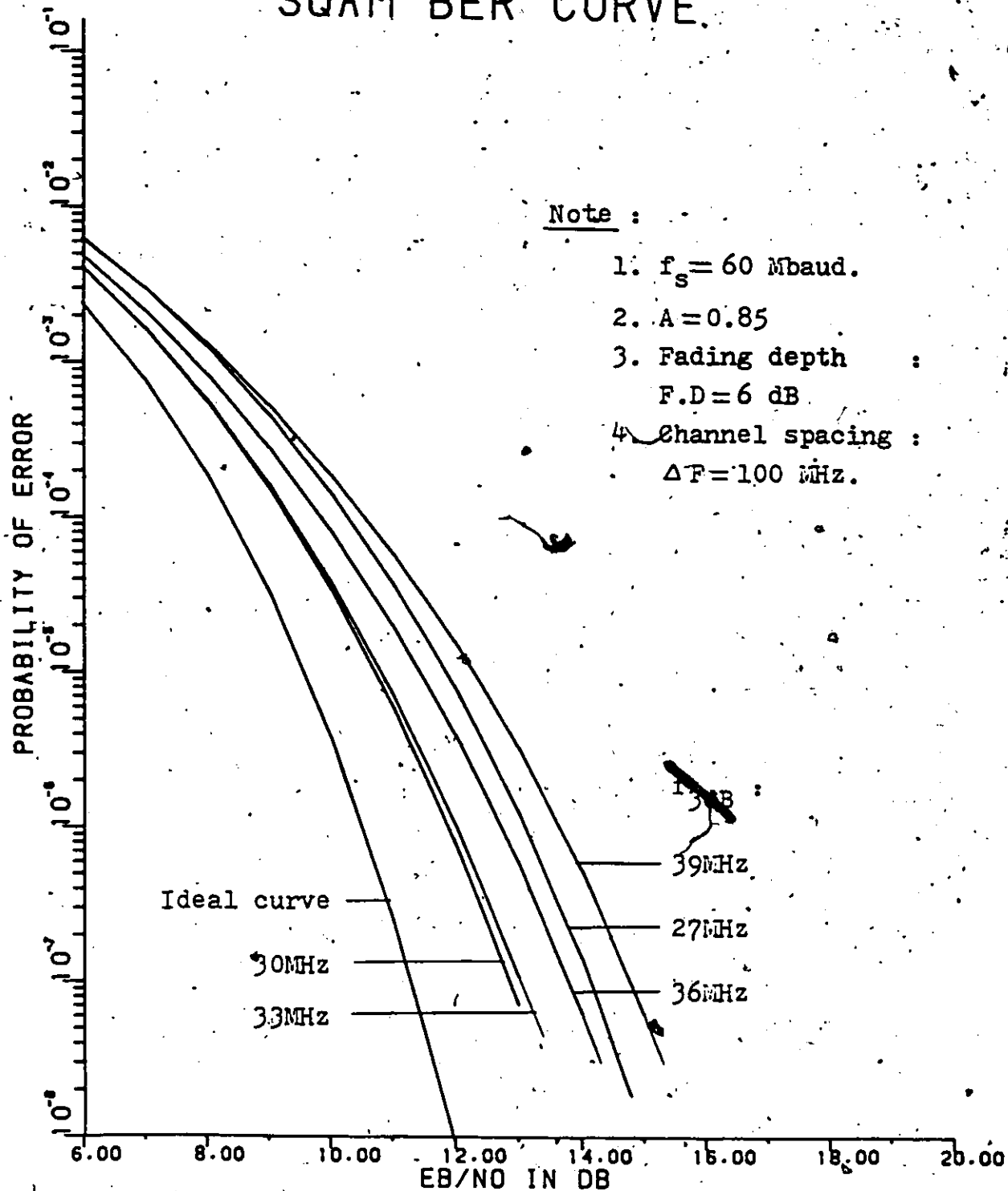


Fig.4.5(b) P_e performance of SQAM modem in a hardlimited multi-channel system (vs. f_{3dB}).

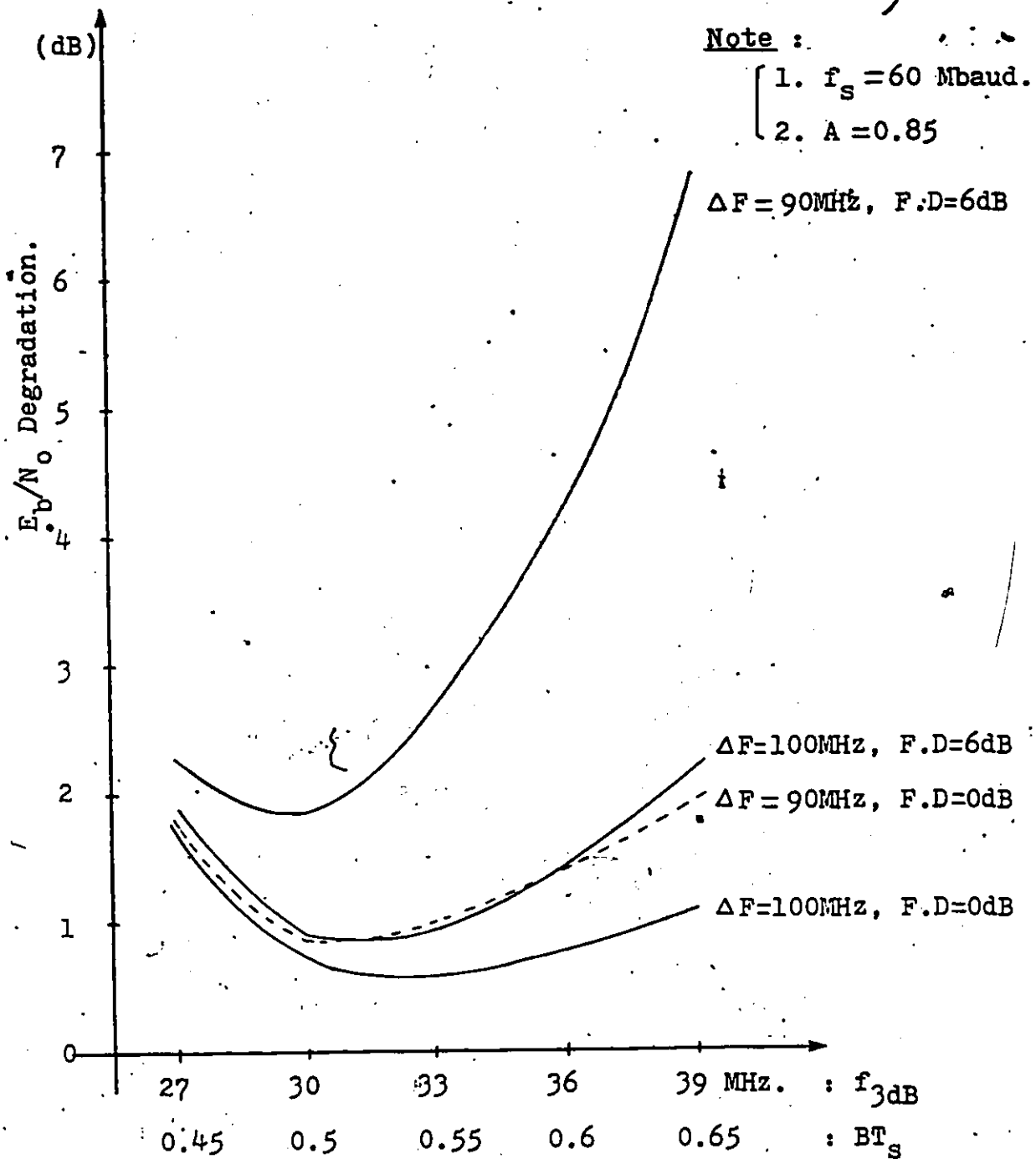


Fig.4.5(c) E_b/N_0 degradation vs. BT_s products of receive filter (5th order Butterworth LPF) in a hard-limited multi-channel SQAM system.

4.2.4 Effects of Channel Frequency Separation (Spacing)

In this simulation, we assume that the interfering signals have equal power compared to the desired signal, and the 3dB bandwidth of the receive low pass filter is 30 MHz (Nyquist minimum bandwidth). The $P(e)$ performance results of the SQAM modem for different channel spacing are shown in Fig.4.6(a). The $P(e)$ performance degradation, as a function of a normalized channel spacing (or spectral efficiency), is shown in Fig.4.6(b), where the normalized channel spacing is expressed in $\Delta F/f_b$ (i.e. channel spacing /bit rate). The performance of the SQAM modem, for a hardlimited multichannel system, is also compared to those of OQPSK, MSK and IJF-OQPSK modems.[11,16,27]. The filtering strategies, which have been used for the generation of these results, are summarized in Table 4.1. Note that for $\Delta F/f_b > 80/120$, the SQAM modem outperforms all the other schemes studied here. It is also noticed that the performance of MSK modem without transmit filters is much worse than that with transmit filters. This is so because the bandlimiting filters in the MSK transmitter confine the bandwidth of the transmitted signals, and reduce the ACI. Note that for the large channel spacings, that is, when $\Delta F/f_b > 110/120$, the performance is getting close to the performance in a single channel environment, and the ACI is predominantly caused by the spectral spreading of the modulated adjacent carriers.

SQAM BER CURVE

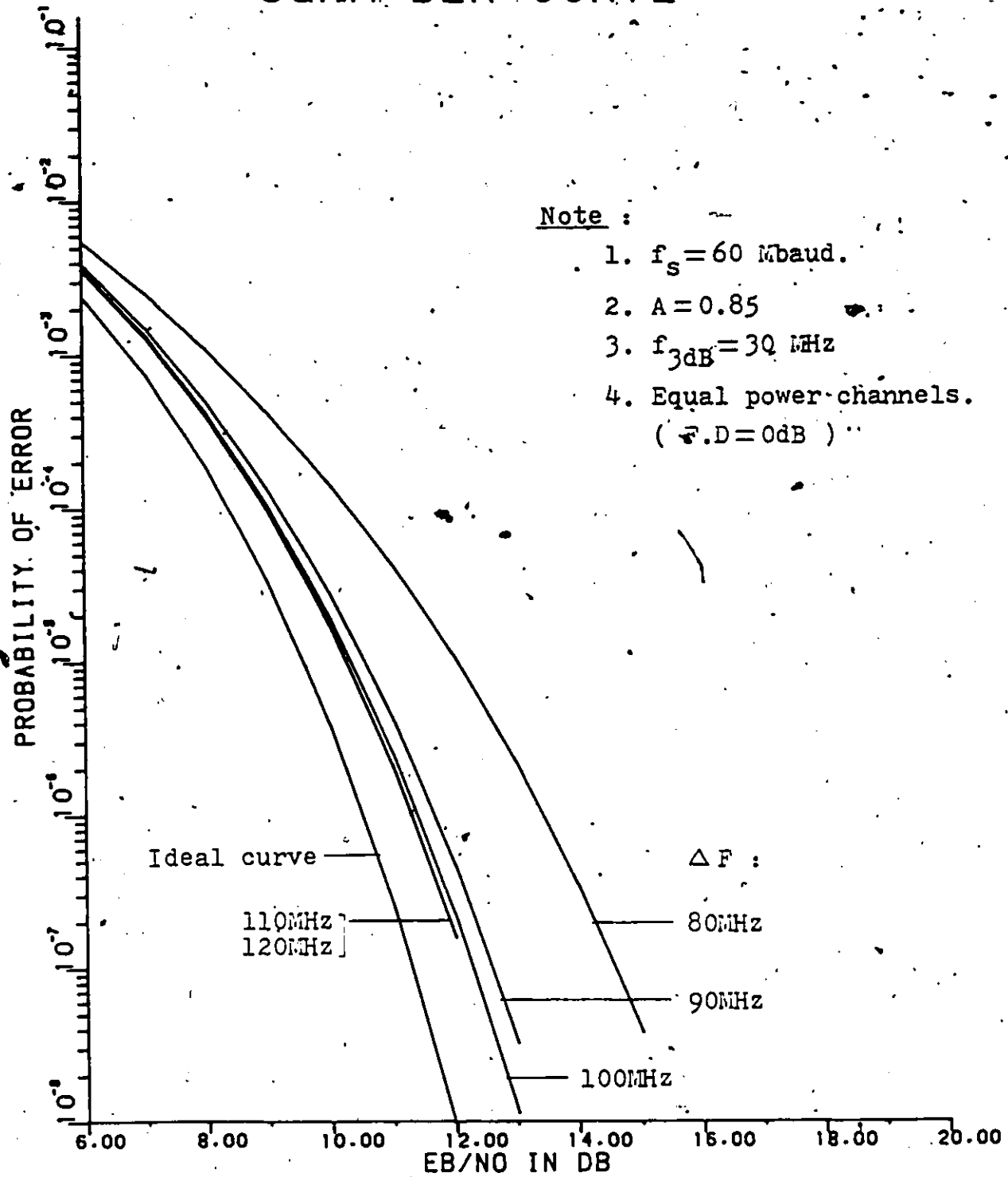
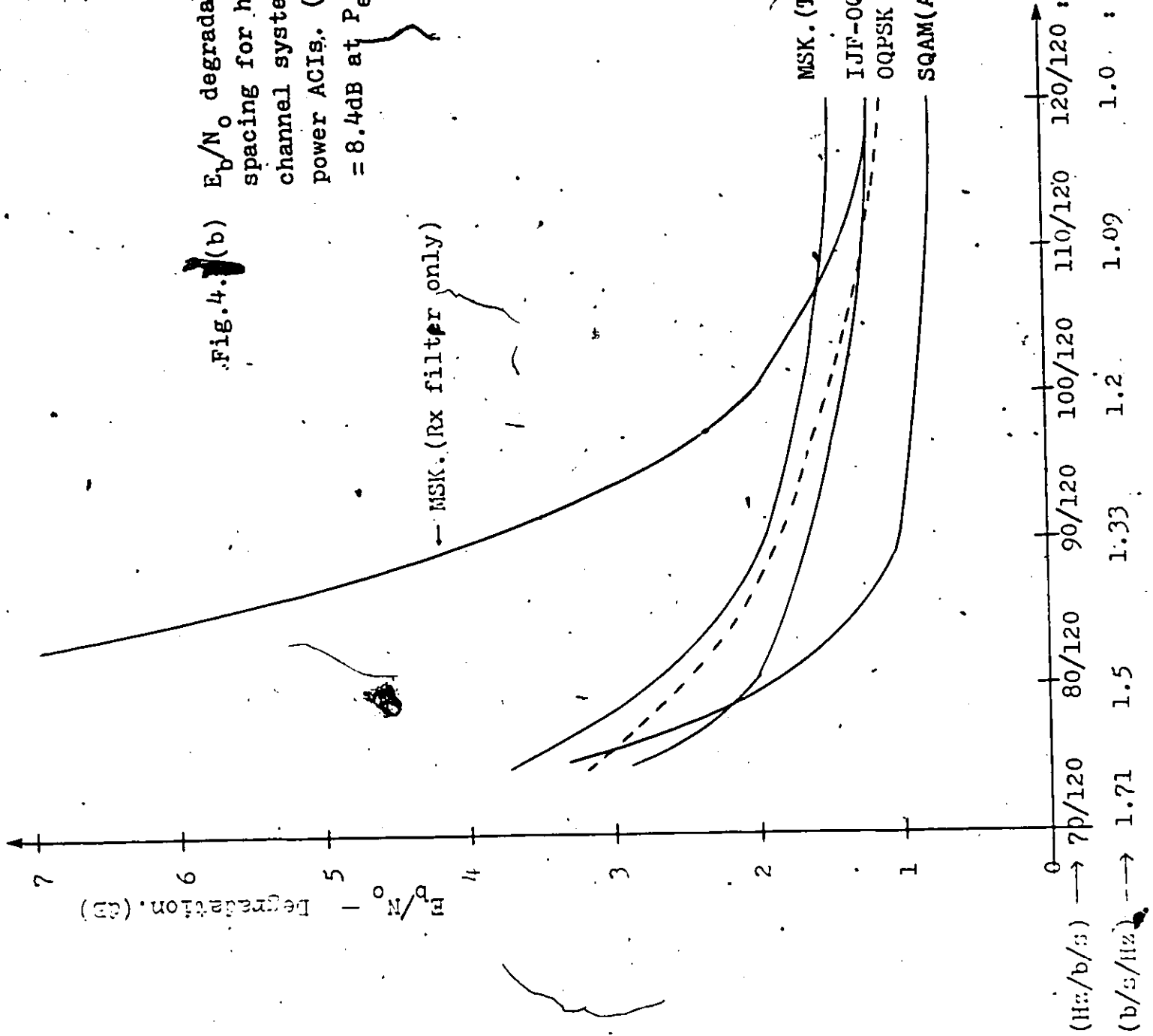


Fig.4.6(a) P_e performance of SQAM modem in a hardlimited multi-channel system (vs. ΔF).

Fig. 4.1(b) E_b/N_0 degradation* vs. channel spacing for hardlimited multi-channel system with two equal-power ACIS. (* Compared to $E_b/N_0 = 8.4\text{dB}$ at $P_e = 1 \times 10^{-4}$)



(Hz/b/s) → 70/120 80/120 90/120 100/120 110/120 120/120 ; normalized ch. spacing;
 (b/s/Hz) → 1.71 1.5 1.33 1.2 1.09 1.0 ; spectral efficiency.

Table 4.1 Filtering Strategies for Different Modems.

Modem	Transmit Filter	Receive Filter
QPSK, OQPSK	aperture equalizer ($x/\sin x$) + square-root raised-cosine filter	square-root raised- cosine filter. ($\alpha=0.4$)
MSK	5th order Butterworth LPF. ($f_{3dB}=f_s/2$)	5th order Butterworth LPF. ($f_{3dB}=f_s/2$)
SQAM (IJF-OQPSK)	Nil	5th order Butterworth LPF. ($f_{3dB}=f_s/2$)

4.2.5 Effects of Fade Depth on the Desired Signal

In our study, we assume that the desired signal (main channel) suffers fading due to the rain in the uplink, and the fade depth is varied from 0 dB to 14 dB with different channel spacings. The $P(e)$ performance results of the SQAM modem for different fade depths are shown in Figs.4.7(a)

and (b), for channel spacings $\Delta F=90$ and 100 MHz. The $P(e)$ performance degradation as a function of the fade depth are shown in Figs.4.8(a),(b), and the performance of SQAM modem is compared to those of OQPSK, MSK and IJF-OQPSK modems. Note that SQAM modem followed by IJF-OQPSK modem outperforms the other modems for every fade depth. This can be explained from the fact that the out-of-band energy of SQAM signal, for linearly and nonlinearly amplified systems, is much lower than those of other signals. [Refer to Figs.2.10(a) and (b).] Thus, the SQAM signal causes less ACI compared to other signals. It is also noticed that in a narrow channel spacing or at low levels of fade depth, the OQPSK modem outperforms the MSK modem. This is so because in MSK the sidelobe roll-off is faster, but its mainlobe bandwidth is 50 % wider than that of OQPSK. Note that in the ACI environment, the performance of MSK modem without transmit filter is much worse than that with transmit filter, especially at high levels of fade depths or with narrow channel spacing. Simulated eye patterns of the demodulated and filtered MSK, IJF-OQPSK and SQAM signals are shown in Figs.4.9(a),(b) and (c) respectively.

SQAM BER CURVE

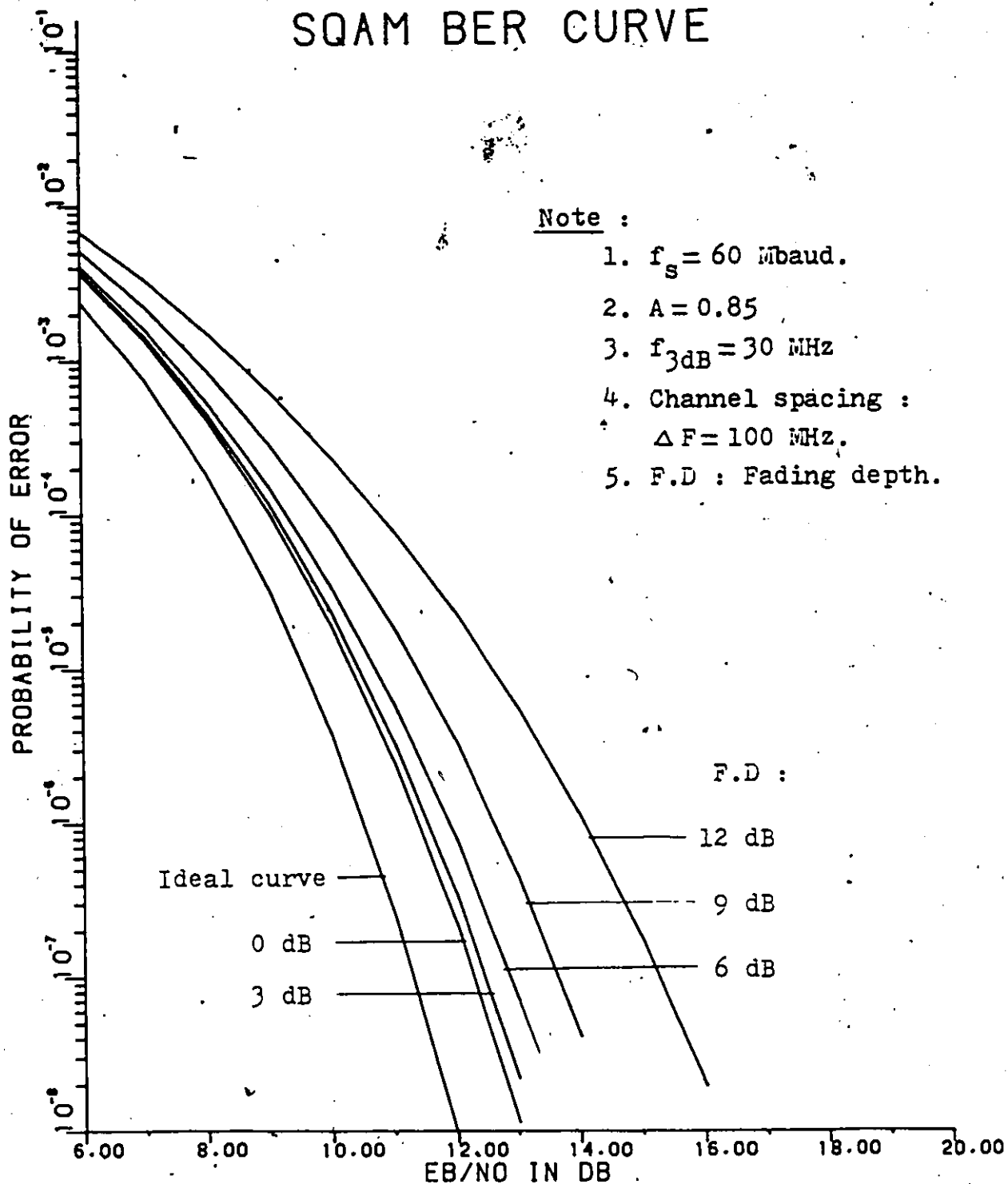


Fig.4.7(a) P_e performance of SQAM modems in a hardlimited multi-channel system (vs. F.D).

SQAM BER CURVE

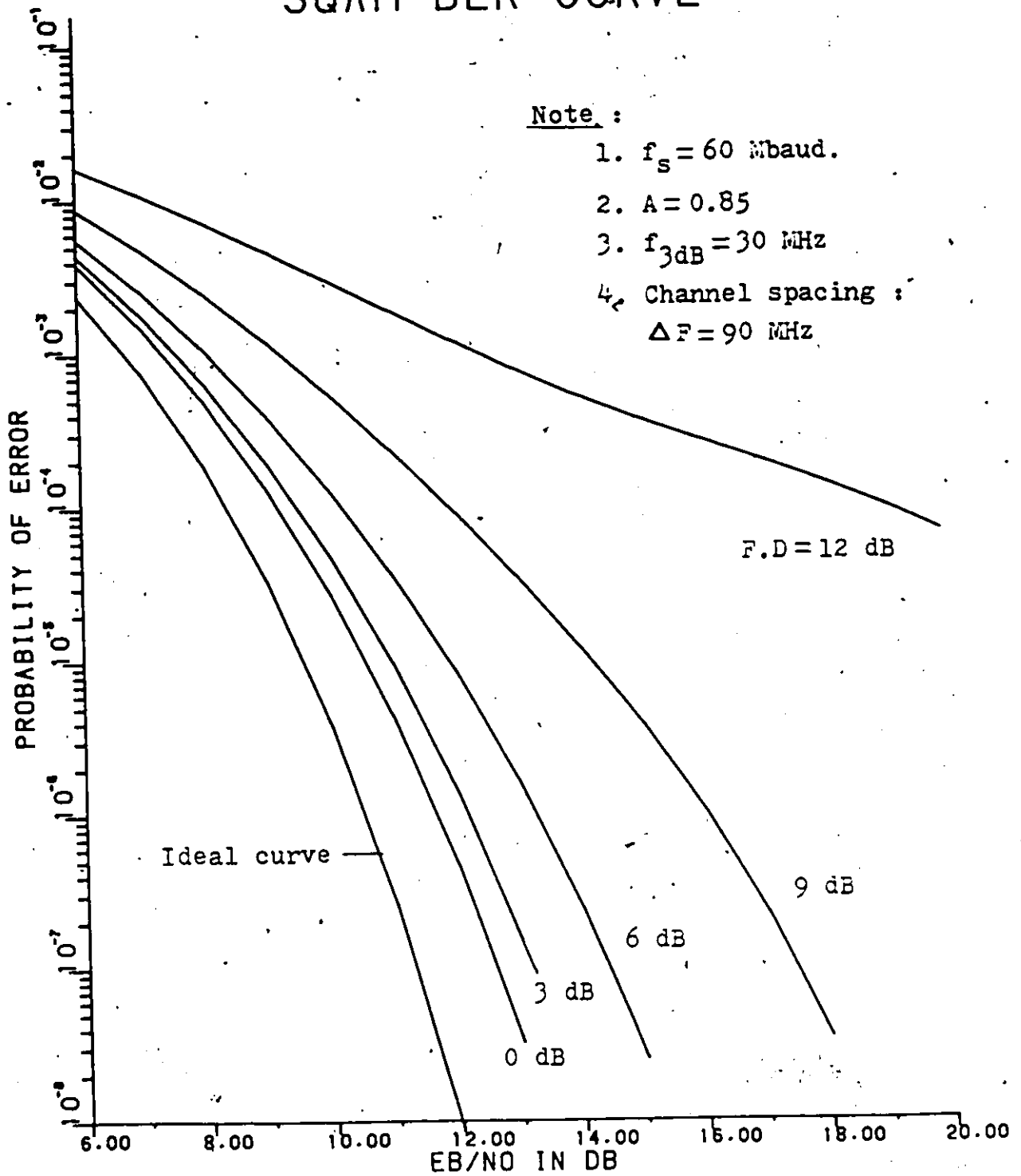


Fig.4.7(b) P_e performance of SQAM modem in a hardlimited multi-channel system (vs. F.D.).

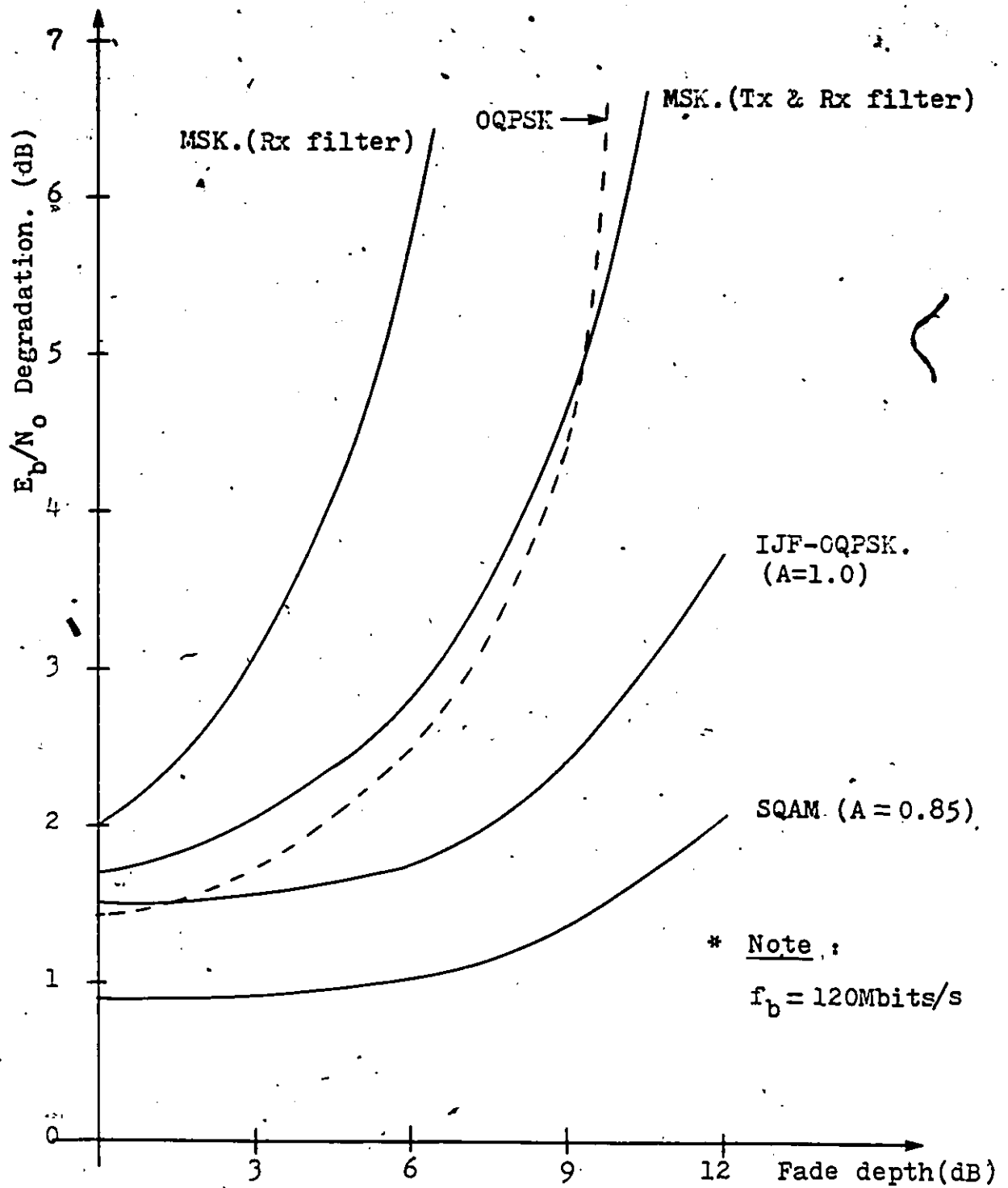


Fig.4.8(a) E_b/N_0 degradation vs. fade depth of the desired channel for hardlimited multichannel system. (Channel spacing : $\Delta F = 100$ MHz)

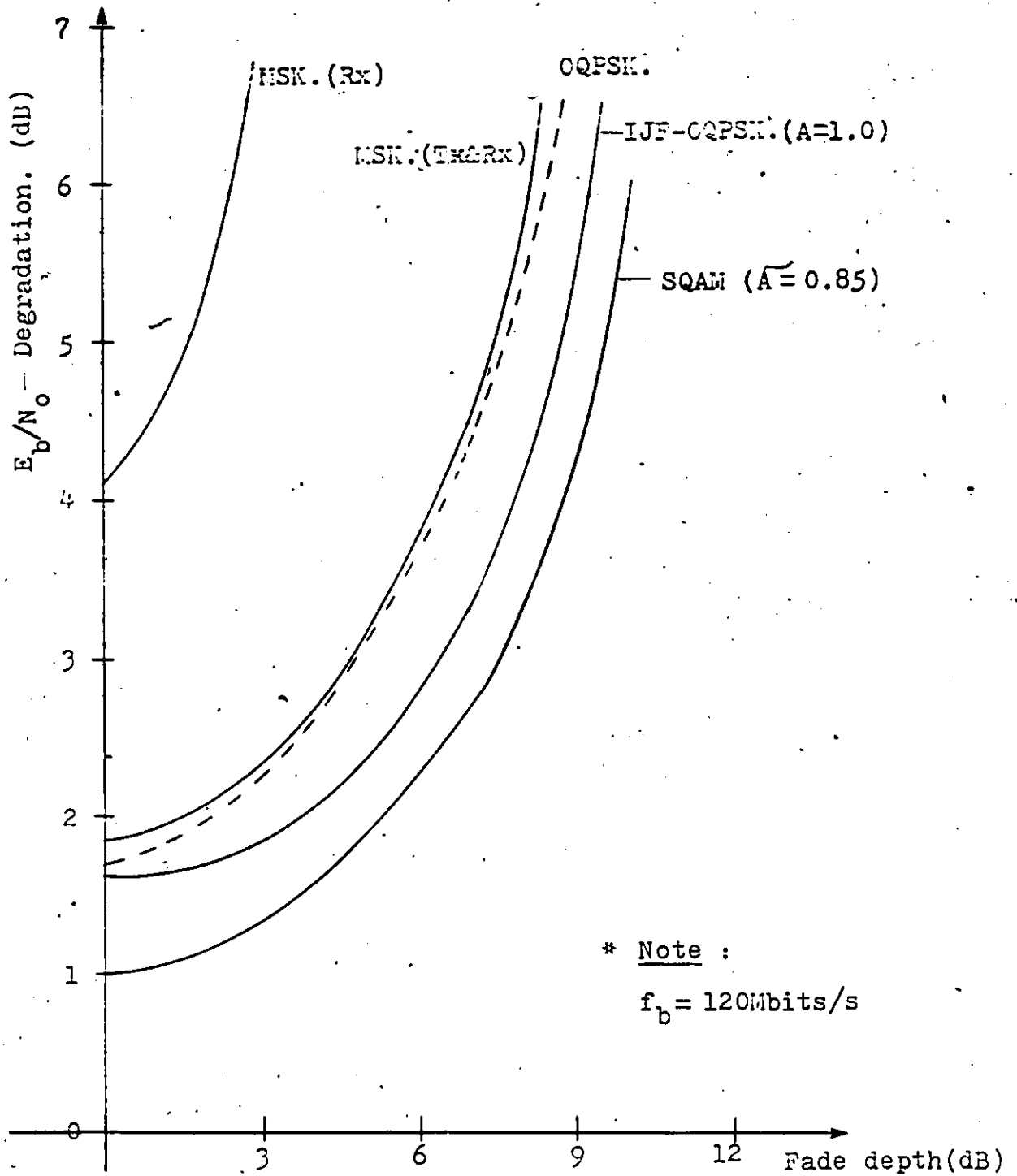
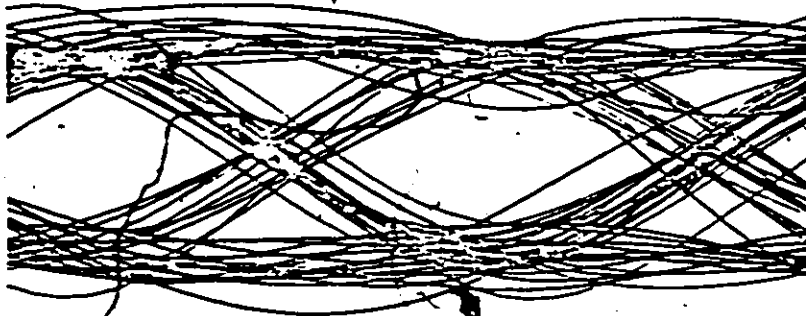
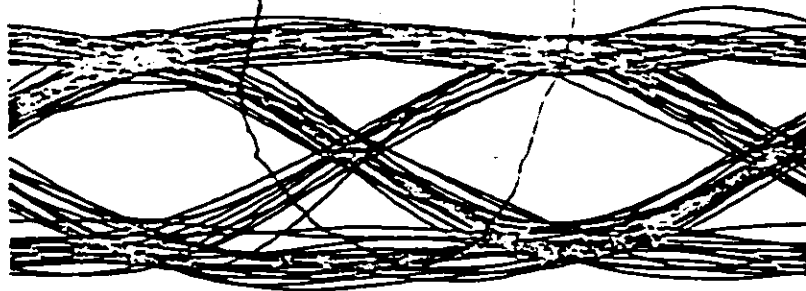


Fig.4.8(b) E_b/N_0 degradation vs. fade depth of the desired channel for hardlimited multichannel system.
 (Channel spacing : $\Delta F = 90 \text{ MHz}$)

(a) MSK..



(b) IJF-QPSK (or SQRC)



(c) SQAM ($A=0.85$)

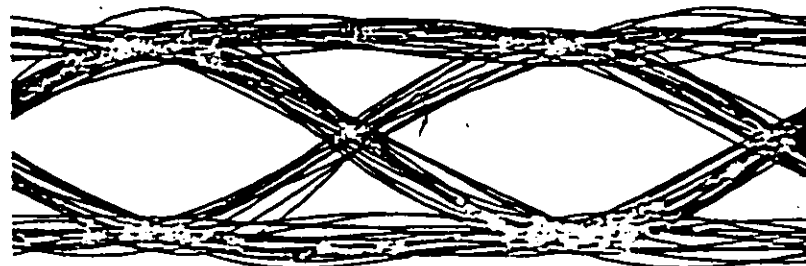


Fig. 4.9 Eye patterns of demodulated and filtered MSK , IJF-QPSK and SQAM signals in a hardlimited multi-channel system ($\Delta F=100\text{MHz}$, F.D=6 dB).

4.2.6 Effects of CCI on P(e) Performance of SQAM Modems

In a frequency-reuse communication system, co-channel interference (CCI) is one of the major sources of the performance impairment. [13,15,17]. A simulation model of a co-channel system is shown in Fig.4.10, while its frequency allocation is shown in Fig.4.11. In this simulation, an interfering channel, centered at the same carrier frequency as the main channel (i.e., $\Delta F=0$), is introduced, and 5th order phase-equalized Butterworth LPFs are used in the SQAM receiver. The P(e) performance results of the SQAM modem at different levels of main-channel carrier-to-cochannel interference (C/I) ratio, are shown in Fig.4.12. The P(e) performance degradation of the SQAM modem, as a function of C/I ratio for different BT_s product, is shown in Fig.4.13. It is noticed that ISI, in addition to CCI, is also a major source of the performance impairment. The P(e) performance degradation of the SQAM modem as a function of C/I ratio is compared to those of OQPSK, MSK and IJF-OQPSK modems in Fig.4.14. Note that SQAM outperforms all the other modems studied here. It is also noticed that MSK modem without transmit filter outperforms the one with a transmit filter. This is so because as the bandlimiting of the filter becomes severe, the ISI increases, thus, the performance is degraded in a CCI environment. [Refer to Fig.3.13 and eq.(4.12)'.]

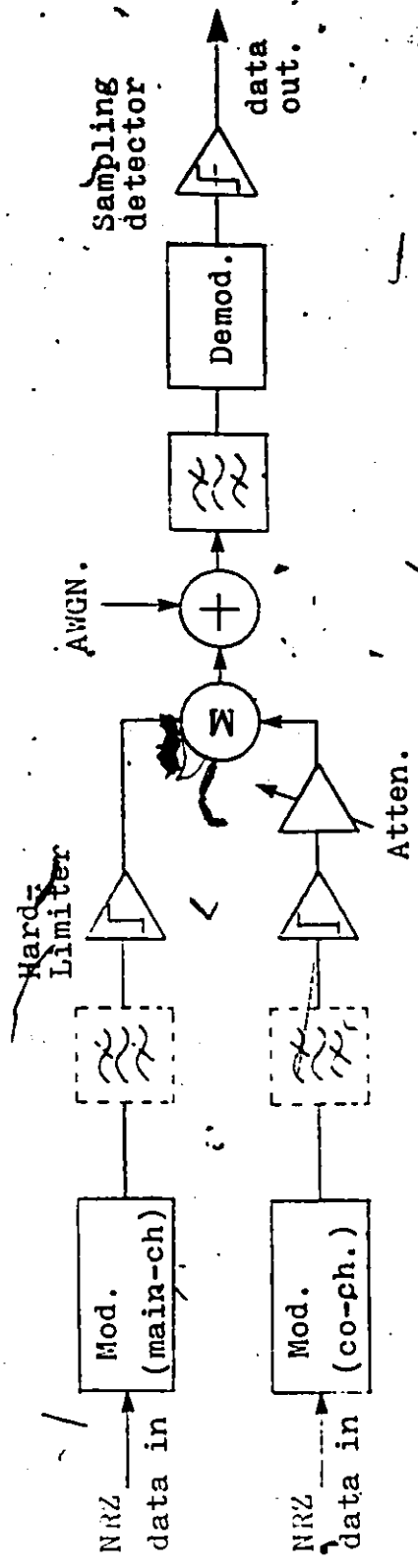


Fig.4.10: A simulation model of co-channel system.

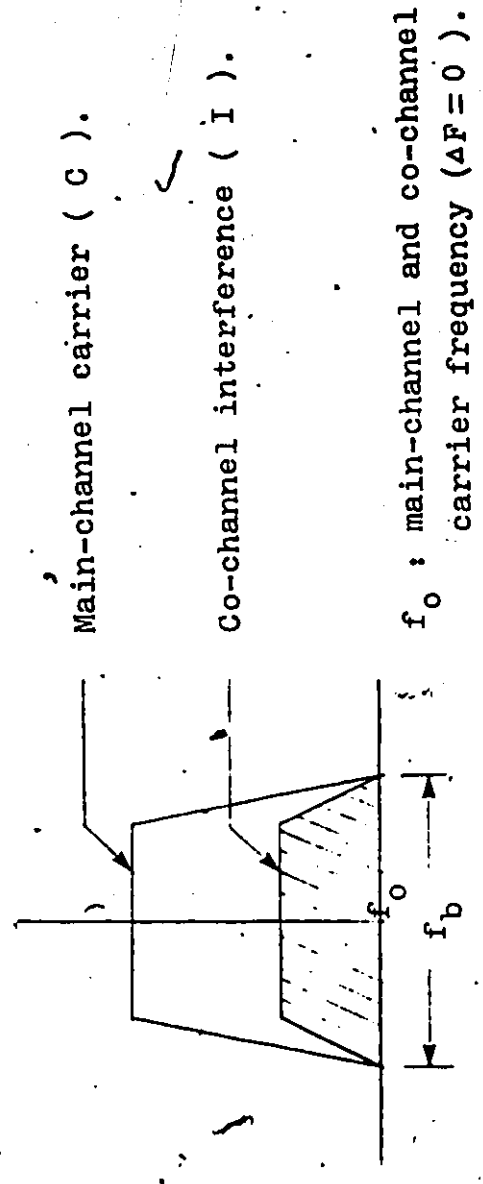


Fig.4.11 Frequency allocation for co-channel system.

SQAM BER CURVE

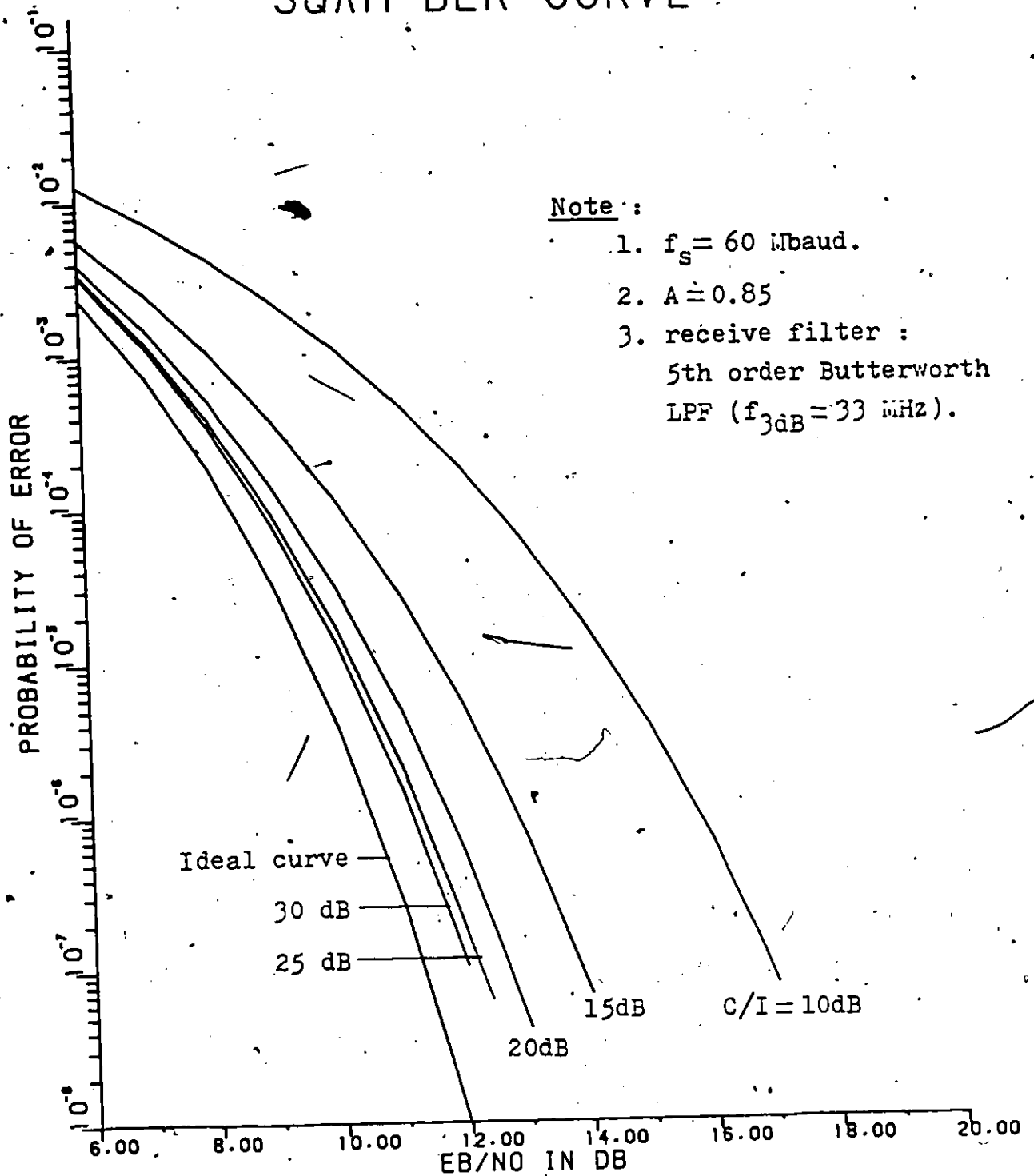


Fig.4.12 P_e performance of SQAM modem in a hardlimited co-channel system (vs. C/I).

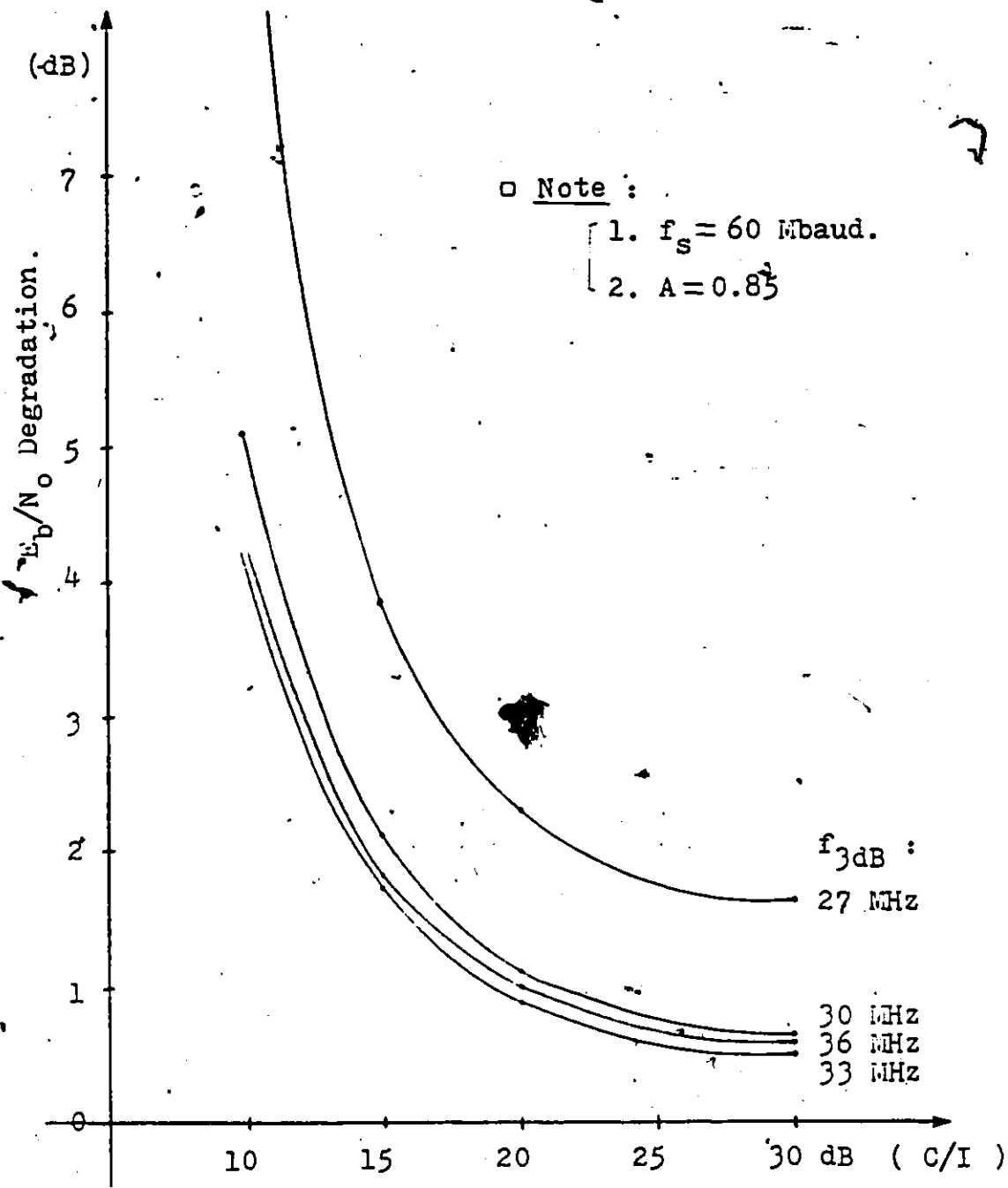
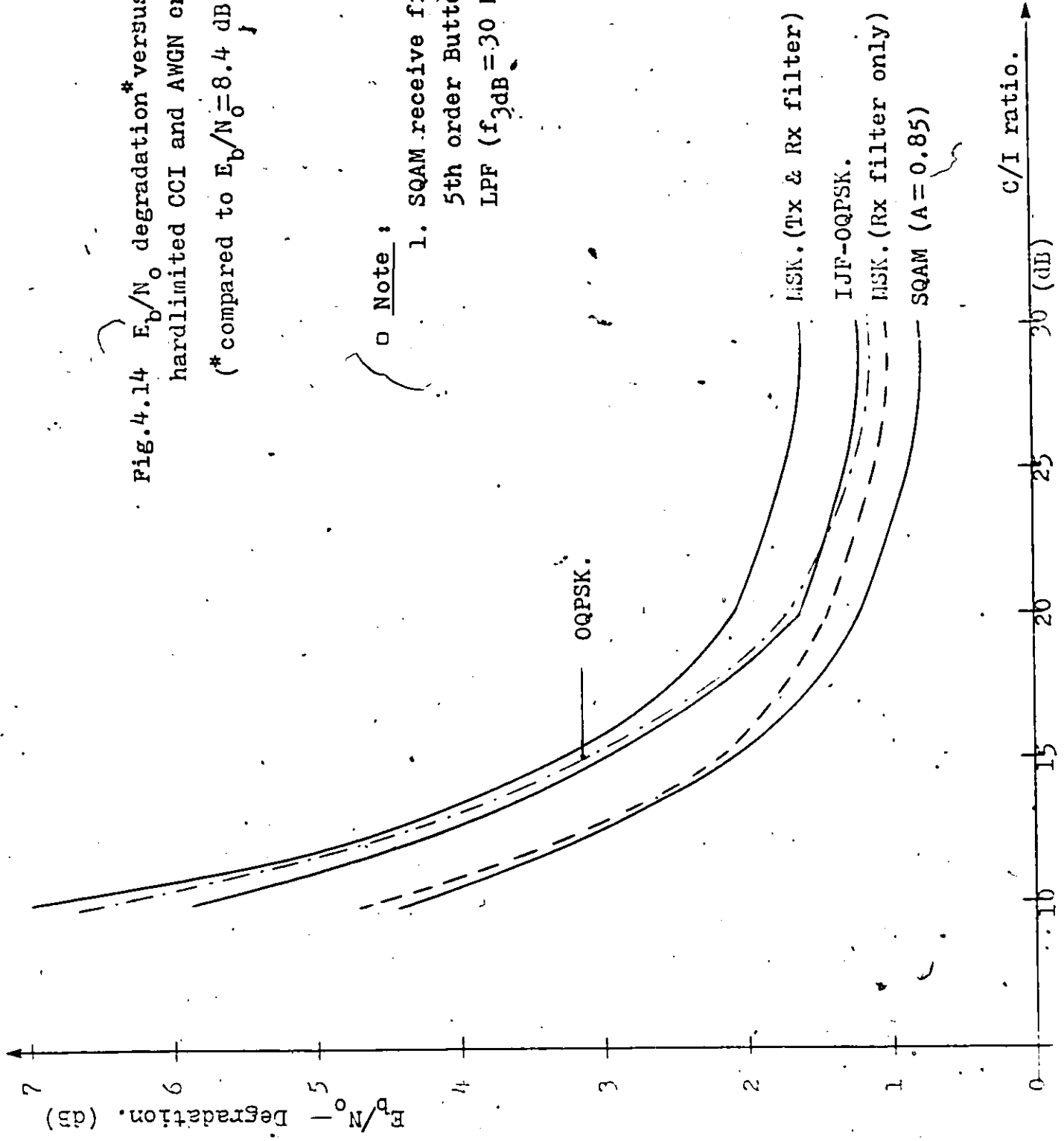


Fig.4.13 E_b/N_0 degradation vs. C/I ratio for different f_{3dB} of receive filter in a hardlimited co-channel SQAM system.

Fig. 4.14 E_b/N_0 degradation* versus C/I in a hardlimited CCI and AWGN environment.
 (* compared to $E_b/N_0 = 8.4$ dB at $P_c = 1 \times 10^{-4}$)



Note :

1. SQAM receive filter : 5th order Butterworth LPF ($f_{3dB} = 30$ MHz).

Chapter V

RECOMMENDED FURTHER RESEARCH

For a good power efficiency, a constant envelope modulation technique may be preferable, and this leads to the use of frequency modulations. In FM schemes, to narrow the power spectrum, a pulse shaping filter (i.e. premodulation filter) prior to the frequency modulator is required. In TFM (or CORPSK), a premodulation filter, composed of a correlative encoder and an aperture-equalized raised-cosine filter, is used to achieve smooth phase transitions, and thus good spectral properties. However the implementation of the filter is complicated. The impulse response of the premodulation filter in TFM is shown in Fig.5.1, and the block diagram of TFM transmitter is shown in Fig.5.2.

In SQAM, the phase is a smooth function of time, and correlated between the consecutive symbols. (Refer to section 2.2.) The impulse response of SQAM signal encoder $s(t)$ is shown in Fig.2.1.(b), where its generation is quite simple as shown in Fig.2.3.

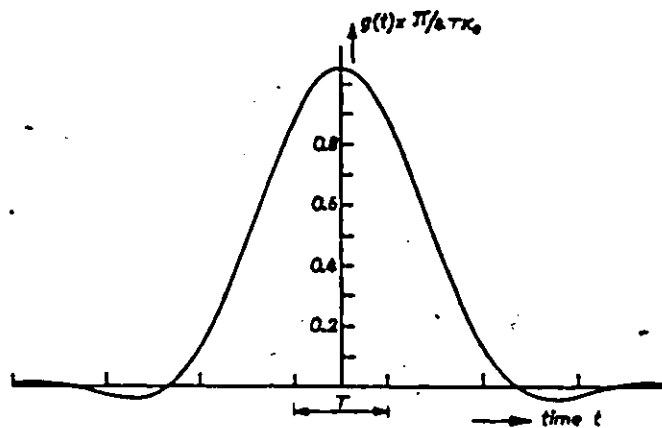


Fig.5.1 Impulse response of TFM premodulation filter.

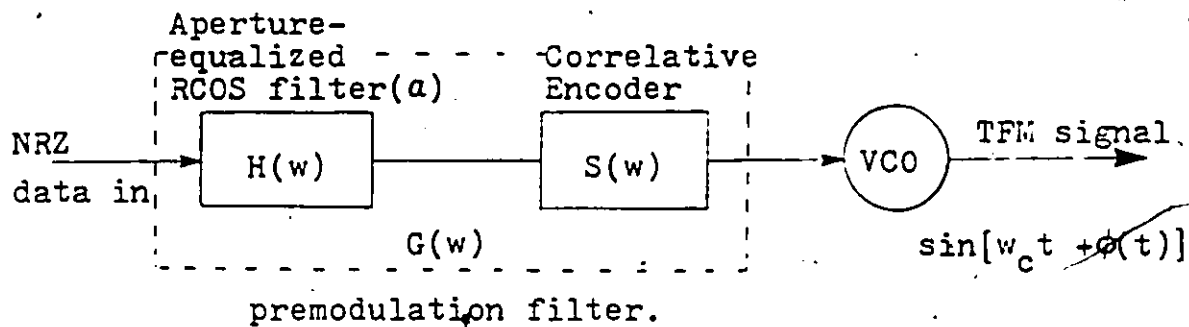
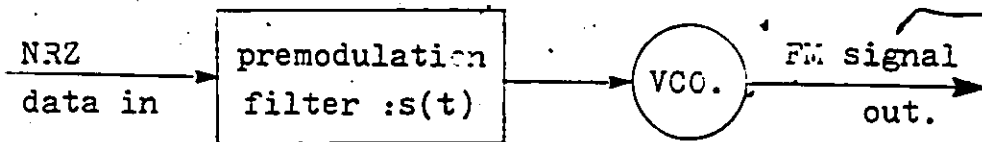


Fig.5.2 Block diagram of TFM transmitter.

In SQAM, the phase behavior is very similar to TFM for $A=1.0$, and similar to CCPSK[20] for $A<1.0$. Hence, if we use the SQAM signal encoder as a premodulation filter in digital FM scheme, the resulting frequency modulated signal will retain a constant envelope and good spectral properties. Fig.5.3 shows the suggested block diagram.



($s(t)$: Impulse response defined in eq.(2.3).)

Fig.5.3 Digital FM transmitter combined with SQAM encoder.

In order to improve further the spectral properties of the SQAM signals, 'duo-binary SQAM technique', where SQAM baseband signal processing is combined with the duo-binary ($1+D$; class I) technique [21], is suggested. A duo-binary SQAM encoder is composed of a SQAM encoder and a duo-binary encoder. The block diagram of a duo-binary SQAM encoder is shown in Fig.5.4. The power spectral density function of the duo-binary SQAM signal is derived and plotted in Appendix B. This result shows that duo-binary SQAM signals provide a lower out-of-band energy and a faster spectral roll-off, compared to conventional SQAM signals.

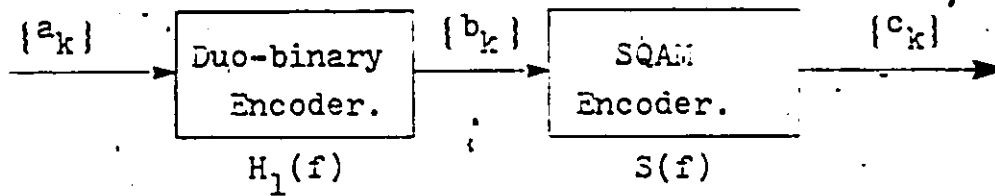


Fig.5.4 Block diagram of Duo-binary SQAM Encoder.

A further study of modulated duobinary SQAM signals, being a similar approach to the previous chapters, could lead to additional valuable results.

We also suggest an extension of the pulse overlapping interval (i.e. multi-symbol interval) in SQAM systems, or a partial response[25] SQAM for a better power spectrum.

Chapter VI

CONCLUSION

A spectral and power efficient modulation technique- SQAM has been introduced. In SQAM, by superposing two baseband waveshapes which have different symbol-intervals and weighting factors, a good power and spectral efficiency was achieved.

In the first part of this thesis, a power spectral density function of the SQAM signal was derived, and the spectral characteristics and the $P(e)$ performance in a single-channel environment were compared with those of other schemes. Experimental and simulation results showed that SQAM signals have significant spectral advantages over QPSK, OQPSK and MSK signals and better $P(e)$ performance than other constant envelope modulation schemes, such as MSK and TFM. In SQAM, the envelope fluctuation and power spectrum can be controlled to minimize the $P(e)$ performance degradation in a particular operating environment, by adjusting the amplitude parameter A .

In the second part of this thesis, the performance of a SQAM modem, in a nonlinearly amplified multichannel environment, in the presence of AWGN, ISI, ACI and/or CCI,

was investigated and compared to those of OQPSK, MSK and IJF-OQPSK modems. The effects of ACI and CCI on the performance of SQAM modem were investigated under different channel conditions, such as different channel spacing, filter bandwidth symbol duration product (BT_s) and flat fade depth. It has been found that our SQAM modem outperforms OQPSK, MSK and IJF-OQPSK modems for certain system environments, and that ACI is one of the major sources of the performance impairment of multichannel systems, especially under flat fadings. It was also found that the proper selection of modulation techniques, type of modem filters (transmit and receive) and their BT_s values can minimize the degradation of $P(e)$ performance caused by ACI or CCI.

These desirable performance characteristics, combined with the simple hardware implementation of SQAM modems, may lead to numerous satellite and terrestrial radio systems applications.

Appendix A

DERIVATION OF THE PSD OF SQAM SIGNAL

(Equation (2.22) in Chapter 2.)

The impulse method [19] is applied to derive the frequency spectrum of the SQAM baseband signals. This method uses the differentiation and the time domain shift properties of the Fourier transform. In (2.3) and (2.4), a SQAM double-interval pulse is defined as :

$$s(t) = g(t) + d(t) \quad (\text{A.1})$$

First, consider the double-interval raised-cosine pulse $g(t)$ of the SQAM signal :

$$g(t) = \begin{cases} 1/2 (1 + \cos \pi t / T_s) & |t| \leq T_s \\ 0 & |t| > T_s \end{cases} \quad (\text{A.2})$$

(See Fig.A.1.)

Now differentiate the pulse $g(t)$ a sufficient number of times to produce impulse functions. The derivatives of $g(t)$ with respect to 't' are given by :

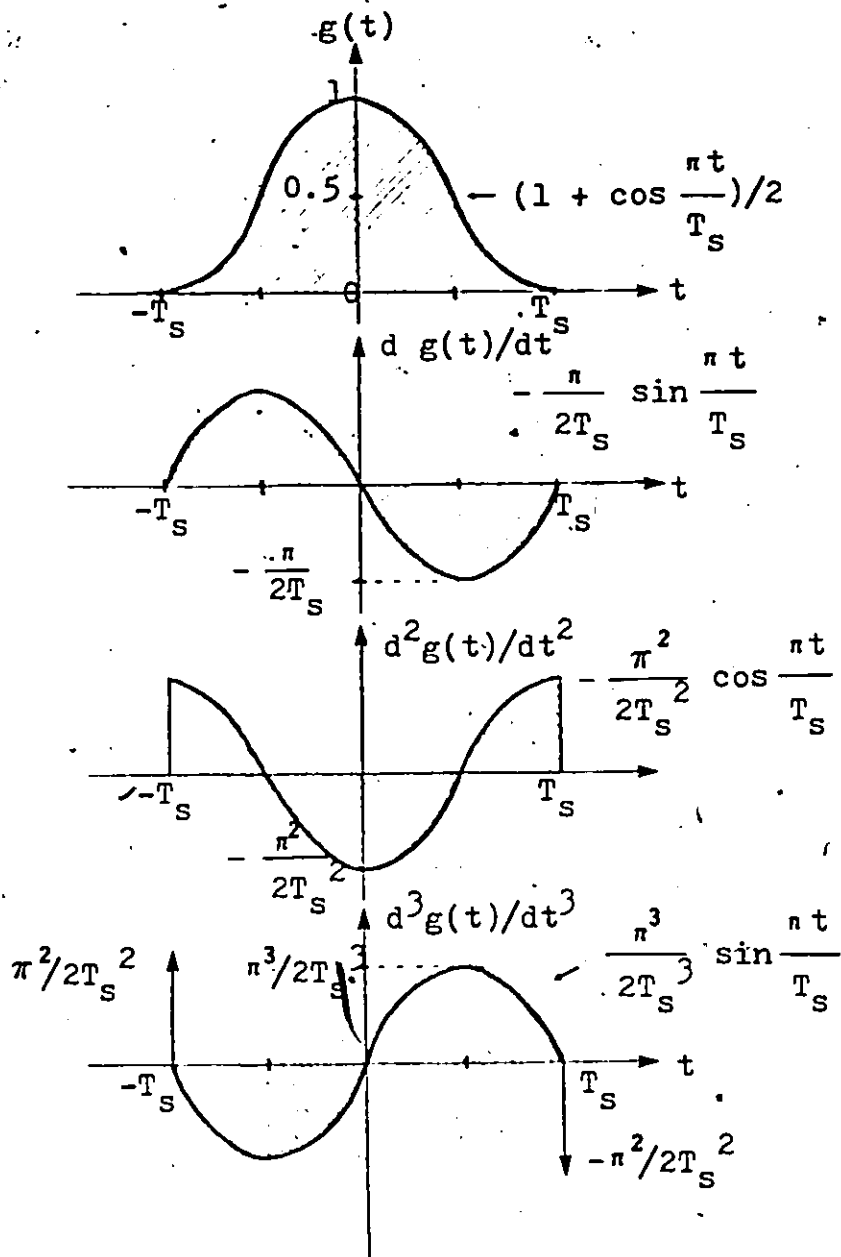


Fig.A.1. A double-interval raised-cosine pulse and its first three derivatives.

$$\frac{dg(t)}{dt} = \begin{cases} \frac{\pi}{2T_s} \cdot \sin \frac{\pi t}{T_s} & |t| \leq T_s \\ 0 & |t| > T_s \end{cases} \quad (\text{A.3})$$

$$\frac{d^2g(t)}{dt^2} = \begin{cases} -\frac{\pi^2}{2T_s^2} \cdot \cos \frac{\pi t}{T_s} & |t| \leq T_s \\ 0 & |t| > T_s \end{cases} \quad (\text{A.4})$$

$$\frac{d^3g(t)}{dt^3} = \begin{cases} \frac{\pi^3}{2T_s^3} \cdot \sin \frac{\pi t}{T_s} - \frac{\pi^2}{2T_s^2} [\delta(t-T_s) - \delta(t+T_s)] & |t| \leq T_s \\ 0 & |t| > T_s \end{cases} \quad (\text{A.5})$$

From eq. (3) and (5)

$$\frac{d^3g(t)}{dt^3} = \begin{cases} -\frac{\pi^2}{T_s^2} \cdot \frac{dg(t)}{dt} + \frac{\pi^2}{2T_s^2} [\delta(t+T_s) - \delta(t-T_s)] & |t| \leq T_s \\ 0 & |t| > T_s \end{cases} \quad (\text{A.6})$$

From differential and time shift properties of the Fourier transforms (i.e., $F\{\frac{d^n a(t)}{dt^n}\} = (j2\pi f)^n A(f)$ and $F\{a(t - t_0)\} = A(f)e^{-j2\pi f t_0}$), we can rewrite (6) as:

$$\begin{aligned} (j2\pi f)^3 G(f) &= -\frac{\pi^2}{T_s^2} (j2\pi f) G(f) + \frac{\pi^2}{2T_s^2} (e^{j2\pi f T_s} - e^{-j2\pi f T_s}) \\ &= -\frac{\pi^2}{T_s^2} (j2\pi f) G(f) + \frac{\pi^2}{2T_s^2} (j2) \sin 2\pi f T_s \end{aligned} \quad (\text{A.7})$$

Solving for $G(f)$, we find the frequency spectrum of the double-interval raised-cosine pulse to be:

$$G(f) \left[-(2\pi f)^3 + \frac{\pi^2}{T_s^2} (2\pi f) \right] = \frac{\pi^2}{T_s^2} \cdot \sin 2\pi f T_s \quad (\text{A.8})$$

$$\begin{aligned} \therefore G(f) &= \frac{\pi^2/T_s^2}{\pi^2/T_s^2 - (2\pi f)^2} \cdot \frac{\sin 2\pi f T_s}{2\pi f} \\ &= \frac{T_s}{1 - 4f^2 T_s^2} \cdot \frac{\sin 2\pi f T_s}{2\pi f T_s} \end{aligned} \quad (\text{A.9})$$

Now let's derive the frequency spectrum of the weighted single-interval raised-cosine pulse $d(t)$ shown in Fig.A.2.

$$d(t) = \begin{cases} -\frac{1-A}{2} \left(1 - \cos \frac{2\pi t}{T_s} \right) & |t| \leq T_s \\ 0 & |t| > T_s \end{cases} \quad (\text{A.10})$$

The derivatives of $d(t)$ with respect to t are given by:

$$\frac{d d(t)}{dt} = \begin{cases} -\frac{1-A}{2} \cdot \frac{2\pi}{T_s} \cdot \sin \frac{2\pi t}{T_s} & |t| \leq T_s \\ 0 & |t| > T_s \end{cases} \quad (\text{A.11})$$

$$\frac{d^2 d(t)}{dt^2} = \begin{cases} -\frac{1-A}{2} \left(\frac{2\pi}{T_s} \right)^2 \cdot \cos \frac{2\pi t}{T_s} & |t| \leq T_s \\ 0 & |t| > T_s \end{cases} \quad (\text{A.12})$$

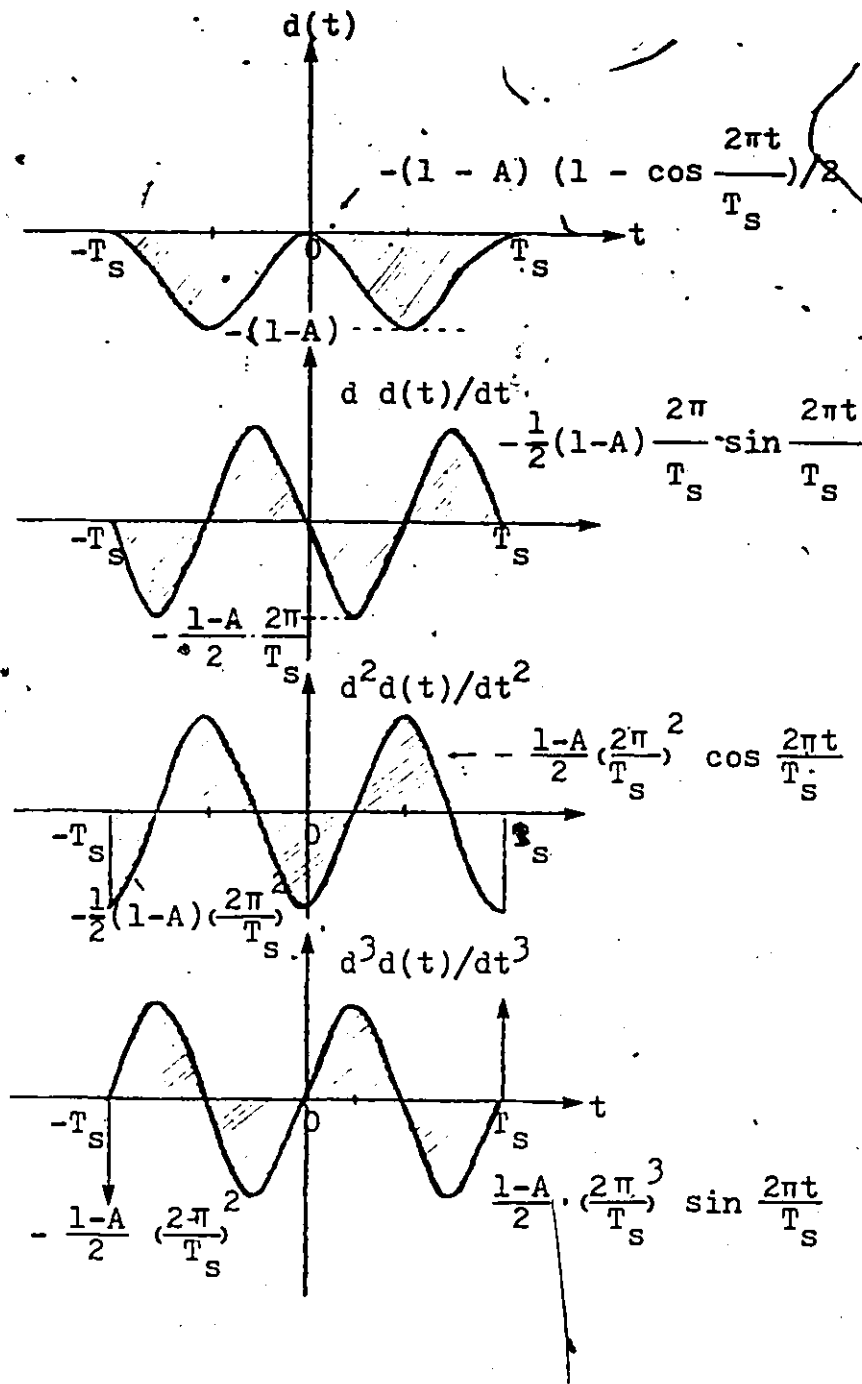


Fig.A.2. A weighted single-interval raised-cosine pulse and its first three derivatives.

$$\frac{d^3 d(t)}{dt^3} = \begin{cases} \frac{1-A}{2} \left(\frac{2\pi}{T_s}\right)^2 \left\{ \frac{2\pi}{T_s} \cdot \sin \frac{2\pi t}{T_s} + [\delta(t-T_s) - \delta(t+T_s)] \right\} & |t| \leq T_s \\ 0 & |t| > T_s \end{cases} \quad (\text{A.13})$$

From eq. (11) and (13)

$$\frac{d^3 d(t)}{dt^3} = -\left(\frac{2\pi}{T_s}\right)^2 \frac{d d(t)}{dt} - \frac{1-A}{2} \left(\frac{2\pi}{T_s}\right)^2 [\delta(t+T_s) - \delta(t-T_s)] \quad (\text{A.14})$$

From properties of Fourier transform, eq. (14) can be rewritten as:

$$(j2\pi f)^3 D(f) = -\left(\frac{2\pi}{T_s}\right)^2 (j2\pi f) D(f) - \frac{1-A}{2} \left(\frac{2\pi}{T_s}\right)^2 (j2) \sin 2\pi f T_s \quad (\text{A.15})$$

Solving for D(f)

$$\begin{aligned} D(f) [-(2\pi f)^3 + \left(\frac{2\pi}{T_s}\right)^2 2\pi f] &= -(1-A) \left(\frac{2\pi}{T_s}\right)^2 \sin 2\pi f T_s \\ \therefore D(f) &= \frac{-(1-A) \left(\frac{2\pi}{T_s}\right)^2 \sin 2\pi f T_s}{\left(\frac{2\pi}{T_s}\right)^2 - (2\pi f)^2} \quad (\text{A.16}) \\ &= \frac{-(1-A) T_s}{1 - f^2 T_s^2} \frac{\sin 2\pi f T_s}{2\pi f T_s} \end{aligned}$$

As the frequency spectrum of s(t) is given by:

$$S(f) = G(f) + D(f) \quad (\text{A.17})$$

$$\therefore S(f) = \left(\frac{T_s}{1 - 4f^2 T_s^2} + \frac{(A-1) T_s}{1 - f^2 T_s^2} \right) \frac{\sin 2\pi f T_s}{2\pi f T_s} \quad (\text{A.18})$$

and

$$S(0) = A T_s \quad (\text{A.19})$$

Therefore the normalized PSD function of the SQAM signal $s(t)$ is :

$$\therefore \left| \frac{S(f)}{S(0)} \right|^2 = \frac{1}{A^2} \left(\frac{1}{1 - 4f^2 T_s^2} + \frac{A-1}{1 - f^2 T_s^2} \right)^2 \left(\frac{\sin 2\pi f T_s}{2\pi f T_s} \right)^2 \quad (\text{A.20})$$

Appendix B
POWER SPECTRUM OF DUOBINARY SQAM

B.1 DUO-BINARY ENCODER

The block diagram of the duo-binary encoder is shown in Fig.B.1..

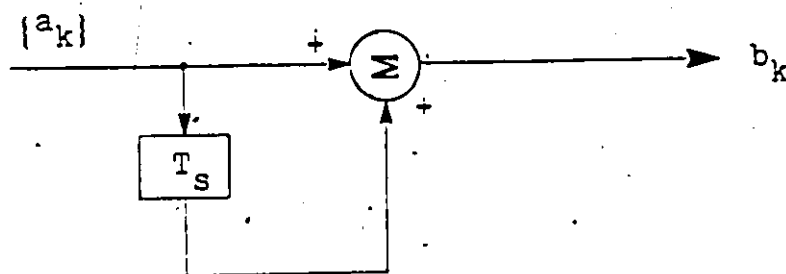


Fig.B.1. Block diagram of the Duo-binary encoder.

where

$a_k = \pm 1$ with equal probability

$T_s =$ one symbol interval delay-line (D flip/flop).

and

$$b_k = a_k + a_{k-1}$$

(B.1)

B.2 POWER SPECTRUM OF DUO-BINARY SQAM SIGNALS

Let the Duo-binary encoder have an impulse response $h_1(t)$ shown in Fig.B.2.

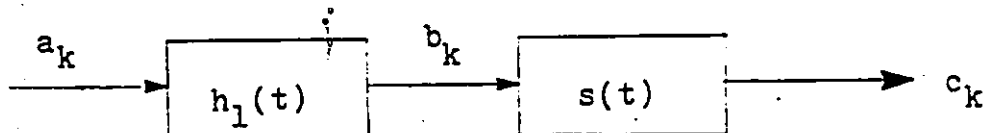


Fig.B.2. Impulse response of the Duo-binary SQAM encoder

From (B.1), $h_1(t)$ is given by :

$$h_1(t) = \delta(t) + \delta(t - T_s) \quad (\text{B.2})$$

where

$\delta(t)$: Dirac delta function.

Therefore, the transfer function $H_1(f)$ is expressed as :

$$\begin{aligned} H_1(f) &= F\{h_1(t)\} \\ &= 1 + e^{-j2\pi f T_s} \end{aligned} \quad (\text{B.3})$$

The impulse response $s(t)$ and transfer function $S(f)$ of the SQAM encoder are given in (2.3), (2.4) and (2.23).

Therefore, the overall transfer function $V(f)$ is given by :

$$V(f) = H_1(f) S(f)$$

$$= T_S (1 + e^{-j2\pi f T_S}) \left(\frac{1}{1 - T_S^2 f^2} + \frac{A - 1}{1 - T_S^2 f^2} \right) \times \left(\frac{\sin 2\pi f T_S}{2\pi f T_S} \right) \quad (\text{B.4})$$

and

$$V(0) = 2AT_S \quad (\text{B.5})$$

The normalized PSD function of the Duo-binary SQAM signal is given by :

$$\begin{aligned} \left| \frac{V(f)}{V(0)} \right|^2 &= \frac{1 + \cos 2\pi f T_S}{2A^2} \left(\frac{1}{1 - T_S^2 f^2} + \frac{A - 1}{1 - T_S^2 f^2} \right) \times \left(\frac{\sin 2\pi f T_S}{2\pi f T_S} \right)^2 \\ &= \left(\frac{\cos \pi f T_S}{A} \right)^2 \left(\frac{1}{1 - T_S^2 f^2} + \frac{A - 1}{1 - T_S^2 f^2} \right)^2 \times \left(\frac{\sin 2\pi f T_S}{2\pi f T_S} \right)^2 \quad (\text{B.6}) \end{aligned}$$

where A is the amplitude parameter of SQAM signal.

The normalized PSD is plotted in Fig.B.3. It is noticed that Duo-binary SQAM signal has a lower out-of-band energy and a faster spectral roll-off, compared to the conventional SQAM signal. Note that Duo-binary SQAM signals have a 1st spectral null at the Nyquist frequency (i.e. $f_n = f_s/2$).

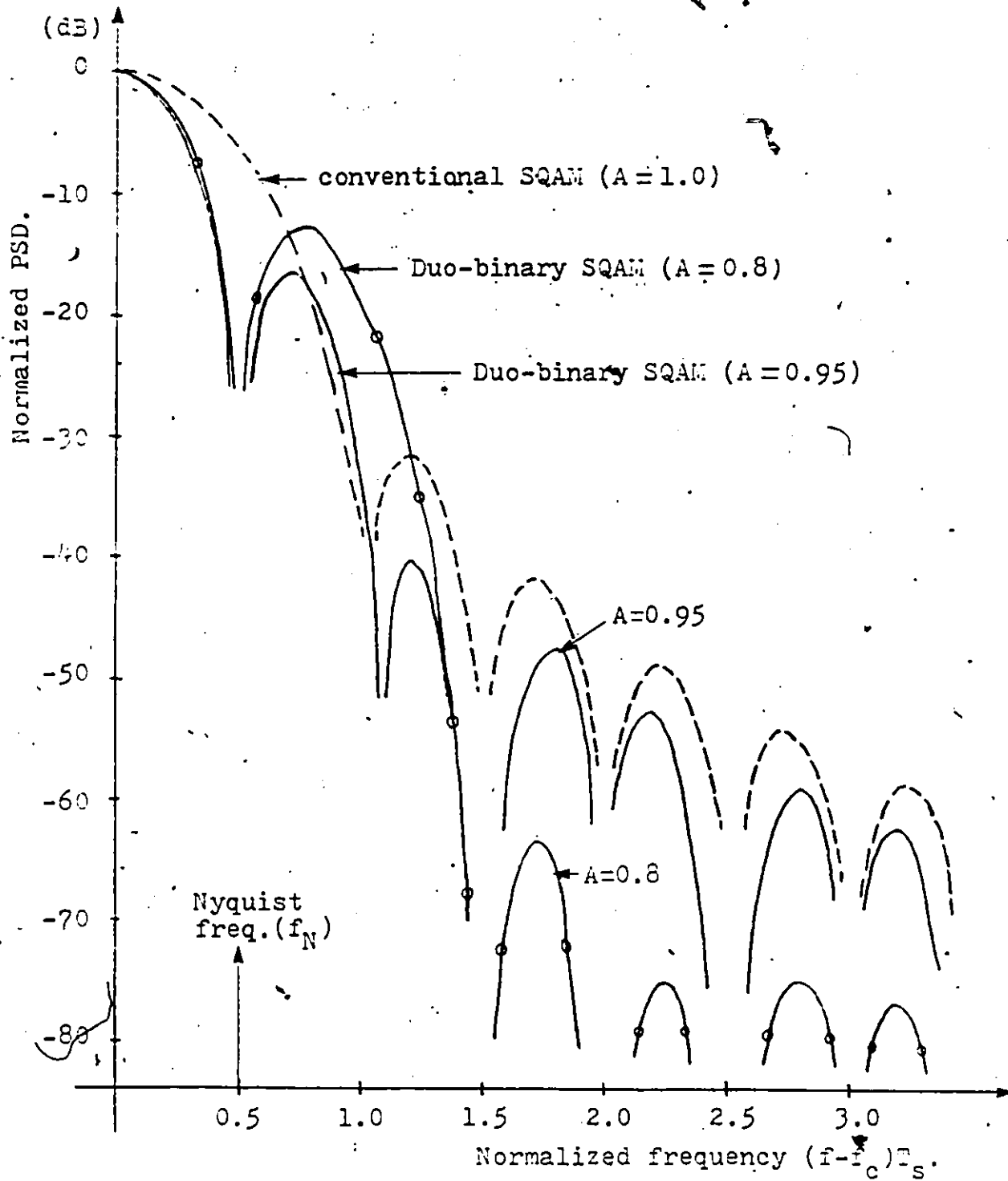


Fig.B.3. Normalized PSD of Duo-binary SQAM signals.

Appendix C

PROGRAMS TO SIMULATE PERFORMANCE OF SQAM MODEM

The following programs are used to simulate the performance of the SQAM modems, in an AWGN single-channel (linear and nonlinear) environment and in a nonlinear multichannel environment. The data source is an equiprobable NRZ signal with a bit rate of 120 Mb/s. The simulation here is based on the equivalent baseband concepts of the modulated system. In the simulation, the earth station HPA (high power amplifier), operating in the saturation mode, is approximated by an ideal hardlimiter. Using this simulation, the P(e) performance of the required system model can be evaluated, and power spectrum, eye-pattern, waveshape, phase transition and signal state-space diagram can be obtained. The simulation models, in a single-channel environment and in a multi-channel environment, are shown in Fig.3.9 and Fig.4.2(or Fig.4.10) respectively.

This program was developed from our available software computer simulation systems called COMSIM, which was developed at the Digital Communication Group of the University of Ottawa.

```

//          JOB          , 'SE013' , CLASS=J
//          EXEC        PLOTG, FORM=0111, PARM.GO= (SIZE=250K' , TIME=5
//FORT.SYSIN          DD          *

```

```

C *****
C PROGRAM TO SIMULATE THE P(E) PERFORMANCE OF SQAM MODEM IN
C AN AWGN SINGLE-CHANNEL ENVIRONMENT.
C *****
C

```

```

COMMON                                LDIM, IOFF
COMMON/PARA/LSAMPL, NSYMB, NO1, NO2, BAUD, SBANDW
COMPLEX TF(2048), TF1(2048), TF2(2048), TF3(2048), TF4(2048)
COMPLEX                                DATA(2048), DATA1(2048)
DIMENSION PEI(25), EBNO(25), IPNI(128), IPNQ(128)
DIMENSION IWK(12), PO(65), IPNI1(128), IPNQ1(128)
DIMENSION XARRAY(27), YARRAY(27), APEI(25)
COMMON                                /AA/A

```

```

C          INITIALIZE          PROGRAM.
C

```

```

IOFF=8
ICEL=4
NSYMB=128
LSAMPL=16
BAUD=60.
FOF=0.
DATA                                NSNR/25/
DATA                                NRUNS/4/
DATA          FBW1, FBW2, FBW3, FBW4/33.0, 30.0, 40.0, 40.0/
DATA                                ALPHA1, ALPHA2/0.4, 0.4/
SBANDW=FLOAT(LSAMPL)*BAUD
LDIM=LSAMPL*NSYMB
NO1=LDIM/2+1
NO2=NO1+1

```

```

C          END          OF          INITIALIZATION.
C

```

```

C          START          OF          COMPUTATIONS.
C

```

```

A=0.60
DO          500          KM=1, NRUNS
A=A+.10
CALL          LOAD4(DATA, IPNI, IPNQ)
CALL          BUT(TF, FBW1, ICEL)
CALL          HLIM(DATA)
C          CALL          RCOS(SBANDW, FBW2, TF, ALPHA1, LDIM, FOF)
CALL          ENERGY(DATA, EB, BAUD)
CALL          FILTER(DATA, TF)
CALL          HHGG(TF, PNOISE)
CALL          DECOD4(DATA, PNOISE, IPNI, IPNQ,
#EBNO, PEI, NSNR, EB)
DO          5          I=1, NSNR
PEI(I)=PEI(I)/FLOAT(NSYMB)
5          EBNO(I)=FLOAT(I)
WRITE(6,150)
150  FORMAT(5X, 'EB/NO', 10X, 'PROB. OF. ERROR', /)

```

```

172 WRITE(6,172) (EBNO(I),PEI(I),I=1,NSNR)
DO XARRAY(I)=EBNO(I) 99 FORMAT(5X,F5.1,10X,E13.6)
99 CALL YARRAY(I)=PEI(I) I=1,NSNR
500 CALL DRAW(XARRAY,YARRAY,NSNR,KM,NRUNS)
STOP CONTINUE
END

```

```

C*****
C THE FOLLOWING SUBROUTINE PERFORMS THE FILTERING
C PROCESS ON THE DATA SEQUENCE.
C*****

```

```

SUBROUTINE FILTER(SIGNAL,TF)
COMMON LDIM,IOFF
COMPLEX SIGNAL(1),TF(1)
DIMENSION IWK(12)
CALL FFT2C(SIGNAL,11,IWK)
DO 1 I=1,LDIM
1 SIGNAL(I)=CONJG(SIGNAL(I)*TF(I))
CALL FFT2C(SIGNAL,11,IWK)
DO 2 I=1,LDIM
2 SIGNAL(I)=CONJG(SIGNAL(I))/FLOAT(LDIM)
RETURN
END

```

```

C*****
C THIS SUBROUTINE COMPUTES THE EFFECTIVE NOISE (PNOISE)
C AT THE OUTPUT OF THE RECEIVE FILTER
C*****

```

```

SUBROUTINE HHGG(TF,PNOISE)
COMMON LDIM
COMMON/PARA/LSAMPL,NSYMB,NO1,NO2,BAUD,SBANDW
COMPLEX TF(1)
SUM=0.0
DO 1 L=1,LDIM
1 HH=(CABS(TF(L)))**2
SUM=SUM+HH
PNOISE=SUM*SBANDW/FLOAT(LDIM)/2.
PP=PNOISE*2./BAUD
RETURN
END

```

```

C*****
C          BIT          ENERGY          COMPUTATION
C*****

```

```

SUBROUTINE          ENERGY (DATA, EB)
COMMON              LDIM
COMMON/PARA/LSAMPL, NSYMB, NO1, NO2, BAUD, SBANDW
COMPLEX              DATA (1)
WATTS=0.
DO                   1          I=1, LDIM
WATTS=WATTS+((CABS (DATA (I)))**2.)
1
WATTS=WATTS/FLOAT (LDIM)
EB=WATTS/(2.*BAUD)
RETURN
END

```

```

C*****
C          SUBROUTINE          HLIM (DATA)
C*****

```

```

COMMON              LDIM
COMMON/PARA/LSAMPL, NSYMB, NO1, NO2, BAUD, SBANDW
COMPLEX              DATA (1)
DO                   10         I=1, LDIM
10          DATA (I)=DATA (I)/CABS (DATA (I))
RETURN
END

```

```

C*****
C          THIS SUBROUTINE DECODES THE PROCESSED DATA
C*****

```

```

SUBROUTINE          DECOD4 (DATA, PNOISE, IPNI, IPNQ,
#EBNO, PEI, NSNR, EB)
COMMON              LDIM, IOFF
COMMON/PARA/LSAMPL, NSYMB, NO1, NO2, BAUD, SBANDW
COMPLEX              DATA (1), AMP
DIMENSION           EBNO (1), PEI (1), IPNI (1), IPNQ (1)
DATA                NERROR, NOLD, NOF, NN, MI, MQ/0, 0, 0, 0, 1, 1/
IF                  (IOFF.EQ.0)          GO          TO          111
DO                   9          K=1, IOFF
XX=AIMAG (DATA (1))
LD=LDIM-1
DO                   5          KK=1, LD
5          DATA (KK)=CMLX (REAL (DATA (KK)), AIMAG (DATA (KK+1)))
9          DATA (LDIM)=CMLX (REAL (DATA (LDIM)), XX)
C          SYNCHRONIZE          THE          RECEIVED          DATA
111          LFU=2*NSYMB
300          DO          10          K=1, LDIM

```

```

NEW=0
DO                                200                                J=1, NSYMB
J1=K+(J-1)*LSAMPL
IF(J1.GT.LDIM)                    J1=J1-LDIM
XB=REAL(DATA(J1))
YB=AIMAG(DATA(J1))
IF      (SIGN(1.,XB).EQ.IPNI(J))    NEW=NEW+1
IF      (SIGN(1.,YB).EQ.IPNQ(J))    NEW=NEW+1
200  CONTINUE
IF(NEW-NOLD)                       399,12,13
12  GO                                TO                                NN=NN+1
13  GO                                TO                                10
NOLD=NEW
NOF=K
GO                                TO                                NN=0
399  IF(NOLD.EQ.LFU)                GO                                TO                                10
10  GO                                TO                                400
400  CONTINUE
NOF1=NOF+NN/2
NOF1
60  WRITE(6,60)
    FORMAT(5X,'SAMPLING TIME IS DELAYED TO ',I2,
$        'SIXTEENTHS OF THE SYMBOL INTERVAL',/)
IF      (NOF1.EQ.0)                GO                                TO                                230
LO=LDIM-1
DO                                250                                I=1,NOF1
AMP=DATA(I)
DO                                240                                J=1,LO
DATA(J)=DATA(J+1)
240  CONTINUE
DATA(LDIM)=AMP
250  CONTINUE
230  EOI=FLOAT(NSYMB)+1.
EOQ=FLOAT(NSYMB)+1.
SNR=PNOISE*EB/5.
SIGMA=SQRT(SNR)
DO                                110                                J=1,LSAMPL
EI=0.
EQ=0.
DO                                100                                K=1,NSYMB
J1=(K-1)*LSAMPL+J
AXBAR=(REAL(DATA(J1))+REAL(DATA(J1+1)))/2.
AYBAR=(AIMAG(DATA(J1))+AIMAG(DATA(J1+1)))/2.
IF(SIGN(1.,AXBAR).NE.IPNI(K))      EI=EI+1
IF(SIGN(1.,AYBAR).NE.IPNQ(K))      EQ=EQ+1
ARGI=ABS(AXBAR)/SIGMA
ARGQ=ABS(AYBAR)/SIGMA
EI=EI+ERFC(ARGI)/2.
EQ=EQ+ERFC(ARGQ)/2.
100  CONTINUE
IF(EOI.LE.EI)                      GO                                TO                                120
EOI=EI
MI=J
120  CONTINUE
IF      (EQQ.LE.EQ)                GO                                TO                                110

```

```

EQQ=EQ
MQ=J
110                                     CONTINUE
      MOFF=IABS(MI-MQ)
      IF      (MOFF.NE.0)                WRITE(6,160)      MOFF
160  FORMAT(5X,'SAMPLING POINTS FOR I AND Q CHANNELS DIFFER BY',
#I2,' SIXTEENTHS OF THE SYMBOL INTERVAL',/)
      MOFF=(MQ+MI)/2-1
      OFF=(FLOAT(MOFF)+FLOAT(NOF1))/FLOAT(LSAMPL)
      WRITE(6,161)
161  FORMAT(5X,'RECEIVED DATA IS DELAYED BY ',E9.3,' SYMBOLS',/)
      DO      2      K=1,NSYMB
      JI=(K-1)*LSAMPL+MI
      JQ=(K-1)*LSAMPL+MQ
      AXBAR=(REAL(DATA(JI))+REAL(DATA(JI+1)))/2.
      AYBAR=(AIMAG(DATA(JQ))+AIMAG(DATA(JQ+1)))/2.
      INDEXX=0
      IF(SIGN(1.,AXBAR).NE.IPNI(K))      INDEXX=1
      INDEXY=0
      IF(SIGN(1.,AYBAR).NE.IPNQ(K))      INDEXY=1
      IF((INDEXX.EQ.1).OR.(INDEXY.EQ.1))  NERROR=NERROR+1
C    COMPUTE THE PROBABILITY OF ERROR FOR THIS SYMBOL
      DO      4      M=1,NSNR
      XM=FLOAT(M)/10.
      SNR=PNOISE*EB/(10.**XM)
      SIGMA=SQRT(SNR)
      ARG=(ABS(AXBAR))/(SIGMA*SQRT(2.))
      IF      (ARG.GT.12.)                ARG=12.
      EX=ERFC(ARG)/2.
      IF      (INDEXX.EQ.1)              EX=1.-EX
      ARG=(ABS(AYBAR))/(SIGMA*SQRT(2.))
      IF      (ARG.GT.12.)                ARG=12.
      EY=ERFC(ARG)/2.
      IF      (INDEXY.EQ.1)              EY=1.-EY
      IF      (EX.LT.1.E-15)             EX=0.
      IF      (EY.LT.1.E-15)             EY=0.
      4      PEI(M)=PEI(M)+((EX+EY)/2.)
      2      CONTINUE
C          DO      5      I=1,NSNR
C          PEI(I)=PEI(I)/FLOAT(NSYMB)
C5         EBNO(I)=FLOAT(I)
C          WRITE(6,150)
C150      FORMAT(5X,'EB/NO',10X,'PROB. OF ERROR',/)
C          WRITE(6,151)      (EBNO(I),PEI(I),I=1,NSNR)
C151      FORMAT(5X,F5.1,10X,E13.6)
C          WRITE      (6,152)      NERROR
C152      FORMAT(/5X,'ERRORS=',I5,/)

      RETURN
      END

```

```

C*****T*****
C          EQUALIZED          BUTTERWORTH          FILTER
C*****

```

```

SUBROUTINE          BUT(TF,FB,ICEL)
COMMON              LDIM,IOFF
COMMON/PARA/LSAMPL,NSYMB,NO1,NO2,BAUD,SBANDW
COMPLEX              TF(1)
A1=1./NSYMB
FBNOR=FB/BAUD
TF(1)=CMPLX(1.0,0.0)
DO                   10              I=2,NO1
  J=I-1
  A2=1./SQRT(1.+(A1*FLOAT(J)/FBNOR)**(2*ICEL))
10                  TF(I)=CMPLX(A2,0.)
DO                   20              I=NO2,LDIM
20                  TF(I)=TF(LDIM+2-I)
RETURN
END

```

```

C*****
C THIS SUBROUTINE GENERATES TWO CHANNELS OF SQAM SIGNAL.
C*****

```

```

SUBROUTINE          LOAD4(DATA,IPNI,IPNQ)
COMMON              LDIM,IOFF
COMMON/PARA/LSAMPL,NSYMB,NO1,NO2,BAUD,SBANDW
COMPLEX              DATA(1)
DIMENSION            NX(7),NY(7),IPNI(1),IPNQ(1),RI(16),RQ(16)
DO                   3              I=1,7
3                    NX(I)=-1
NY(1)=-1
NY(2)=-1
NY(3)=1
NY(4)=1
NY(5)=1
NY(6)=1
NY(7)=-1
DATA                  JLAST/7/
I=0
J=6
KKK=2**JLAST
DO                   1              K=1,KKK
1                    GENERATING      ONE      SYMBOL.
IF                   (I.GE.JLAST)      I=0
IF                   (J.GE.JLAST)      J=0
I=I+1
J=J+1
NX(I)=NX(J)*NX(I)
NY(I)=NY(J)*NY(I)
IPNI(K)=NX(I)
IPNQ(K)=NY(I)

```

```

C   LOAD INTO THE ARRAY TO BE FOURIER TRANSFORMED.
DO      10      K=1,KKK
KML=K-1
IF      (KML.EQ.0)      KML=KKK
MI=IPNI(KML)
MQ=IPNQ(KML)
CALL    SIG(MI,IPNI(K),RI)
CALL    SIG(MQ,IPNQ(K),RQ)
J1=(K-1)*LSAMPL
DO      10      I=1,16
10     DATA(J1+I)=CMPLX(RI(I),RQ(I))
IF      (IOFF.EQ.0)      GO      TO      20
DO      15      I=1,IOFF
A=AIMAG(DATA(LDIM))
DO      13      L=2,LDIM
K=LDIM+2-L
13     DATA(K)=CMPLX(REAL(DATA(K)),AIMAG(DATA(K-1)))
DATA(1)=CMPLX(REAL(DATA(1)),A)
15
20     CONTINUE
      RETURN
END

```

```

C   *****
C   SUBROUTINE      SIG(M,IP,R)
C   *****

COMMON      /AA/A
REAL      R(16)
P=3.14159265/16.
IF(M.EQ.IP)      GOTO      20
IF(IP.EQ.1)      GOTO      10
DO      1      I=1,16
1     R(I)=COS((I+0.5)*P)
GOTO      40
10     DO      11      I=1,16
11     R(I)=-COS((I+0.5)*P)
GOTO      40
20     IF(IP.EQ.1)      GOTO      30
DO      21      I=1,16
21     R(I)=-A-(1.0-A)*COS(2.*(I+0.5)*P)
GOTO      40
30     DO      31      I=1,16
31     R(I)=A+(1.0-A)*COS(2.*(I+0.5)*P)
40     CONTINUE

RETURN
END

```

```

C*****
C THIS SUBROUTINE DRAWS PROBABILITY OF ERROR CURVES FOR
C P(E) AS LOW AS 1.0E-8 AND A C/N RATIO AS HIGH AS 30 DB.
C*****

```

```

SUBROUTINE DRAW(XARRAY, YARRAY, NSNR, JCURV, JLAST)
DIMENSION XARRAY(27), YARRAY(27), X(9), Y(9)
IF(JCURV.GT.1) GOTO 2

C C C ESTABLISH THE SURFACE AREA.
CALL PLOTS(30.0, 27.5)
C C C ESTABLISH THE ORIGIN.
CALL PLOT(3.0, 3.0, -3)
C C C DRAW THE LOGARITHMIC Y-AXIS.
CALL LGAXS(0.0, 0.0, 20, PROBABILITY OF ERROR, 20, 18.,
+90., 1.0E-8, .4)
C C C DRAW THE LINEAR X-AXIS.
CALL AXIS(0.0, 0.0, 11, HEB/NO IN DB, -11,
+14.0, 0.0, 6.0, 1.0)
C C C WRITE THE TITLE OF THE GRAPH.
CALL SYMBOL(4.0, 23.0, 0.49, 14, HSQAM BER CURVE, 0.0, 20)
C C C PLOT THE IDEAL CURVE.
DO 5 J=1, 7
JJ=J+5
X(J)=FLOAT(JJ)
Y(J)=.5*ERFC(SQRT(10.**(.1*JJ)))
C C C CALL NEWPEN(2)
CALL LGLIN(X, Y, 7, 1, 0, 0, 1)
CONTINUE
C C C PLOT THE DATA IN LOG-LINEAR MODE.
M=NSNR
DO 1 K=1, M
KK=K+5
IF(KK.GT.M) KK=M
XARRAY(K)=XARRAY(KK)
YARRAY(K)=YARRAY(KK)
IF(YARRAY(K).LE.1.0E-8) GOTO 3
GOTO 1
M=K-1

```

```

1      GOTO 4
4
      I=M+1
      II=I+1
      XARRAY(I)=6.0
      XARRAY(II)=1.0
      YARRAY(I)=1.E-8
      YARRAY(II)=0.4
C      CALL NEWPEN(1)
      CALL LGLIN(XARRAY,YARRAY,M,1,0,0,1)
      IF(JCURV.EQ.JLAST) CALL PLOT(0.0,0.0,999)
      RETURN
      END

```

```

C*****
C      RAISED COSINE FILTER WITH ARBITRARY ALPHA
C*****

```

```

      SUBROUTINE RCOS(SBANDW,FBANDW,TF,ALPHA,LDIM,FOF)
      COMPLEX TF(1)
      COMPLEX XX
      COMMON /AA/A
C***** FF(X) IS THE INVERSE BASEBAND SPECTRUM
      FF(X)=2.*X*(1.-(4./(3.141592**2))*(X**2))/SIN(2.*X)
C      B(X)=(1.-A)/((X/3.141592)**2-1.)C # 1./(1.-4.*(X/3.141592)**2)
C      FF(X)=2.*X/(B(X)*SIN(2.*X))
      QQ=2.
      NO=LDIM/2
      NO1=NO+1
      IF (ALPHA.EQ.0) ALPHA=0.0001
      FN=LDIM*(FBANDW/SBANDW)
      F1=(1.-ALPHA)*FN
      F2=(1.+ALPHA)*FN
      IFN=IFIX(FN)
      IF1=IFIX(F1)+1
      IF2=IFIX(F2)+1
      A1=3.141592/(2.*FLOAT(IFN))
      TF(1)=CMPLX(1.0,0.0)
      DO 8 I=2,IF1
        J=I-1
        A2=FF(FLOAT(J)*A1)
        TF(I)=CMPLX(A2,0.0)
8      JK=IF1+1
      DO 9 I=JK,IF2
        J=JK,IF2
        I=J-1
        A3=QQ
        IF(I.NE.FN) A3=FF(FLOAT(I)*A1)
        A=(3.141592/(2.0*ALPHA))*((FLOAT(I)/FLOAT(IFN))-1.)
        TF(J)=CMPLX((0.5*(1.0-SIN(A))),0.0)
        TF(J)=TF(J)*CMPLX(A3,0.0)

```

```

9          CONTINUE
  JH=IF2+1
  DO          10          I=JH,NO1
  TF(I)=CMLPX(0.0,0.0)
10          CONTINUE
  NO2=NO1+1
  DO          5          I=NO2,LDIM
  TF(I)=TF(LDIM+2-I)
5          CONTINUE
  IFOF=IFIX(FOF*FLOAT(LDIM)/SBANDW)
  IF(IFOF.EQ.0)          RETURN
  IF(IFOF.LT.0)          GO          TO          50
  DO          20          K=1,IFOF
  XX=TF(LDIM)
  JJ=LDIM-1
  DO          30          I=1,JJ
  TF(LDIM+1-I)=TF(LDIM-I)
30          CONTINUE
  TF(1)=XX
20          CONTINUE
  RETURN
50          IFOF=-IFOF
  JJ=LDIM-1
  DO          70          K=1,IFOF
  XX=TF(1)
  DO          60          I=1,JJ
  TF(I)=TF(I+1)
60          CONTINUE
  TF(LDIM)=XX
70          CONTINUE
  RETURN
  END

```

```

C*****
C          GENERATES TWO CHANNELS OF MSK SIGNAL
C*****

```

```

SUBROUTINE          LOAD7          (DATA,IPNI,IPNQ)
COMMON          LDIM,IOFF
COMMON/PARA/LSAMPL,NSYMB,NO1,NO2,BAUD,SBANDW
COMPLEX          DATA(1)
DIMENSION          IPNI(1),IPNQ(1),NX(7),NY(7),RI(16),RQ(16)
DATA          NX(1),NX(2),NX(3),NX(4),NX(5),NX(6),NX(7)/-1,-1,-1,
#          -1,-1,-1,-1/
DATA          NY(1),NY(2),NY(3),NY(4),NY(5),NY(6),NY(7)/-1,-1,1,
#          1,1,1,-1/
  IOFF=8
  DATA          JLAST,J,I/7,6,0/
  DO          1          K=1,128
  IF(I.GE.7)          I=0
  IF(J.GE.7)          J=0
  I=I+1
  J=J+1

```

```

NX(I)=NX(J)*NX(I)
NY(I)=NY(J)*NY(I)
IPNI(K)=NX(I)
1
DO 10 IPNQ(K)=NY(I)
CALL K=1,128
CALL MSK(IPNI(K),RI)
J1=(K-1)*16 MSK(IPNQ(K),RQ)
DO 10 I=1,16
DATA(J1+I)=CMPLX(RI(I),RQ(I))
IF(IOFF.EQ.0) GOTO 20
DO 15 I=1,IOFF
A=AIMAG(DATA(2048))
DO 13 L=2,2048
K=2050-L
DATA(K)=CMPLX(REAL(DATA(K)),AIMAG(DATA(K-1)))
DATA(1)=CMPLX(REAL(DATA(1)),A)
15 CONTINUE
20 RETURN
END

```

C*****
SUBROUTINE MSK(IP,R)
C*****

```

REAL R(16)
P=3.14159265/16.
IF(IP.EQ.1) GOTO 10
DO 1 I=1,16
R(I)=-SIN((I+0.5)*P)
GOTO 40
DO 10 I=1,16
R(I)=SIN((I+0.5)*P)
11 CONTINUE
40 RETURN
END

```

EXEC
// FORT.SYSIN

JOB , 'SEO E, CLASS=J
PLOTG, FORM=0111, PARM.GO=' SIZE=250K', TIME=5
DD *

PROGRAM TO PLOT EYE-PATTERNS, WAVESHAPES, STATE-SPACE
DIAGRAMS AND PHASE TRANSITIONS OF SQAM BASEBAND SIGNALS.

COMMON LDIM, IOFF
COMMON/PARA/LSAMPL, NSYMB, NO1, NO2, BAUD, SBANDW
COMPLEX TF(2048), TF1(2048), TF2(2048), TF3(2048), TF4(2048)
COMPLEX DATA(2048), DATA1(2048)
DIMENSION PEI(25), EBNO(25), IPNI(128), IPNQ(128)
DIMENSION IWK(12), PO(65), IPNI1(128), IPNQ1(128)
DIMENSION XARRAY(27), YARRAY(27), APEI(25)
REAL TR(514)
COMMON /AA/A

INITIALIZE PROGRAM.

IOFF=8
ICEL=4
NSYMB=128
LSAMPL=16
BAUD=60.
DATA NRUNS/1/
DATA FBW1, FBW2, FBW3, FBW4/33.0, 30.0, 40.0, 40.0/
DATA ALPHA1, ALPHA2/0.4, 0.4/
SBANDW=FLOAT(LSAMPL)*BAUD
LDIM=LSAMPL*NSYMB
NO1=LDIM/2+1
NO2=NO1+1

START OF COMPUTATIONS.

A=0.70
DO 500 KM=1, NRUNS
A=A+.10
CALL LOAD4(DATA, IPNI, IPNQ)
CALL TRAN(DATA, TR)
WRITE(6, 100) (DATA(I), TR(I), I=1, 512)
100 FORMAT(5X, F12.7, 20X, F12.7)
CALL HLIM(DATA)
CALL BUT(TF, FBW1, ICEL)
CALL FILTER(DATA, TF)
CALL EYEQQ(DATA, 16, 128, KM, NRUNS)
CALL WAVSH2(DATA)
CALL SPACE(DATA, KM, NRUNS)
500 CONTINUE
STOP
END

```

C*****
C   THIS SUBROUTINE DRAWS THE WAVE SHAPE FOR
C   2*64 BIT DURATION.
C*****

```

```

SUBROUTINE WAVSH2(DATA)
COMMON LDIM,IMOD,IOFF
COMMON/PARA/LSAMPL,NSYMB,NO1,NO2,BAUD,SBANDW
DIMENSION DATA2(259),DATA3(259),MOD(2)
COMPLEX DATA(1)

C ESTABLISH THE SURFACE AREA.
CALL PLOTS(36.0,27.5)

C ESTABLISH THE ORIGIN.
CALL PLOT(2.5,19.5,-3)

C WRITE THE TITLE OF THE GRAPH.
C DRAW THE TIME AXIS.
CALL AXIS(0.0,0.0,1H,-1,32.5,0.0,0.0,0.5)

C DRAW THE AMPLITUDE AXIS.
CALL AXIS(0.0,-2.0,1H,1,4.0,90.0,-1.0,0.5)

C ESTABLISH THE SURFACE AREA.
C PLOT THE DATA.
DATA2(258)=0.0
DATA2(259)=0.5
DATA3(258)=0.5
DATA3(259)=8.
DO 4 KK=1,257
DATA2(KK)=REAL(DATA(KK))
DATA3(KK)=FLOAT(KK)
4 CALL LINE(DATA3,DATA2,257,1,0,0)
C ESTABLISH THE ORIGIN.
CALL PLOT(0.0,-13.0,-3)
C DRAW THE TIME AXIS.
CALL AXIS(0.0,0.0,1H,-1,32.5,0.0,17.,0.5)
C DRAW THE AMPLITUDE AXIS.
CALL AXIS(0.0,-2.0,1H,1,4.0,90.0,-1.0,0.5)
C PLOT THE DATA.
DO 7 KK=1,256
DATA2(KK)=REAL(DATA(KK+256))
DATA3(KK)=FLOAT(KK)
7 DATA2(257)=REAL(DATA(1))
DATA3(257)=FLOAT(257)
CALL LINE(DATA3,DATA2,257,1,0,0)
CALL PLOT(0.0,0.0,999)
RETURN
END

```

```

C*****
C THIS SUBROUTINE DRAWS THE EYE-PATTERNS FOR A
C SYMBOL DURATION.
C*****

```

```

SUBROUTINE EYEQQ(DATA,LSAMPL,NSYMB,JCURV,JLAST)
DIMENSION DATA2(64),DATA3(64)
COMPLEX DATA(1)
IF(JCURV.GT.1) GOTO 3
CALL ESTABLISH THE SURFACE AREA.
CALL ESTABLISH THE PLOTS(20.0,27.5)
CALL WRITE THE TITLE OF THE GRAPH.
CALL SYMBOL(0.0,18.0,0.49,16HSQAM EYE DIAGRAM,0.0,16)
CALL DRAW THE TIME AXIS.
CALL DRAW AXIS(0.0,-6.0,1H , -1,12.,0.0,0.0,3.0)
CALL DRAW THE AMPLITUDE AXIS.
CALL DRAW AXIS(0.0,-6.0,1H , 1,1.0,90.0,0.0,0.60)
CALL PLOT THE DATA.
P=0.0
JJ=2*LSAMPL
3 DATA2(JJ+1)=P
DATA2(JJ+2)=0.6
DATA3(JJ+1)=1.0
DATA3(JJ+2)=3.0
M2=NSYMB/2
DO 4 KK=1,M2
DO 2 I=1,JJ
II=(KK-1)*2*LSAMPL+I
DATA2(I)=REAL(DATA(II))
2 CALL LINE(DATA3,DATA2,JJ,1,0,0)
4 P=P-4.0
IF(JCURV.EQ.JLAST) CALL PLOT(0.0,0.0,999)
RETURN
END

```

```

C*****
C THIS SUBROUTINE DRAWS SIGNAL STATE-SPACE DIAGRAMS.
C*****

```

```

SUBROUTINE SPACE(DATA,JCURV,JLAST)
REAL X(2050),Y(2050)
COMPLEX DATA(1)
IF(JCURV.GT.1) GOTO 2
CALL ESTABLISH SURFACE AREA
CALL ESTABLISH PLOTS(30.0,27.5)
CALL ESTABLISH ORIGIN
CALL PLOT(15.0,12.5,-3)
CALL TITLE

```

```

C      CALL SYMBOL(-6.0,12.5,0.49,13HSPACE  DIAGRAM,0.0,13)
C      DRAW AXIS
CALL      AXIS(-8.0,0.0,1H      ,1,16.0,0.0,-2.0,0.25)
CALL      AXIS(0.0,-8.0,1H      ,1,16.0,90.0,-2.0,0.25)
X(2049)=0.0
X(2050)=0.25
Y(2049)=0.0
Y(2050)=0.25

C      PLOT DIAGRAM
2      CONTINUE
DO      21 I=1,2048
C      X(I)=REAL(DATA(I))
C      Y(I)=AIMAG(DATA(I))
21      CALL LINE(X,Y,2048,1,0,0)
IF(JCURV.EQ.JLAST) CALL PLOT(0.0,0.0,999)
WRITE(6,61)
61      FORMAT(5X,' ---SPACE DIAGRAM IS REQUESTED ---')
RETURN
END

```

```

C *****
C      DRAW PHASE TRANSITIONS OF SQAM SIGNAL.
C *****

```

```

SUBROUTINE TRAN(DATA,TR)
REAL X(514),Y(514),TR(514),B(514)
COMPLEX DATA(1)
C      ESTABLISH THE SURFACE AREA.
CALL PLOTS(36.0,27.5)
C      ESTABLISH THE ORIGIN.
CALL PLOT(2.5,13.5,-3)
C      DRAW THE TIME AXIS.
CALL AXIS(0.0,0.0,1H , -1,32.5,0.0,0.0,1.0)
C      DRAW THE AMPLITUDE AXIS.
CALL AXIS(0.0, -2.0,1H , 1,4.0,90.0,-2.0,1.0)
TR(513)=0.0
TR(514)=1.0
B(513)=0.5
B(514)=16.
DO 4 I=1,512
C      X(I)=REAL(DATA(I))
C      Y(I)=AIMAG(DATA(I))
C      TR(I)=-ATAN(Y(I)/X(I))
C      B(I)=FLOAT(I)
4      CALL LINE(B,TR,512,1,0,0)
CALL PLOT(0.0,0.0,999)
RETURN
END

```

```
//  
// EXEC  
// FORT.SYSIN
```

```
JOB 'SUN2', CLASS=B  
PLOTG, FORM=0111, PARM.GO='SIZE=500K', TIME=5  
DD
```

```
C *****  
C PROGRAM TO COMPUTE AND PLOT THE P.S.D. AND THE OUT-OF-BAND  
C ENERGY OF SQAM BASEBAND SIGNALS.  
C *****  
C
```

```
COMMON LDIM, IOFF  
COMMON/PARA/LSAMPL, NSYMB, NO1, NO2, BAUD, SBANDW  
COMPLEX DATA(16384)  
DIMENSION PEI(25), EBNO(25), IPNI(1024), IPNQ(1024)  
DIMENSION IWK(12), PO(129), IPNI1(1024), IPNQ1(1024)  
DIMENSION XARRAY(27), YARRAY(27), APEI(25), TPO(129)  
COMMON /AA/A
```

```
C  
C INITIALIZE PROGRAM.  
C
```

```
IOFF=8  
NSYMB=1024  
LSAMPL=16  
BAUD=60.  
DATA NRUNS/2/  
SBANDW=FLOAT(LSAMPL)*BAUD  
LDIM=LSAMPL*NSYMB  
NO1=LDIM/2+1  
NO2=NO1+1
```

```
C  
C START OF COMPUTATIONS.  
C  
A=0.60  
DO 500 KM=1, NRUNS  
A=A+.20  
CALL LOAD4(DATA, IPNI, IPNQ)  
CALL HLIM(DATA)  
CALL SPECT(DATA, PO, TPO)  
CALL DRAW5(TPO, KM, NRUNS)  
CONTINUE  
500 STOP  
END
```

```
C *****  
C THIS SUBROUTINE GENERATES BASEBAND SQAM SIGNALS.  
C *****
```

```
SUBROUTINE LOAD4(DATA, IPNI, IPNQ)  
COMMON LDIM, IOFF  
COMMON/PARA/LSAMPL, NSYMB, NO1, NO2, BAUD, SBANDW  
COMPLEX DATA(1)  
DIMENSION NX(10), NY(10), IPNI(1), IPNQ(1), RI(16), RQ(16)  
DO 3 I=1, 10
```

```

3
NY(1)=-1
NY(2)=-1
NY(3)=1
NY(4)=1
NY(5)=1
NY(6)=1
NY(7)=-1
NY(8)=-1
NY(9)=1
NY(10)=1
DATA
I=0
J=9
KKK=2**JLAST
DO
C          GENERATING          ONE          K=1, KKK
          (I.GE.JLAST)          SYMBOL.
IF          (J.GE.JLAST)          I=0
J=J+1          J=0
NX(I)=NX(J)*NX(I)
NY(I)=NY(J)*NY(I)
IPNI(K)=NX(I)
C          IPNQ(K)=NY(I)
LOAD INTO THE ARRAY TO BE FOURIER TRANSFORMED.
DO          10          K=1, KKK
KML=K-1
IF          (KML.EQ.0)          KML=KKK
MI=IPNI(KML)
MQ=IPNQ(KML)
CALL          SIG(MI, IPNI(K), RI)
CALL          SIG(MQ, IPNQ(K), RQ)
J1=(K-1)*LSAMPL
DO          10          I=1, 16
          DATA(J1+I)=CMPLX(RI(I), RQ(I))
10 IF          (IOFF.EQ.0)          GO          TO          20
DO          15          I=1, IOFF
A=AIMAG(DATA(LDIM))
DO          13          L=2, LDIM
K=LDIM+2-L
13          DATA(K)=CMPLX(REAL(DATA(K)), AIMAG(DATA(K-1)))
          DATA(1)=CMPLX(REAL(DATA(1)), A)
15          CONTINUE
20          RETURN
END

```

```

C*****
C          GENERATES TWO CHANNELS OF MSK SIGNAL
C*****

```

```

SUBROUTINE          LOAD7          (DATA,IPNI,IPNQ)
COMMON              LDIM,IOFF
COMMON/PARA/LSAMPL,NSYMB,NO1,NO2,BAUD,SBANDW
COMPLEX
DIMENSION          NX(10),NY(10),IPNI(1),IPNQ(1),RI(16),RQ(16)
DO                  3              I=1,10
                                NX(I)=-1
3
NY(1)=-1
NY(2)=-1
NY(3)=1
NY(4)=1
NY(5)=1
NY(6)=1
NY(7)=-1
NY(8)=-1
NY(9)=1
NY(10)=1
DATA
I=0
J=9
KKK=2**JLAST
DO
C          GENERATING          ONE          K=1,KKK
                                SYMBOL.
IF          (I.GE.JLAST)          I=0
IF          (J.GE.JLAST)          J=0
I=I+1
J=J+1
NX(I)=NX(J)*NX(I)
NY(I)=NY(J)*NY(I)
IPNI(K)=NX(I)
                                IPNQ(K)=NY(I)
C          LOAD INTO THE ARRAY TO BE FOURIER TRANSFORMED.
DO          10              K=1,KKK
CALL          MSK(IPNI(K),RI)
CALL          MSK(IPNQ(K),RQ)
J1=(K-1)*LSAMPL
DO          10              I=1,16
                                DATA(J1+I)=CMPLX(RI(I),RQ(I))
10          IF          (IOFF.EQ.0)          GO          TO          20
DO          15              I=1,IOFF
A=AIMAG(DATA(LDIM))
DO          13              L=2,LDIM
K=LDIM+2-L
13          DATA(K)=CMPLX(REAL(DATA(K)),AIMAG(DATA(K-1)))
15          DATA(1)=CMPLX(REAL(DATA(1)),A)
20
                                CONTINUE
                                RETURN
END

```

```

C*****
C THIS SUBROUTINE COMPUTES THE P.S.D. AND OUT-OF-BAND ENERGY.
C*****

```

```

SUBROUTINE SPECT(SIGNAL,PO,TPO)
COMMON LDIM,I OFF
COMMON/PARA/LSAMPL,NSYMB,NO1,NO2,BAUD,SBANDW
COMPLEX SIGNAL(1)
COMPLEX CWK(258)
DIMENSION X(32768),PO(1),IWK(8),WK(128),TPO(129)
S=0.
DO 10 I=1,LDIM
L=I-I OFF
IF(L.LE.0) L=L+LDIM
X(I)=REAL(SIGNAL(I))
X(I+16384)=AIMAG(SIGNAL(L))
10 S=S+X(I)+X(I+16384)
S=S/FLOAT(32768)
DO 20 I=1,32768
X(I)=X(I)-S
20 CALL FTFPS(X,Y,32768,256,0,PO,PSY,XPS,IWK,WK,CWK,IER)
PMA X=PO(1)
TPO(129)=PO(129)

```

```

C
C **** CALCULATE P.S.D. ****
C

```

```

C DO 30 I=1,129
C30 TPO(I)=-10.*ALOG10(PO(I)/PMA X)
C WRITE(6,1) (TPO(I),I=1,129)
C1 FORMAT(2X,'POWER SPECTRUM',/ ,10(2X,F6.1))
C

```

```

C ***** CALCULATE OUT-OF-BAND ENERGY *****
C

```

```

C DO 40 I=1,127
C40 TPO(129-I)=TPO(130-I)+2.*PO(129-I)
TPO(1)=TPO(2)+PO(1)
TPMA X=TPO(1)
C DO 50 I=1,129
C50 TPO(I)=-10.*ALOG10(TPO(I)/TPMA X)
WRITE(6,2) (TPO(I),I=1,129)
2 FORMAT(2X,'OUT OF BAND TO TOTAL POWER RATIO' /
&,10(2X,F6.1))
C

```

```

C RETURN
END

```

C*****
 C THIS SUBROUTINE DRAWS THE NORMALIZED P.S.D.
 C*****

```

SUBROUTINE DRAW5(TPO, JCURV, JLAST)
COMMON LDIM, IOFF
COMMON/PARA/LSAMPL, NSYMB, NO1, NO2, BAUD, SBANDW
DIMENSION TPO(1), DATA2(131), DATA3(131)
COMPLEX DATA(1)
IF(JCURV.GT.1) GOTO 2
C ESTABLISH THE SURFACE AREA.
CALL PLOTS(20.0, 27.5)
C ESTABLISH THE ORIGIN.
CALL PLOT(3.0, 7.0, -3)
C WRITE THE TITLE OF THE GRAPH.
CALL SYMBOL(5.0, 17.0, 0.35, 19HSQAM POWER SPECTRUM, 0.0, 24)
C DRAW THE FREQ AXIS.
CALL AXIS(0.0, 0.0, 20HNORMALIZED FREQUENCY, -20, 5., 0.0, 0.0, 1.0)
C DRAW THE NORMALIZED PSD AXIS.
CALL AXIS(0.0, 0.0, 18HNORMALIZED PSD DB, 18, 9., +90.,
#-80.0, 10.)
DATA2(66)=-80.
DATA2(67)=10.
DATA3(66)=0.0
DATA3(67)=1.0
2 CONTINUE
DO 4 KK=1, 65
DATA2(KK)=-TPO(KK)
DATA3(KK)=(FLOAT(KK)-1.0)*16./256.
4 CONTINUE
CALL LINE(DATA3, DATA2, 65, 1, 0, 0)
5 IF(JCURV.EQ.JLAST) CALL PLOT(0.0, 0.0, 999)
RETURN
END

```

```

//
// EXEC JOB 'SUN1', CLASS=B
// FORT.SYSIN PLOTG, FORM=0111, PARM.GO='SIZE=500K', TIME=5 DD
C
C*****
C PROGRAM TO SIMULATE THE P(E) PERFORMANCE OF SQAM MODEM IN
C A NONLINEARLY AMPLIFIED MULTICHANNEL ENVIRONMENT.
C*****
C
COMMON LDIM, IOFF
COMMON/PARA/LSAMPL, NSYMB, NO1, NO2, BAUD, SBANDW
COMPLEX TF(2048), TF1(2048), TF2(2048), TF3(2048), TF4(2048)
COMPLEX DATA(2048), DATA1(2048), BUFF(2048)
DIMENSION PEI(25), EBNO(25), IPNI(128), IPNQ(128)
DIMENSION IWK(12), PO(65), IPNI1(128), IPNQ1(128)
DIMENSION XARRAY(27), YARRAY(27), APEI(25)
REAL MP, MP1, MP2, MP0, MPF
COMMON /AA/A

C
C INITIALIZE PROGRAM.
C
IOFF=8
NSYMB=128
LSAMPL=16
BAUD=60.
DATA NSNR/25/
DATA NRUNS/8/
DATA ALPHA1, ALPHA2/0.4, 0.4/
DATA ALPHA3, ALPHA4/0.1, 0.2/
DATA BAKOFH, BAKOFT/7.0, 2.0/
C
C SBANDW=FLOAT(LSAMPL)*BAUD
C LDIM=LSAMPL*NSYMB
C NO1=LDIM/2+1
C NO2=NO1+1
C
C DATA PSHIF1, PSHIF2/1.70, 3.14/
C DATA ITSH1, ITSH2/672, 1344/
C
C SET SYSTEM PARAMETERS
C
A=0.85
DATA AT1, AT2/ -0., -0./
DATA FOF, FOF1, FOF2/0., 100., -100./
DATA NOA/5/
DATA ICEL/5/
DATA FBW1, FBW2, FBW3, FBW4/30.0, 30.0, 40.0, 35.0/
C
C OFF=FLOAT(IOFF)/FLOAT(LSAMPL)
C PO1=0.0
C
1 PRINT
FORMAT(2X, '** SIMULATION OF SQAM MODEM IN ACI **')
WRITE (6,6) BAUD
6 FORMAT(5X, 'SYMBOL RATE:', F7.2, ' MBAUD')
WRITE(6,2) FBW1
2 FORMAT(5X, 'RX FILTER CUTOFF FREQ=', F4.1, ' MHZ')

```

C
C
C

START OF COMPUTATIONS.

```

DO 600 KA=1,NOA
PSHIF1=1.7
PSHIF2=3.14
ITSH1=672
ITSH2=1344
DO 19 I=1,NSNR
APEI(I)=0.0

```

19

```

DO 500 CONTINUE
KM=1,NRUNS

```

C

```

CALL CALL LOAD4(DATA,IPNI,IPNQ)
CALL CALL BUT(TF,FBW1,ICEL,FOF)
CALL CALL RCOS(FBW1,TF,ALPHA1,FOF)
CALL CALL HLIM(DATA)
CALL CALL POWER(DATA,MP,PF)
CALL CALL ENERGY(DATA,EB,BAUD)
CALL CALL FILTER(DATA,TF,FOF)

```

C

```

CALL CALL LOAD4(DATAL,IPNI1,IPNQ1)
CALL CALL HLIM(DATAL)
CALL CALL PHASE(DATAL,PSHIF1)
CALL CALL FSM1(DATAL,ITSH1)
CALL CALL ATT(DATAL,AT1)
CALL CALL POWER(DATAL,MP1,PF1)
CALL CALL FILTER(DATAL,TF,FOF1)
DO 10 I=1,LDIM
DATA(I)=DATA(I)+DATAL(I)

```

10

C

```

CALL CALL LOAD4(DATAL,IPNI1,IPNQ1)
CALL CALL HLIM(DATAL)
CALL CALL PHASE(DATAL,PSHIF2)
CALL CALL FSM1(DATAL,ITSH2)
CALL CALL ATT(DATAL,AT2)
CALL CALL POWER(DATAL,MP2,PF2)
CALL CALL FILTER(DATAL,TF,FOF2)
DO 11 I=1,LDIM
DATA(I)=DATA(I)+DATAL(I)

```

11

```

CALL CALL POWER(DATA,MPF,PF)
CALL CALL HHGG(TF,PNOISE)

```

```

ACI1=10.*ALOG10(MP/MP1)
ACI2=10.*ALOG10(MP/MP2)
CALL DECOD4(DATA,PNOISE,IPNI,IPNQ,
#EBNO,PEI,NSNR,EB)
DO 5 I=1,NSNR

```

```

PEI(I)=PEI(I)/FLOAT(NSYMB)
EBNO(I)=FLOAT(I)
APEI(I)=APEI(I)+PEI(I)
IF((PEI(I).LT..1E-03.AND.PEI(I).GT..1E-04).AND.(KM.EQ.1)) KL=I
CONTINUE
POL=(PEI(KL)**2.)+POL

```

C
5
C

```

ITSH1=ITSH1-1

```

```

PSHIF1=PSHIF1+.22
PSHIF2=PSHIF2+.46
ITSH2=ITSH2+1
500 CONTINUE
WRITE(6,4) A
4 FORMAT(5X,'A=',F3.2)
N=1
WRITE(6,3) N,FOF1,AT1,ACI1
N=2
WRITE(6,3) N,FOF2,AT2,ACI2
3 FORMAT(///,2X,'CHANNEL ',I1,' CHARACTERISTICS'///,2X,
&'OFFSET FREQ.: ',F6.1,' MHZ', ' ATTENUATION:',F4.1,' DB',
&' CARRIER TO INT. RATIO: ',F5.1,' DB')
DO 64 I=1,NSNR
APEI(I)=APEI(I)/FLOAT(NRUNS)
64 CONTINUE
WRITE(6,150)
150 FORMAT(5X,'EB/NO',10X,'PROB. OF. ERROR',/)
WRITE(6,172) (EBNO(I),APEI(I),I=1,NSNR)
172 FORMAT(5X,F5.1,10X,E13.6)
DO 99 I=1,NSNR
XARRAY(I)=EBNO(I)
99 YARRAY(I)=APEI(I)
CALL DRAW(XARRAY,YARRAY,NSNR,KA,NOA)
CALL EYEQQ(DATA,16,128,KA,NOA)
C CALL CHANGE SYSTEM PARAMETERS
AT1=AT1-3.
AT2=AT2-3.
C
600 CONTINUE
STOP
END

```

```

C*****
C THIS SUBROUTINE ATTENUATES THE SIGNAL POWER.
C*****

```

```

SUBROUTINE ATT(DATA,AT)
COMMON LDIM
COMMON/PARA/LSAMPL,NSYMB,NO1,NO2,BAUD,SBANDW
COMPLEX DATA(1)
ATT=10.**(-AT/20.)
DO 10 I=1,LDIM
DATA(I)=DATA(I)*ATT
10 RETURN
END

```

```

C*****
C   THIS      SUBROUTINE      SHIFTS      THE      SIGNAL
C*****

```

```

SUBROUTINE                                TIME(DATA,IT)
COMMON                                    LDIM
COMMON/PARA/LSAMPL,NSYMB,NO1,NO2,BAUD,SBANDW
COMPLEX                                    DATA(1),DAT
DO                                          I=1,IT
DAT=DATA(1)                                10
DO                                          20
                                          J=2,LDIM
DATA(J-1)=DATA(J)
DATA(LDIM)=DAT
20
10
RETURN
END

```

```

C*****
C   COMPUTATION      OF      MEAN      POWER
C*****

```

```

SUBROUTINE                                POWER(DATA,MP,PF)
COMMON                                    LDIM
COMMON/PARA/LSAMPL,NSYMB,NO1,NO2,BAUD,SBANDW
COMPLEX                                    DATA(1)
REAL                                        MP
PF=0.
MP=0.0
DO                                          I=1,LDIM
MP=MP+((CABS(DATA(I)))**2.)
IF(PF.LT.CABS(DATA(I)))                    PF=CABS(DATA(I))
10                                          CONTINUE
MP=MP/FLOAT(LDIM)/2.
PF=(PF**2.)/MP
PF=10.*ALOG10(PF)
RETURN
END

```

```

C*****
C   THE FOLLOWING SUBROUTINE PERFORMS THE FILTERING
C   PROCESS      ON      THE      DATA      SEQUENCE.
C*****

```

```

SUBROUTINE                                FILTER(SIGNAL,TF,FOF)
COMMON                                    LDIM,IOFF
COMMON/PARA/LSAMPL,NSYMB,NO1,NO2,BAUD,SBANDW
COMPLEX                                    SIGNAL(1),TF(1),XX
DIMENSION                                  IWK(12)
CALL                                        FFT2C(SIGNAL,11,IWK)
IFOF=IFIX(FOF*FLOAT(LDIM)/SBANDW)
CALL                                        FSM1(SIGNAL,IFOF)

```

```

1 DO 1 I=1, LDIM
    SIGNAL(I)=CONJG(SIGNAL(I)*TF(I))
CALL FFT2C(SIGNAL, 11, IWK)
DO 2 I=1, LDIM
2 SIGNAL(I)=CONJG(SIGNAL(I))/FLOAT(LDIM)
RETURN
END

```

```

C*****
C THIS SUBROUTINE COMPENSATES THE PHASE SHIFT
C DUE TO THE CARRIER OFFSET.
C*****

```

```

SUBROUTINE PHASE(DATA, PSHIFT)
COMMON LDIM
COMPLEX EPS, DATA(1)
EPS=CMPLX(COS(PSHIFT), -SIN(PSHIFT))
DO 10 I=1, LDIM
10 DATA(I)=DATA(I)*EPS
RETURN
END
CONTINUE

```

```

C*****
C THIS SUBROUTINE DECODES THE PROCESSED DATA
C*****

```

```

SUBROUTINE DECOD4(DATA, PNOISE, IPNI, IPNQ,
#EBNO, PEI, NSNR, EB)
COMMON LDIM, IOFF
COMMON/PARA/LSAMPL, NSYMB, NO1, NO2, BAUD, SBANDW
COMPLEX DATA(1), AMP
DIMENSION EBNO(1), PEI(1), IPNI(1), IPNQ(1)
DATA NOLD, NOF/0, 0/
IF (IOFF.EQ.0) GO TO 111
DO 9 K=1, IOFF
XX=AIMAG(DATA(1))
LD=LDIM-1
DO 5 KK=1, LD
5 DATA(KK)=CMPLX(REAL(DATA(KK)), AIMAG(DATA(KK+1)))
9 DATA(LDIM)=CMPLX(REAL(DATA(LDIM)), XX)
C SYNCHRONIZE THE RECEIVED DATA
C111 IF(KN.GT.1) GOTO 210
111 LFU=2*NSYMB
C NOLD=0
C NOF=0
NERROR=0
K=1
300 NEW=0
CONTINUE

```

```

DO      200      J=1, NSYMB
J1=K+(J-1)*LSAMPL
IF(J1.GT.LDIM)      J1=J1-LDIM
XB=REAL(DATA(J1))
YB=AIMAG(DATA(J1))
IF      (SIGN(1.,XB).EQ.IPNI(J))      NEW=NEW+1
IF      (SIGN(1.,YB).EQ.IPNQ(J))      NEW=NEW+1
200      CONTINUE
IF(NOLD.GE.NEW)      GOTO      12
NOLD=NEW
NOF=K
12      K=K+1
IF(NOLD.LT.LFU.AND.K.LE.LDIM)      GOTO      300
NOS=NOF-1
ND=-NOS
CALL      FSM1(DATA,ND)
C      IF(KN.GT.1)      GOTO      110
230      MI=1
MQ=1
EOI=FLOAT(NSYMB)+1.
EQ=FLOAT(NSYMB)+1.
SNR=PNOISE*EB/10.
SIGMA=SQRT(SNR)
DO      110      J=1, LSAMPL
EI=0.
EQ=0.
DO      100      K=1, NSYMB
J1=(K-1)*LSAMPL+J
AXBAR=(REAL(DATA(J1))+REAL(DATA(J1+1)))/2.
AYBAR=(AIMAG(DATA(J1))+AIMAG(DATA(J1+1)))/2.
IF(SIGN(1.,AXBAR).NE.IPNI(K))      EI=EI+1
IF(SIGN(1.,AYBAR).NE.IPNQ(K))      EQ=EQ+1
ARGI=ABS(AXBAR)/SIGMA
ARGQ=ABS(AYBAR)/SIGMA
EI=EI+ERFC(ARGI)/2.
EQ=EQ+ERFC(ARGQ)/2.
100      CONTINUE
IF(EOI.LE.EI)      GO      TO      120
EOI=EI
MI=J
120      CONTINUE
IF      (EQ.LE.EQ)      GO      TO      110
EQ=EQ
MQ=J
110      CONTINUE
MOFF=IABS(MI-MQ)
MOFF=(MQ+MI)/2
OFF=(FLOAT(MOFF)+FLOAT(NOF)-8.0)/FLOAT(LSAMPL)
DJPP=((8.0-FLOAT(MOFF))/FLOAT(LSAMPL))*2
DO      11      M=1, NSNR
11      PEI(M)=0.0
DO      2      K=1, NSYMB
2      JI=(K-1)*LSAMPL+MI
      JQ=(K-1)*LSAMPL+MQ

```

```

AXBAR=(REAL(DATA(JI))+REAL(DATA(JI+1)))/2.
AYBAR=(AIMAG(DATA(JQ))+AIMAG(DATA(JQ+1)))/2.
INDEXX=0
IF(SIGN(1.,AXBAR).NE.IPNI(K)) INDEXX=1
INDEXY=0
IF(SIGN(1.,AYBAR).NE.IPNQ(K)) INDEXY=1
IF((INDEXX.EQ.1).OR.(INDEXY.EQ.1)) NERROR=NERROR+1
C COMPUTE THE PROBABILITY OF ERROR FOR THIS SYMBOL
DO 4 M=1,NSNR
XM=FLOAT(M)/10.
SNR=PNOISE*EB/(10.**XM)
SIGMA=SQRT(SNR)
ARG=(ABS(AXBAR))/(SIGMA*SQRT(2.))
IF (ARG.GT.12.) ARG=12.
EX=ERFC(ARG)/2.
IF (INDEXX.EQ.1) EX=1.-EX
ARG=(ABS(AYBAR))/(SIGMA*SQRT(2.))
IF (ARG.GT.12.) ARG=12.
EY=ERFC(ARG)/2.
IF (INDEXY.EQ.1) EY=1.-EY
IF (EX.LT.1.E-15) EX=0.
IF (EY.LT.1.E-15) EY=0.
PEI(M)=PEI(M)+((EX+EY)/2.)
CONTINUE
C WRITE (6,152) NERROR
C152 FORMAT(/5X,'ERRORS=',I5,/)
RETURN
END

```

```

C*****
C APERTURE EQUALIZED RAISED COSINE FILTER WITH ARBITRARY ALPHA
C*****

```

```

SUBROUTINE RCOS(FBANDW,TF,ALPHA,FOF)
COMMON LDIM,IOFF
COMMON/PARA/LSAMPL,NSYMB,NO1,NO2,BAUD,SBANDW
COMPLEX TF(1)
C*** FF(X) IS THE INVERSE BASEBAND SPECTRUM
FF(X)=2.*X*(1.-(4./(3.141592**2))*(X**2))/SIN(2.*X)
QQ=2.
C FF(X)=X/SIN(X)
C QQ=3.14159265/2.
C ALPHA=0.0001
IF (ALPHA.EQ.0)
FN=LDIM*(FBANDW/SBANDW)
F1=(1.-ALPHA)*FN
F2=(1.+ALPHA)*FN
IFN=IFIX(FN)
IF1=IFIX(F1)+1
IF2=IFIX(F2)+1
A1=3.141592/(2.*FLOAT(IFN))
TF(1)=CMPLX(1.0,0.0)

```

```

DO          8          I=2,IF1
  J=I-1
  A2=FF(FLOAT(J)*A1)
  TF(I)=CMPLX(A2,0.0)
8          CONTINUE
  JK=IF1+1
  DO          9          J=JK,IF2
    I=J-1
    A3=QQ
    IF(I.NE.FN)          A3=FF(FLOAT(I)*A1)
    A=(3.141592/(2.0*ALPHA))*((FLOAT(I)/FLOAT(IFN))-1.)
    TF(J)=CMPLX(0.5*(1.0-SIN(A)),0.0)
    TF(J)=TF(J)*CMPLX(A3,0.0)
9          CONTINUE
  JH=IF2+1
  DO          10         I=JH,NO1
    TF(I)=CMPLX(0.0,0.0)
10         CONTINUE
  DO          5          I=NO2,LDIM
    TF(I)=TF(LDIM+2-I)
5          CONTINUE
  IFOF=IFIX(FOF*FLOAT(LDIM)/SBANDW)
  CALL          FSML(TF,IFOF)
  RETURN
  END

```

```

C*****T*****
C          PHASE      EQUALIZED      BUTTERWORTH      FILTER
C*****

```

```

SUBROUTINE          BUT(TF,FB,ICEL,FOF)
COMMON          LDIM,IOFF
COMMON/PARA/LSAMPL,NSYMB,NO1,NO2,BAUD,SBANDW
COMPLEX          TF(1)
A1=1./NSYMB
FBNOR=FB/BAUD
TF(1)=CMPLX(1.0,0.0)
DO          10         I=2,NO1
  J=I-1
  A2=1./SQRT(1.+(A1*FLOAT(J)/FBNOR)**(2*ICEL))
10         TF(I)=CMPLX(A2,0.)
  DO          20         I=NO2,LDIM
    TF(I)=TF(LDIM+2-I)
20
  IFOF=IFIX(FOF*FLOAT(LDIM)/SBANDW)
  CALL          FSML(TF,IFOF)
  RETURN
  END

```

C*****
 C THIS SUBROUTINE SHIFTS THE SIGNAL IN TIME DOMAIN. *
 C*****

```

SUBROUTINE                                , FSML(DATA, IOF)
COMMON                                     LDIM, IOFF
COMMON/PARA/LSAMPL, NSYMB, NO1, NO2, BAUD, SBANDW
COMPLEX                                   DATA(1), BUFF(2048)
J=LDIM-IABS(IOF)
K=J+1
IF      (IOF.EQ.0)                         GOTO          9
IF      (IOF.LT.0)                         GOTO          4
DO      1                                I=1, J
1      DO      2                                BUFF(I)=DATA(I)
2      DO      2                                I=K, LDIM
2      DO      2                                DATA(I-J)=DATA(I)
3      DO      3                                I=1, J
3      DO      3                                DATA(I+IOF)=BUFF(I)
4      GOTO          9
4      L=IOF+1
DO      5                                I=L, LDIM
5      DO      6                                BUFF(I-IOF)=DATA(I)
6      DO      6                                I=1, IOF
6      DO      7                                DATA(I+J)=DATA(I)
7      DO      7                                I=1, J
9      DATA(I)=BUFF(I)
9      RETURN
END

```

REFERENCES

1. T. Le-Ngoc, K. Feher, H. Pham-Van, "New Modulation Technique for Low-Cost Power and Bandwidth Efficient Satellite Earth Stations", IEEE Trans. on Comm., vol. COM-30, Jan. 1982.
2. V.K. Prabhu, "PSK-Type Modulation with Overlapping Baseband Pulses", IEEE Trans. on Comm., vol. COM-25, Sept. 1977.
3. F. deJager, C.B. Dekker, "Tamed Frequency Modulation, A Novel Method to Achieve Spectrum Economy in Digital Transmission", IEEE Trans. on Comm., vol. COM-26, May, 1978.
4. J.C.Y. Huang, K. Feher, M. Gendron, "Techniques to Generate ISI and Jitter-Free Bandlimited Nyquist Signals and a Method to Analyze Jitter Effects", IEEE Trans. on Comm., vol. COM-27, Nov. 1979.
5. K. Feher, "Filter, Nonlinear Digital", Canadian and U.S. Patent Disclosure, Canada No.372 365, May 1979, U.S. No. 4 339 724, July 1982
6. M.C. Austin, M.V. Chang, "Quadrature Overlapped Raised-Cosine Modulation", IEEE Trans. on Comm., vol. COM-29, Mar. 1981.
7. S. Kato, K. Feher, "XPSK - A New Cross-Correlated Phase Shift Keying Modulation Technique", IEEE Trans. on Comm., vol. COM-31, May 1983.
8. I. Sasase, Y. Harada, S. Mori, "Bandwidth Efficient Quadrature Overlapped Modulation", ICC'82, June 1982.
9. H. Pham-Van, K. Feher, "A Class of Two-Symbol-Interval Modems for Nonlinear Radio-Systems", IEEE Trans. on Comm., vol. COM-31, Mar. 1983.
10. K. Feher, "Digital Communications : Satellite/Earth Station Engineering", Englewood Cliffs, NJ: Prentice-Hall, 1983.
11. T. Le-Ngoc, K. Feher, "Performance of IJF-OQPSK Modulation Schemes in a Complex Interference Environment", IEEE Trans. on Comm., vol. COM-31, Jan. 1983.

12. K. Feher, "Digital Modulation Techniques for New Earth Stations", Satellite Communications Magazine, Feb. 1983.
13. D.J. Kennedy, O. Shimbo, "Cochannel Interference in Nonlinear QPSK Satellite Systems", IEEE Trans. on Comm., vol. COM-29, May 1981.
14. T.C. Huang, J.K. Omura, "Analysis of Coherent Satellite Communication Systems in the Presence of Interference and Noise", IEEE Trans. on Comm., vol. COM-29, May 1981.
15. V.K. Prabhu, "Error Rate Considerations for Coherent Phase-Shift Keyed Systems with Co-Channel Interference", B.S.T.J., Mar. 1969.
16. R.J.F. Fang, "Quaternary Transmission Over Satellite Channels with Cascaded Nonlinear Elements and Adjacent Channel Interference", IEEE Trans. on Comm., vol. COM-29, May 1981.
17. J.R. Cruz, R.S. Simpson, "Cochannel and Intersymbol Interference in Quadrature Carrier Modulation", IEEE Trans. on Comm., vol. COM-29, Mar. 1981.
18. J.S. Seo, K. Feher, "Modified Minimum Shift Keyed (MMSK) Modem for Satellite Systems", Proceedings of the Satellite Communications Conference, SCC'83, Ottawa, June 1983.
19. S. Stein, J.J. Jones, "Modern Communication Principles", McGraw-Hill, NY., 1967.
20. S. Asakawa, F. Sugiyama, "A Compact Spectrum Constant Envelope Digital Phase Modulation", IEEE Trans. Veh. Technol., vol. VT-30, No.3, Aug. 1981.
21. A. Lender, "The Duobinary Technique for High Speed Data Transmission", IEEE Trans. Comm. and Electronics, Vol.82, May 1963.
22. D. Divsalar, M.K. Simon, "The Power Spectral Density of Digital Modulations Transmitted over Nonlinear Channels", IEEE Trans. on Comm., Vol. COM-30, No.1, Jan. 1982.
23. V.K. Prabhu, "Bandwidth Occupancy in PSK Systems", IEEE Trans. on Comm., Vol. COM-24, Apr. 1976.
24. S.A. Gronemeyer, A.L. McBride, "MSK and Offset QPSK Modulation", IEEE Trans. on Comm., Vol. COM-24, Aug. 1976.

25. P. Kabal, S. Pasupathy, "Partial-Response Signaling", IEEE Trans. on Comm., Vol. COM-23, Sep. 1975.
26. D. Mulwijk, "Correlative Phase Shift Keying - A Class of Constant Envelope Modulation Techniques", IEEE Trans. on Comm., Vol. COM-29, Mar. 1981.
27. I. Korn, "Simple Expression for Interchannel and Intersymbol Interference Degradation in MSK Systems with Application to Systems with Gaussian Filters", IEEE Trans. on Comm., Vol. COM-30, Aug. 1982.
28. S.A. Rhodes, "FSOQ, A New Modulation Technique That Yields A Constant Envelope", NTC'80, 1980.

VITA

Name : Seo , Jong-Soo
Born : Jan. 7 , 1952 , Busan , Korea
School : Dept. of Electronic Eng., Yonsei Univ.,
Seoul , Korea (B.A.Sc., 1975.)
Career : Central Research Lab., Gold Star Precision
Industries , Gumi , Korea (1975 - 1981)
A .E .L ., Pa., U.S.A. (1977)